A STUDY OF THE $O^{17}(p,\alpha)N^{14}$ REACTION

Thesis by

Ronald E. Brown

In Partial Fulfillment of the Requirements

for the Degree of

Doctor of Philosophy

California Institute of Technology

Pasadena, California

1962

ACKNOWLEDGMENTS

The author wishes to express his gratitude and thanks to the entire staff and personnel of the Kellogg Radiation Laboratory for their kind assistance during the course of this work. He is especially indebted to Professor William A. Fowler who suggested the problem and guided the work to its completion. Special thanks are also expressed to Barbara A. Zimmerman for her help with many of the computations.

The author is also grateful for the graduate fellowships received from the National Science Foundation and for the financial support of this research by the joint program of the Office of Naval Research and the U. S. Atomic Energy Commission.

ABSTRACT

An experimental measurement of the absolute cross section for the $O^{17}(p,\alpha)N^{14}$ reaction has been carried out in the energy range from 490- to 1580-kev proton bombarding energy at a laboratory angle of 150^{o}. Resonances were observed at bombarding energies of 518, 672, 747, 825, 927, 1096, 1101, 1247, 1274, and 1335 kev. Other level parameters were assigned where possible. The 747-kev resonance corresponds to a level in F^{18} at 6302-kev excitation which does not appear to have been previously reported.

A calculation of the ratio O^{17}/O^{16} formed at equilibrium at various temperatures in the CNO-cycle in stars is made, and it is concluded that the terrestrial material which has been processed in the CNO-cycle underwent this processing at a temperature of about $17 \times 10^{6}\ ^{o}K$.

TABLE OF CONTENTS

I. INTRODUCTION

In recent years theoretical work on the properties of the mass-18 system (Redlich, 1954, 1958; Elliott, 1955, 1958a, 1958b) has stimulated a good deal of work on the levels of F^{18}--especially the low-lying levels (Ajzenberg-Selove, 1959). In this thesis the results of an investigation of several of the higher levels of F^{18} by means of the $O^{17}(p,\alpha)N^{14}$ reaction is reported. Also reported is an application of our present knowledge of the F^{18} level structure to an estimate of the $O^{17}(p,\alpha)N^{14}$ reaction rate in stars.

In the present experiment an excitation curve at a laboratory angle of 150° was taken with protons ranging in energy from 490 to 1580 kev. This covers the region of excitation in F^{18} from 6.06 to 7.09 Mev. Below 1-Mev bombarding energy several very narrow, well isolated resonances were found, and above this energy several narrow anomalies superimposed on rather broad resonances were observed. Previous work on the $O^{17}(p,\alpha)N^{14}$ reaction had been carried out in the region of 1- to 3-Mev bombarding energy (Ahnlund, 1957). In the present work some structure near 1250 kev was seen that was not reported by Ahnlund (1957). The present work and the work of Ahnlund (1957) are the only reported investigations of the $O^{17}(p,\alpha)N^{14}$ reaction to this date. This is presumably because the very low concentration (.04%) of O^{17} in natural oxygen makes large enrichment factors necessary. Recently enrichments of O^{17} of up to 4% have become available.*

---

*Weizmann Institute of Science, Rehovoth, Israel; Isomet Corporation, Palisades Park, New Jersey.

Several other reactions have been used to investigate this region of excitation in F^{18}. The $F^{19}(He^3,\alpha)F^{18}$ reaction has been used to measure the level positions in F^{18} (Hinds, 1959). Several of the angular momentum and parity properties have been investigated by means of $N^{14}(\alpha,\alpha)N^{14}$ elastic scattering experiments (Heydenburg, 1953; Kashy, 1958; Herring, 1958a, 1958b; Silverstein, 1960). Also investigated have been $N^{14}(\alpha,p)O^{17}$ (Heydenburg, 1953; Kashy, 1958; Herring, 1958a) and $N^{14}(\alpha,\gamma)F^{18}$ (Phillips, 1958). In Section V-D some of these results will be compared with those obtained in the present experiment.

The importance of the $O^{17}(p,\alpha)N^{14}$ reaction in theories of element synthesis in stars comes from its occurrence in the well-known carbon-nitrogen-oxygen cycle (CNO-cycle) in which it acts as a feedback into the main part of the cycle. The reactions occurring in the CNO-cycle are (Fowler, 1960)

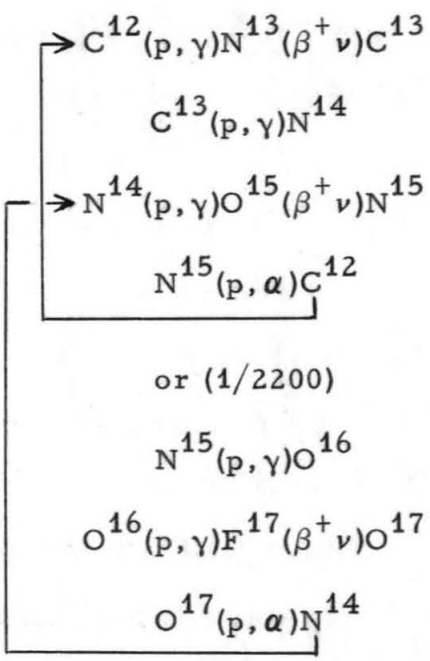

Knowledge of the ratio of the amount of O^{16} to the amount of O^{17} formed in the CNO-cycle then depends on a knowledge of the cross sections for $O^{16}(p,\gamma)$ which forms the O^{17} and for $O^{17}(p,\alpha)$ which destroys it. This ratio is important in the light of a recent paper by Fowler, Greenstein, and Hoyle (1961) which discusses element formation in the early history of the solar system.

This thesis thus consists of two main parts. In Sections II through V we discuss the experimental determination of the $O^{17}(p,\alpha)N^{14}$ cross section and the assignment of level parameters to the various states in F^{18}. Section VI deals with the astrophysical problem in the light of the suggestions of Fowler et al. (1961).

II. APPARATUS

A. General Discussion

The Kellogg Laboratory 2-Mv electrostatic generator was used to accelerate the protons for this experimental determination of the energy excitation curve for $O^{17}(p,\alpha)N^{14}$. The proton beam was passed through an 80^{o} electrostatic analyzer into a target chamber. A signal taken from the horizontal slits at the bottom of the analyzer was used to regulate the generator voltage. The analyzer slits were set such that the energy resolution was about 0.2%. A double focusing magnetic spectrometer with an equilibrium orbit radius of 10.5 inches (Snyder, 1950) was used to analyze the reaction products. The target surface defines the object plane; at the image plane a CsI crystal was mounted on a lucite light pipe, the optical contact being made with Dow Corning high vacuum grease. The other end of the lucite was sealed in the same manner to the surface of a Dumont 6291 photomultiplier. The output pulses from this photomultiplier were passed through a standard preamplifier and pulse amplifier. The output of the pulse amplifier was fed into a biased amplifier and then into a 10-channel pulse height analyzer. The 10-channel analyzer was set in the five-volts-per-channel mode and the biased amplifier allowed this 50-volt window to be positioned in the desired region of pulse heights.

In order to integrate the beam current a capacitor of known capacitance was charged by means of a bank of mercury batteries of known voltage. The beam current was then allowed to discharge this capacitor. At complete discharge the counting equipment was automatically gated off by a system of relays. In this way the total

number of bombarding protons per run could be found. In order to avoid electron leakage to or from the target when the beam is on, two precautions were taken. The target was raised to a potential of 300 volts above ground in order to prevent electrons from leaving the target when the beam strikes it. Also, a screen at a potential of 300 volts below ground was placed at the entrance to the target chamber. This prevented electrons which were produced at the slit systems from finding their way to the target. This arrangement requires that 0.3 kev be subtracted from the proton energy E_e at the electrostatic analyzer exit to obtain the proton energy E_{1B} at the target surface.

B. Electrostatic Analyzer Energy Calibration

The voltage across the plates of the electrostatic analyzer is determined by tapping off a fraction of this voltage and reading it with a potentiometer; call this reading V_e. Let M and Z be the mass and charge number of the particle with energy E_e which passes through the analyzer. Following the derivation of Mozer (1956) but using the notation of Bardin (1961) we may write

$$E_e = k_e Z V_e (1 + E_e/2Mc^2) \qquad (1)$$

Here k_e is the calibration constant, and c is the speed of light.

In order to determine k_e the gamma rays from the 873-kev resonance in the $F^{19}(p,\alpha\gamma)O^{16}$ reaction were observed by means of a sodium iodide crystal, photomultiplier arrangement. A thick CaF target was prepared by evaporation onto a Cu backing. The

Cu backing consisted of Cu evaporated onto a clean glass microscope slide. The midpoint of the step in the thick target gamma ray yield was observed to occur at a setting of $V_e = 0.8686$ decivolts. It is assumed that this value corresponds to the resonant energy E_{res} for the $F^{19}(p,\alpha\gamma)O^{16}$ reaction. After a survey of the energy determinations of this resonance (Bondelid, 1959, and references therein) the following value was adopted:

$$E_{res} = 872.7 \pm 0.4 \text{ kev}$$

This is to be compared with the recent value of 872.5 ± 0.4 kev adopted by Marion (1961) in his article on energy calibrations. Correction for the target potential gives $E_e = 873.0 \pm 0.4$ kev, and solving Eq. (1) for k_e gives

$$k_e = 1.0047 \pm 0.0006 \text{ Mev/decivolt}$$

C. Magnetic Spectrometer Energy Calibration

The magnetic field in the spectrometer is measured and regulated to one part in one thousand by means of a rotating coil fluxmeter and optical lever system (Milne, 1953). The current in the fluxmeter coil is determined by measuring the voltage across a precision resistor; call this voltage V_m. If we again follow the derivation of Mozer (1956) and use the notation of Bardin (1961) we may write

$$E_m = \frac{k_m Z^2 M_p}{V_m^2 M} (1 - E_m/2Mc^2) \qquad (2)$$

where E_m is the energy of a particle of charge number Z and mass M passing through the spectrometer, and k_m is the calibration constant.

In order to determine the spectrometer constant k_m the reaction Cu(p,p)Cu was observed at a laboratory angle of 150°. Thick Cu targets were prepared by evaporation onto clean glass microscope slides. Protons of approximately 1 Mev were scattered from the Cu and a target profile was taken (the term target profile will henceforth denote number of counts N_0 versus fluxmeter setting V_m for a fixed bombarding energy E_{1B}). The bombarding energy is known from the electrostatic analyzer calibration, and the energy of the protons which are elastically scattered from Cu atoms at the target surface can be calculated from kinematics. The fluxmeter setting corresponding to the midpoint on the target profile rise is taken to correspond to the scattered proton energy at the target surface. The small correction due to the target potential was again made. The result of several trials is

$$k_m = 384\,100 \pm 200 \quad \text{Mev-mv}^2$$

The determination of the solid angle of the spectrometer will be discussed in Section V-A.

III. TARGETS

A. Preparation

The relative abundance of O^{17} in natural oxygen is about 0.04% so that a considerable enrichment of the O^{17} is needed for the present experiment. Two types of targets were used. One was a 1/16-inch thick stainless steel disc which had been bombarded in a mass separator with O^{17} in the form of the ion $N^{14}O^{17}$. This resulted in a thin, nonuniform target of O^{17}. This target was brought to the Institute from Sweden by Katarina Ahnlund for her investigation of the $O^{17}(p,\alpha)N^{14}$ reaction (Ahnlund, 1957). Upon completion of her work here she kindly left the target at the Institute. In what follows this target will be referred to as the iron oxide target.

The other type of target used was a thick, uniform nickel oxide target. These targets were prepared by oxidizing clean, polished, 15-mil thick nickel blanks in an induction heater. The oxygen gas used was obtained from the Weizmann Institute of Science, Rehovoth, Israel, and was of composition 3.97% O^{17}, 43.70% O^{18}, and 52.33% O^{16}. Their isotopic analysis has been assumed to be correct. At an early stage of the experiment a sample of oxygen gas enriched to 2.77% O^{17} and 71.7% O^{18} was obtained from the Isomet Corporation, Palisades Park, New Jersey. The alpha-particle yield at several bombarding energies was found to be in the ratio 3.97/2.77 for the two targets, thus lending support to the above quoted O^{17} concentrations. Nickel was decided on as the element to be oxided with the enriched gas after a series of trials were made in oxiding different metals (using natural oxygen). The elements W, Cu, Ni, Mo, Ti, and stainless steel were all tried. Protons were then scattered

from the oxided targets to determine the degree of oxidation and uniformity of the oxide layer as described in Section III-B below. It was found that it was easiest to obtain a good NiO target, hence Ni was chosen. The oxide was found to be stable--no oxygen loss was detectable with the beam currents of the order of 1 microamp or less and the beam spot size of the order of 1 mm x 2 mm used in this experiment.

B. Nickel Oxide Target Analysis

To obtain the absolute cross section one must know the number of reacting target atoms per cm^3 in the target. It is thus important to know what fraction of the nickel atoms in the target are oxidized. In order to determine this a target profile was taken of 1-Mev protons elastically scattered from the target. From the profile both the degree of oxidation of the nickel and the thickness of the oxide layer can be determined. Such a profile along with a profile taken from a pure nickel target is shown in Fig. 1. The protons counted in both cases are those elastically scattered from the nickel atoms. The decrease in counts at the step in the oxided target is due to the influence of the stopping power of the oxygen. When the magnet setting is such that the observed scattered protons start coming from behind the oxided layer then the yield approaches that from pure nickel; thus the thickness of the oxide layer can be determined. Let the symbol [X] stand for the number of X atoms (or molecules) per unit volume in the target, and ϵ_X stand for the stopping cross section per atom (or molecule) for material X. We then define two quantities α and μ by

$$\alpha = \frac{[NiO]}{[Ni]} \tag{3}$$

$$\epsilon_{NiO} = \mu (\epsilon_{Ni} + \epsilon_{O}) \tag{4}$$

It should be stressed that the symbol [Ni] is meant to include all the nickel in the target--including that contained in the nickel oxide. Thus α measures the degree to which the oxide layer has been oxidized ($\alpha = 1$ for pure NiO) and μ measures the error made in assuming that the additivity of stopping powers is valid ($\mu = 1$ for no error). We now derive a formula which compares the yield at the step in the two cases. The same proton energy is used so that the Rutherford cross section is the same in both cases. For the same cross section, the scattered proton yield is directly proportional to [Ni]t, the number of nickel atoms per cm^2 as seen by the spectrometer. For the case of elastic scattering and where the normal to the target surface bisects the angle between the incident particles and the outgoing particles we have

$$[Ni]t \propto \frac{1}{\epsilon_1(\epsilon_2/\epsilon_1 + E_2/E_1)}$$

where ϵ_1 is the stopping cross section per nickel atom for the incoming proton, ϵ_2 is the stopping cross section per nickel atom for the scattered proton, and E_2/E_1 is the ratio of the scattered energy to the incident energy as determined from kinematics (Brown, 1951). Let N be the number of counts at the step in the NiO target and $N + \Delta N$ be the number of counts at the step in the Ni target. Then we find

$$[\epsilon_1(N + \Delta N)(\epsilon_2/\epsilon_1 + E_2/E_1)]_{Ni} = [\epsilon_1 N(\epsilon_2/\epsilon_1 + E_2/E_1)]_{NiO} \quad (5)$$

On assuming $\alpha = 1$, $\mu = 1$, the terms $\epsilon_2/\epsilon_1 + E_2/E_1$ are found to be very nearly equal in the two cases; thus this term will be cancelled from the equation giving

$$(N + \Delta N)\epsilon_{Ni} = N\epsilon_T \quad (6)$$

where ϵ_T is the stopping cross section per nickel atom in the oxided region of the target. It is given by

$$\epsilon_T = \frac{-1}{[Ni]}\frac{dE}{dx} = \frac{1}{[Ni]}\{([Ni] - [NiO])\epsilon_{Ni} + [NiO]\epsilon_{NiO}\} \quad (7)$$

On combining Eqs. (3), (4), (6), and (7) one finds the following relation between α and μ

$$\alpha = \frac{\Delta N}{N}\frac{\epsilon_{Ni}}{\mu\epsilon_O + (\mu - 1)\epsilon_{Ni}} \quad (8)$$

From Fig. 1 we find N = 67 490, ΔN = 21 900. We take the nickel and oxygen stopping cross sections from published curves (Whaling, 1958). Substitution into Eq. (8) then gives the following experimentally determined relation between α and μ.

$$\alpha = \frac{1}{3.06\,\mu - 2.08} \quad (9)$$

This relation is shown graphically in Fig. 2. The physically significant region of the graph is for $\alpha \leq 1$. In order to determine α, the target composition, a value for μ must be chosen. It has been found experimentally that for many compounds μ is close to unity, even at proton energies lower than those used in the present work (Reynolds, 1953). Also, Gray (1943) has pointed out that deviations from

the additivity law should not amount to more than 1%. Platzman (1952), however, believes that 1% may be an underestimate and that in some cases deviations up to even 5% may be present. It must be pointed out, however, that ϵ_O itself is not known; only ϵ_{O_2}, the stopping cross section for the oxygen molecule, can be measured. In the computation of ϵ_{NiO} one assumes $\epsilon_O = \frac{1}{2}\epsilon_{O_2}$ and thus μ will reflect only the difference in binding in O_2 and NiO. One might hope that this difference will be quite small; although Platzman points out that the valence bonding in molecules containing oxygen can vary rather strongly. Thus there is some uncertainty as to the exact value to use for μ. An inspection of Fig. 2 shows that the data are consistent with the values $\alpha = 1$, $\mu = 1$. Also, investigation of several NiO targets of varying thickness showed that ΔN did not change. This suggests $\alpha = 1$, since if all the nickel were not being oxided one would expect α to be a function of the oxidation time (and hence of the thickness of the oxide layer). In the following analysis it will be assumed that $\alpha = 1$, $\mu = 1$. The stopping cross section for NiO will be computed from

$$\epsilon_{NiO} = \epsilon_{Ni} + \frac{1}{2}\epsilon_{O_2} \tag{10}$$

and ϵ_{Ni} and $\frac{1}{2}\epsilon_{O_2}$ will be taken from published data (Whaling, 1958).

The thickness of the oxide layer can also be found from the scattering data. Figure 1 corresponds to an oxide layer thickness of 26 kev to 1-Mev protons.

C. Advantages of Each Type of Target

At a given proton bombarding energy the peak alpha-particle yield from the iron oxide target was found to be about four times that from the nickel oxide targets. In all other respects, however, the iron oxide target was inferior to the nickel oxide. Since it had been used in a previous experiment the iron oxide target had carbon contamination on the surface. The number and distribution of O^{17} atoms in the target was a function of the target spot that was being bombarded. Since the iron oxide target was so thin (about 6 kev to 1-Mev protons) it was necessary to take a complete target profile at each bombarding energy. This fact and the carbon build up during the bombardment made it extremely difficult to obtain any quantitative data with this target at the several very narrow resonances observed in this work. Relative cross section measurements were made with the iron oxide target at several energies away from the very narrow resonances, particularly where the cross section was quite low and the low yield prohibited use of the less enriched nickel oxide targets. These relative cross sections were normalized to the absolute values obtained with the nickel oxide targets.

Even though the yield was lower for the nickel oxide targets the majority of the data was taken with these targets. These targets are thick enough and uniform enough so that the thick target relations (Section V-A) can be used. Thus the magnet setting determines the number of target atoms per cm^2 as long as it is set to detect only particles produced completely in the uniformly oxided region of the target. In order to avoid undesirable effects due to carbon build up

on the target its position relative to the beam can be shifted as often as desired. This is especially important when taking the data at the very narrow resonances.

IV. EXPERIMENTAL PROCEDURE

A. Nickel Oxide Target Data

For this data the targets used were kept as clear of surface contaminants as possible. The ideal case was when the target was removed from the induction heater and placed immediately into the target chamber, which was then pumped down. This procedure was not always followed, however. Many runs were taken with targets which had been under vacuum for several days, either in the target chamber itself or in a separate vacuum jar. It was found that such a waiting period did not affect the experimental results.

There are many protons produced by elastic scattering from the nickel in the target. These have an energy spectrum from zero up to an energy almost equal to that of the bombarding protons. The magnetic spectrometer, besides defining the reaction lamina in the target, also serves the very useful purpose of separating these scattered protons from the alpha particles under observation.

The spectrometer was set to observe the doubly charged alpha particles from the $O^{17}(p,\alpha)N^{14}$ reaction. This reaction has a Q-value of 1.193 Mev as determined from recent mass tables (Everling, 1960). Protons of the same energy as that of the alpha particles will pass through the magnet. At $\theta_{Lab} = 150^{o}$ the maximum energy of the scattered protons becomes equal to that of the alpha particles at about 2-Mev proton bombarding energy. This critical energy becomes larger at smaller scattering angles. However, the Rutherford cross section increases rapidly as one moves to more forward angles. This would tend to greatly increase the number of protons being counted due to scattering through the spectrometer.

It was found that a scattering angle of 150° was a good compromise.

Because of the low alpha-particle yield in this experiment both the entrance apertures and exit slits to the spectrometer were removed. Removing the entrance apertures allowed the full solid angle of the spectrometer to be used. Removing the exit slits increases the counting rate by making the energy resolution poorer--that is, the magnet is allowed to pass a larger portion of the energy spectrum of the particles incident on it.

In taking the data the target chamber entrance slits were first adjusted so that the proton beam hit the target surface in the center of the target chamber. The beam spot was about 1-mm high and 2-mm wide. The target was then positioned so that the normal to the target surface bisected the acute angle formed by the spectrometer (set to give a scattering angle of 150°) and the incoming proton beam. All targets were always positioned in this manner for all the data taken in this experiment. The spectrometer was then set so that the lamina in the target from which the alpha particles were being counted was completely in the oxided layer and below the target surface to a depth of several kev to the bombarding protons. This setting was determined from Eq. (13) (to be discussed in Section V-A1) and was checked by taking a target profile at several bombarding energies. This spectrometer setting is a function of the proton bombarding energy.

For the beam current integration three polystyrene capacitors of nominal value 10 μf each were connected in parallel. The voltage of the bank of mercury batteries used to charge this capacitor combination was measured with a precision voltage divider and potentiometer. This voltage was measured several times during a run

as a check on the condition of the mercury batteries. Normally the voltage was close to 9.45 volts and could be measured to better than one part in five thousand. The total capacitance of the parallel combination was measured by first charging it by means of the mercury batteries--then discharging it with a 300-volt emf and some large resistors in series. The time necessary to accomplish complete discharge was then recorded. From this data the total capacitance C may be calculated. The RC time constant was long compared to the discharge time so that the correction to the capacitance for non-uniform discharge current amounted to a little over 1%. The result of three trials was $C = 29.3 \pm 0.1$ μf. Each integration, then, amounted to a total charge deposited of about 276 microcoulombs, and took approximately ten minutes. After every two and sometimes three integrations the target was shifted so that the proton beam would bombard a clean spot. Even after one integration carbon build up was clearly visible on the target surface. By shifting every two or three integrations it was found that the data taken at the narrow resonances were quite repeatable. This would indicate that the energy shift introduced by the carbon build up from three integrations on a fresh target spot is probably less than 0.5 kev.

As discussed in Section II the alpha-particle pulses were fed into a 10-channel analyzer. It was not strictly necessary to use this analyzer at energies where the cross section was highest but it was extremely convenient and all the nickel oxide target data were taken using it. It was a simple matter to set the pulse amplifier gain and biased amplifier bias so that the peak of the pulse height

distribution fell somewhere in channel five to seven. This could be done empirically at an energy where the yield was relatively high and then the known response of cesium iodide to alpha particles could be used to determine the settings at other energies (Bashkin, 1958). In this way no very accurate bias settings were needed. The work involved in recording the data was greater than had a single scaler been used; however, it was felt that the increased confidence in the data was well worth the effort. The solid histogram in Fig. 3 shows a sample pulse height spectrum for one integration obtained at a bombarding energy of 1.342 Mev.

To keep a check on the background a nickel oxide target was made using natural oxygen. At any time during a run the natural target could be moved into the beam and a background integration taken. The dashed histogram in Fig. 3 shows such a background integration. A spread of five to seven channels was always sufficient to encompass the alpha-particle spectrum. The remaining channels were simply discarded as far as the determination of the number of alpha counts and of background counts was concerned. For instance in Fig. 3 channels one, two, three, and surplus were discarded. It was found that below 1.50-Mev bombarding energy the background ranged from about five to twenty counts per integration depending on the bombarding energy and the general laboratory background at the time. This background is attributed both to laboratory background and to counts due to protons which scatter through the spectrometer and are counted. Above about 1.50 Mev the background increases due to the increasing number of protons passing through the spectrometer until at 1.583 Mev, the highest energy at which

data were taken, the background was 50 counts per integration and the alpha counts were 160 - 50 = 110 counts per integration. The protons did make larger pulses on the average than the alpha particles as was indicated by the large number of counts in the surplus channel. However, the low energy tail of the proton distribution was enough to give 50 counts in the alpha-particle region. At the peaks of the narrow isolated resonances the counting rate ranged from a low of 80 counts per integration at the 825-kev resonance to a high of 290 counts per integration at the 747-kev resonance. An example of the raw data taken at the 672-kev resonance is shown in Fig. 4. The result of each integration is shown on this graph. In the data analysis the points at each energy were averaged together. The highest counting rate was observed at the peak of the broad 1274-kev resonance and amounted to 630 counts per integration.

It will be recalled that there is a considerable amount of O^{18} in the nickel oxide targets (Section III-A). Even though the Q-value for the $O^{18}(p,\alpha)N^{15}$ reaction is about 4 Mev one would suspect that occasionally some of these alpha particles would scatter through the spectrometer and be counted when the spectrometer is set to count the much lower energy alpha particles from the $O^{17}(p,\alpha)N^{14}$ reaction. To check that there actually was a considerable amount of O^{18} in the target a 0.3-mil aluminum foil was inserted between the target and the spectrometer entrance in order to slow down the alpha particles from the O^{18} sufficiently to allow them to be bent by the spectrometer. The target was then bombarded with 846-kev

protons and a target profile was taken. It is known that a resonance in the $O^{18}(p,\alpha)N^{15}$ cross section occurs at this energy and its width is about 50 kev (Carlson, 1961). As expected a large alpha-particle yield was observed. The resonance effect of this yield was observed by shifting the energy several tens of kev to either side of the original bombarding energy. In taking the $O^{17}(p,\alpha)N^{14}$ data with these nickel oxide targets the effect of the alpha particles from the O^{18} was observable only when one attempted to measure rather low, off resonant cross sections. For this reason these targets were not used in these cases. It is reasonable to assume that the O^{18} contamination does not significantly affect the data taken at the narrow resonances and at the higher yield broad resonances since, a) the alpha particles from the O^{18} could hardly be expected to show sharp resonance effects and b) the ratio of the alpha-particle counts found with targets made with the Israel gas to that found with targets made from the Isomet gas was observed to be in the ratio of the O^{17} concentrations in the two gases (Section III-A). If the $O^{18}(p,\alpha)N^{15}$ reaction were making any significant contribution this would not be the case. Thus no corrections were made for the O^{18} contamination--it being assumed that the entire background was given by the bombardment of the targets made with natural oxygen.

B. Iron Oxide Target Data

The general procedure for obtaining data with this target was as follows. First a target profile was obtained at a proton bombarding energy of 1.280 Mev where the alpha-particle yield is high. Figure 5 shows an example of such a profile. This first profile taken at the beginning of each run serves as a reference. All other

data taken at other energies during that run will determine the cross section at those energies relative to the cross section corresponding to the 1.280-Mev bombarding energy. After this reference profile is taken the energy is shifted to some new value at which it is desired to measure the cross section. A complete target profile is then taken at this new energy, and this procedure is repeated if time permits. At the end of the run the energy is again set at 1.280 Mev and the front edge of the target profile is observed. The shift in this front edge determines the amount of carbon deposited on the bombarded target spot during the run. In Section V-A4b it will be described how the data were corrected for this carbon build up. It is not permissible to shift the position of this target during the run as it was for the nickel oxide target since here the O^{17} concentration changes with target position. Because of the length of the runs necessary in the cases of the two lowest measured cross sections (at bombarding energies 804 and 854 kev) it was not possible to take all of the data at the same target spot. In this case for the different runs target spots were chosen which gave similar profiles at 1.280 Mev, although they may have been shifted relative to one another by several millivolts fluxmeter setting. Such a low yield profile which is a combination of three runs is shown in Fig. 6. This was taken at a bombarding energy of 854 kev and corresponds to the lowest cross section measured in the present investigation.

An interesting background problem was encountered with this target. Figure 7, a target profile at 1.005-Mev bombarding energy, illustrates this nicely. At low-yield points it was discovered that the target profiles do not go to zero counts when

the fluxmeter setting is such that no alpha particles from $O^{17}(p,\alpha)N^{14}$ should be observed. Instead it appeared as though there were a continuum of alpha particles underlying the $O^{17}(p,\alpha)N^{14}$ peak. In Fig. 7 this amounts to about 15 counts. These counts are not due to elastically scattered protons since only two or three counts at most were observed from bombardment of a piece of stainless steel under the same circumstances. It did not seem reasonable that these counts could be coming from any elements (N, C, O) known to have been deposited on this target in the mass separator (Ahnlund, 1957). The $O^{18}(p,\alpha)N^{15}$ reaction was investigated for this target in the manner discussed in Section IV-A and the O^{18} concentration was found to be much too low to explain the background. Surface contamination with F^{19} was another possibility; although the bombarding energies used for the iron oxide data were carefully chosen to avoid the known $F^{19}(p,\alpha\gamma)O^{16}$ resonances. A target profile was taken at a bombarding energy of 877 kev and the alpha-particle peak from the F^{19} contamination was observed; however, the continuum background was also observed at fluxmeter settings where no alpha particles from F^{19} should be counted. It was finally decided that perhaps there was some contaminant in the stainless steel backing (presumably made in Sweden) that was not present in the stainless steel which was being used to check for scattered proton background. The back of the target blank was faced off on a lathe, then polished and cleaned. It was then exposed to the proton beam and a profile was taken. The results, shown in Fig. 7, indicate that the observed continuum was being produced in the body of the stainless steel backing. All background data for this target were then taken by bombarding the back

surface of the target. The target holder was arranged so that the front and back of the target could be bombarded alternately simply by rotating the target through 180°. In this way the same target spot was always brought back into the beam. The background points taken in this way are also indicated on Figs. 5 and 6. No attempt was made to determine the actual reaction causing this background.

The 10-channel analyzer was also used in taking the target profiles of the iron oxide target. Figures 8 and 9 are examples of pulse height spectra taken at energies where the alpha-particle yield was relatively low.

In addition to the three integrating capacitors discussed in Section IV-A two other capacitor combinations were made use of in taking the iron oxide data. The capacitance of these was determined in the same manner as before.

V. ANALYSIS OF EXPERIMENTAL DATA

A. Conversion of Data to Cross Section vs Energy

1. The Energy Relation

If one neglects scattering and straggling effects then the following description of the events leading to the production of particles which pass through the spectrometer is valid. A particle passing through the electrostatic analyzer with energy E_e is incident on the target with energy E_{1B}, the bombarding energy. It moves into the target, losing energy as it goes, until its energy is E_1, the reaction energy. The particle then initiates a nuclear reaction producing the particle to be observed with an energy E_2. This particle then emerges from the target with energy E_{20} and proceeds into the spectrometer with energy E_m. For the $O^{17}(p,\alpha)N^{14}$ reaction in the present experiment we have

$$E_{1B} = E_e - Z_1 e V_t = E_e - 0.3 \text{ kev} \tag{11}$$

$$E_{20} = E_m - Z_2 e V_t = E_m - 0.6 \text{ kev} \tag{12}$$

where V_t is the target potential above ground.

For the case where the target normal bisects the angle between the incoming particle direction and the outgoing particle direction the following formula may be derived* (Brown, 1951)

$$E_1 = \frac{\frac{\epsilon_2}{\epsilon_1} E_{1B} + E_{20} + E_{1B} \frac{\partial E_2}{\partial E_1} - E_{2B}}{\frac{\epsilon_2}{\epsilon_1} + \frac{\partial E_2}{\partial E_1}} \tag{13}$$

*The work of Bardin (1961) yields a formula which differs somewhat from Eq. (13). Near the target surface, however, they are essentially the same and so Eq. (13) will be used here.

In this formula $\partial E_2/\partial E_1$ and E_{2B} may be found from kinematics, E_{2B} being the energy of the outgoing particle when the incoming particle had reaction energy E_{1B}. The quantities ϵ_1 and ϵ_2 are the stopping cross sections in the target material for the incoming and outgoing particles respectively. In the present analysis ϵ_1 was evaluated at the energy E_{1B} and ϵ_2 was evaluated at the energy E_{20}. Equation (10) was used to determine the stopping cross section in nickel oxide for both the protons and alpha particles. Data on stopping cross sections of alpha particles is sparse and Whaling's (1958) compilation gives only proton values for nickel and oxygen. The alpha-particle stopping cross section $\epsilon_2(E_\alpha)$ at energy E_α was computed from the proton stopping cross section $\epsilon_1(E_p)$ at energy E_p by use of the following relation:

$$\epsilon_2(E_\alpha) = a\,\epsilon_1(E_p = E_\alpha/3.97) \qquad (14)$$

Here a is a factor that ranged from 3.7 to 4.0 in the present experiment and is tabulated by Whaling (1958) as a function of alpha-particle energy.

For the nickel oxide targets the procedure to obtain the reaction energy E_1 was as follows. From the electrostatic analyzer setting Eqs. (1) and (11) may be used to obtain E_{1B}. From the magnetic spectrometer setting Eqs. (2) and (12) may be used to obtain E_{20}. Equation (13) is then used to calculate E_1. It is this energy that is shown in Fig. 11 and that has been converted to the center of mass (c.m.) energy shown in Fig. 22. The penetration depth into the target before reaction is $E_{1B} - E_1$ and ranged from about 4 to 10 kev in the nickel oxide target data. This depth was always such

that the entire lamina ξ_1 observed by the spectrometer was inside the oxided region of the target. The reaction lamina thickness to the protons in energy units is given by

$$\xi_1 = \frac{2E_m}{R(\epsilon_2/\epsilon_1 + \partial E_2/\partial E_1)} \tag{15}$$

where $R = p/\Delta p$ is the resolution in momentum of the spectrometer (Brown, 1951). In the present work ξ_1 was in the range of 3 to 4 kev.

It will be recalled that for the iron oxide target no shifting of the target during a run was possible; therefore the determination of a reaction energy was complicated somewhat by the carbon contamination on the target surface at the beginning of a run and by the continuing build up of carbon during the run. The mean reaction energy for this case was computed as follows. Let primed symbols refer to those quantities to be evaluated at the reference bombarding energy of 1.280 Mev, and let unprimed symbols denote quantities to be evaluated at the other energies. The proton energy E'_{1M} corresponding to the midpoint on the front edge of the target profile at the beginning of the run and the target thickness ξ'_t in energy units may be found from the reference profile by use of Eq. (13). The initial carbon thickness ξ'_C is then

$$\xi'_C = E'_{1B} - E'_{1M} \tag{16}$$

After the run the midpoint has shifted to a new value $E'_{1M} + \Delta E'_{1M}$ where the energy shift $\Delta E'_{1M}$ is given by

$$\Delta E'_{1M} = E'_{1M}\,(\text{final}) - E'_{1M}\,(\text{initial}) \tag{17}$$

These quantities may be converted to other energies by the relations

$$\xi_C = \frac{\epsilon_C}{\epsilon'_C}\,\xi'_C \qquad \Delta E_{1M} = \frac{\epsilon_C}{\epsilon'_C}\,\Delta E'_{1M} \qquad \xi_t = \frac{\epsilon_{NiO}}{\epsilon'_{NiO}}\,\xi'_t \tag{18}$$

where ϵ_C stands for the proton stopping cross section in carbon, and the stopping cross section for nickel oxide has been used in the oxide region. This was done because the exact target composition is not known. Only a small error will be introduced since it is only the ratio of the stopping cross sections at different energies that is involved.

After Eq. (18) was applied the reaction energy E_1 was calculated by using

$$E_1 = E_{1B} - (\xi_C + \tfrac{1}{2}\Delta E_{1M} + \tfrac{1}{2}\xi_t) \tag{19}$$

2. Charge Exchange in the Target

The magnetic spectrometer was set to count the doubly charged alpha particles emerging from the target. Before emerging from the target surface the alpha particles produced by a reaction in the target undergo a sufficient number of collisions to reach charge equilibrium. In Allison's (1958) notation the equilibrium fraction of He^{++}, He^{+}, and He are denoted by $F_{2\infty}$, $F_{1\infty}$, and $F_{0\infty}$ respectively. The values for these ratios are taken from Allison (1958) and are shown in Fig. 10. The alpha-particle energies in this experiment are in the range 1 to 2 Mev. To obtain the true number of alpha particles produced in the reaction the number that pass through the spectrometer must be divided by $F_{2\infty}$.

3. Thick Target Formula

a. General discussion. The laboratory yield Y_L will be defined here as the number of reactions (or scatterings) produced per incident particle per steradian which, in the absence of charge exchange in the target, would be detected in a given experimental arrangement. If angle effects are neglected the yield may be related to the laboratory cross section σ_L per unit solid angle through

$$Y_L = \int \frac{\sigma_L}{\epsilon_1} f(E)\, dE \tag{20}$$

where ϵ_1 is the stopping cross section per target nucleus for the incident particle, and f(E) is an instrumental resolution function. Target nucleus means that nuclear type which is producing the reaction or scattering under observation. The thick target assumption is that f(E) for the spectrometer cuts the integral off before any depletion in target atoms ($\epsilon_1 \rightarrow \infty$) does. f(E) is taken to be rectangular with length ξ_1 as given by Eq. (15). On the assumption that the cross section is constant over the range of the spectrometer lamina ξ_1 we find

$$\sigma_L(\theta_L) = \frac{\epsilon_1 R Y_L}{2E_m} (\epsilon_2/\epsilon_1 + \partial E_2/\partial E_1) \tag{21}$$

where σ_L has been written $\sigma_L(\theta_L)$ to emphasize that it is the cross section per unit solid angle. The yield is measured by bombarding the target at energy E_{1B} with the spectrometer set at E_m until a charge Q has been deposited on the target and N_0 reactions have been observed. The yield is then given by

$$Y_L = \frac{Ne}{\Omega Q} \tag{22}$$

where e is the electron charge, Ω is the spectrometer solid angle and N, the true number of reactions produced is related to N_0, the observed number, by means of a charge exchange correction. The energy corresponding to the cross section given by Eq. (21) is the reaction energy E_1, Eq. (13).

b. Measurement of spectrometer solid angle. It is seen from Eqs. (21) and (22) that the ratio Ω/R for the spectrometer must be known in order to obtain the cross section. This ratio was measured by observing the Rutherford scattering of protons on a thick, evaporated Cu target. The cross section can be calculated from the Rutherford formula and the number of counts N_0 at the peak of the target profile then yields the ratio Ω/R. Several sets of data were obtained at $E_{1B} = 1.005$ and 1.609 Mev and no correction for charge exchange was made. The result is

$$\Omega/R = (4.03 \pm 0.14) \times 10^{-5} \text{ steradians}$$

From the slope of the front edge of the target profile R was found to be given by

$$R = 107.3 \pm 1.5$$

yielding

$$\Omega = 4.31 \pm 0.17 \text{ millisteradian}$$

This is about 30 % lower than the value given by Snyder et al. (1950) due to the fact that baffles have been inserted into the spectrometer since their paper was published.

c. Application to nickel oxide target data. For the nickel oxide data the charge exchange correction gives $N = N_0/F_{2\infty}$ and $\epsilon_1 = \epsilon_{NiO}/0.0397$ gives the stopping cross section per O^{17} atom. Equations (21) and (22) may then be used to obtain the cross section σ_L vs the reaction energy E_1. In Fig. 11 is shown the results of analyzing the data in this manner. No corrections have been made for instrumental resolution. The width of the narrow resonances below 1.2 Mev is almost entirely due to instrumental resolution and energy straggling (see Section V-C4 below) and thus the ordinate is really not the true cross section for these resonances. The actual cross section is much narrower and rises to a higher maximum value. Figures 12 to 18 show the data from the seven narrowest resonances plotted as alpha-particle yield vs proton bombarding energy at the target surface. The dashed curves on these figures are calculated curves taking into account straggling and the spectrometer resolution. They will be discussed in Section V-C4 below.

4. Thin Target Formula

a. General discussion. In deriving the thin target formula one assumes that the entire target contributes to the yield. f(E) is set equal to one and the cross section is assumed not to vary over the target thickness. Thus from Eq. (20) we have

$$Y_L = \sigma_L \int \frac{dE}{\epsilon_1} = nt\, \sigma_L \qquad (23)$$

where nt is the number of target atoms per cm^2 as seen by the incoming particle beam. Y_L is now the yield from the entire target and Eq. (22) is not valid in this case. To obtain the yield from the

entire target with a magnetic spectrometer a complete target profile N_0 vs V_m must be taken. The yield is then given by

$$Y_L = \frac{eR}{\Omega Q} \int \frac{N}{V_m} dV_m = \frac{eR}{\Omega Q} \int \frac{N_0}{V_m F_{2\infty}} dV_m \qquad (24)$$

Provided that nt is known the cross section may be found from Eqs. (23) and (24).

b. Application to iron oxide target data. From Eqs. (23) and (24) we see that the ratio of the cross section σ_1 at an energy E_1 to the cross section σ_2 at an energy E_2 may be written

$$\frac{\sigma_1}{\sigma_2} = \left[\frac{\int \frac{N_0}{V_m F_{2\infty}} dV_m}{Q} \right]_{E_1} \left[\frac{Q}{\int \frac{N_0}{V_m F_{2\infty}} dV_m} \right]_{E_2} \qquad (25)$$

as long as the same target spot is bombarded so that nt is the same at both energies. By using Eq. (25) the cross section at any energy may be measured in terms of the reference at $E_{1B} = 1.280$ Mev. All the cross sections are then normalized by normalizing the reference to the absolute measurements made with the nickel oxide data.

In order to evaluate the integral appearing in Eq. (25) the quantity $N_0/V_m F_{2\infty}$ was plotted vs V_m and a planimeter was used to find the area under the curve. Such a plot is shown in Fig. 19--this being derived from the data shown in Fig. 5. When significant carbon build up was observed the V_m-value was corrected before the N/V_m spectrum was plotted. If, at the end of a run, a total shift ΔV_m was observed (see Section IV-B) then, before plotting, each V_m-value was shifted an amount $f\Delta V_m$ where f is the ratio of the

charge deposited up to and including the setting V_m to the total charge deposited during the entire profile. This amounts to assuming that the carbon thickness is directly proportional to the amount of charge deposited on the target. This procedure is valid as long as the cross section does not vary rapidly with energy in the region where the profile is taken. In the two cases (see Section IV-B) where more than one reference profile was taken a correction for relative shifts of these reference profiles was also applied. In Fig. 20 is shown the 854-kev data after such corrections are applied. The uncorrected data for this figure is shown in Fig. 6.

Cross section values measured with the iron oxide target are shown, along with nickel oxide values, in Figs. 11 and 22. In order to more clearly display the lowest cross section values which were measured a semi-log presentation of the data between 660 and 1100 kev is given in Fig. 21. In this figure the positions of the narrow resonances are indicated by vertical lines.

B. Error Analysis

The statistical error for all the data below $E_1 = 1.450$ Mev is clearly indicated in Figs. 22, 21, and 12 through 18. Above 1.450 Mev the statistical error was about 6%. Table I shows the errors in the quantities needed to obtain the error in the absolute cross section (error shall mean the rms deviation). Compounding the errors in the quantities used to obtain σ_L results in an error of 10% to be compounded with the statistical error to yield the error in the absolute cross section. The bulk of this error is seen to arise from the uncertainty in the alpha-particle stopping cross section ϵ_2. The following discussion relates in more detail how one

arrives at the errors quoted in Table I.

$F_{2\infty}$: No errors in this quantity are quoted by Allison (1958); however, the bulk of the data is taken from Dissanaike (1953). He quotes an error of 2% in He^{++}/He^{+}. In the range of alpha-particle energies dealt with in this experiment this leads to a 2.6% error in $F_{2\infty}$.

O^{17} concentration: The manufacturer of the enriched gas gave no error in this quantity. One percent is a reasonable guess since the concentration was quoted to three figures and this would give an error of a few in the last figure.

Q: The error here is composed of the error in the capacitor measurements and the error in the measurement of the mercury batteries. These errors are small and lead to a 0.4% error in Q.

Ω/R: The main contributions to this error are from the Cu stopping cross section (4%) and in the value of the integrating capacitor (2%). A small capacitor was used here having $C = 0.319 \pm 0.007$ μf. This gives a 3.6% error in Ω/R.

Kinematics: The kinematic relations are based on the general principles of conservation of momentum and energy and are assumed to hold exactly.

E_m: The 0.2% error in this quantity comes from the error in the spectrometer constant k_m and an assumed 1 part in 1000 long-term stability (Milne, 1953).

ϵ(p in NiO): In assuming a 4% error in the values for ϵ_{Ni} and ϵ_O as read from Whaling's (1958) graphs one obtains the quoted 3.0% error. No error was assigned to the assumption $\mu = 1$ [see Eq. (4)].

ϵ (α in NiO): In Whaling's compilation (1958) in which he tabulates the quantity $\underline{a}$ defined in Eq. (14) he assigns a 20% error to this quantity. It is felt however that in the range where $\underline{a}$ is near 4 this is an overestimate and that something of the order of 10% would not be unreasonable. Thus a 10% error was assumed in the values used for the stopping cross section of alpha particles in nickel oxide.

$\epsilon_1(\partial E_2/\partial E_1) + \epsilon_2$: This quantity is quoted in Table I since it is this combination of stopping cross sections which appears in the cross section formula. Using the above adopted errors for the stopping cross sections it was found that the error in $\epsilon_1(\partial E_2/\partial E_1)+\epsilon_2$ was very close to 9% over the range of energies employed in this experiment.

Compounding these errors then gives a 10% error in the scale of absolute cross sections. Since the iron oxide data was normalized to the nickel oxide data this 10% factor holds for data taken with both targets.

We now discuss the errors to be assigned to the energy scale. The relation between the reaction energy and the bombarding energy may be written

$$E_1 = E_{1B} - E_c \tag{26}$$

where the correction term E_c is given either by

$$E_c = \frac{\epsilon_1(E_{2B}-E_{20})}{\epsilon_2 + \epsilon_1 \dfrac{\partial E_2}{\partial E_1}} \qquad \text{nickel oxide} \tag{27}$$

or by

$$E_c = \xi_C + \frac{1}{2}\Delta E_{1M} + \frac{1}{2}\xi_t \qquad \text{iron oxide} \tag{28}$$

For the nickel oxide target data E_c was in the range of 4 to 10 kev with a percentage error of about 12%. An error of 0.2% is assigned to E_{1B} due to the error in calibrating the electrostatic analyzer and to account for long-term drifts in the equipment. No detailed investigation of long-term drifts was undertaken; however the consistency of the $O^{17}(p,\alpha)N^{14}$ and Cu(p,p)Cu data over a long period testifies to the smallness of this effect. These errors then result in an uncertainty of about 0.25% in E_1. Since this is of the same order as the electrostatic analyzer resolution it is felt that an increase of the assigned error to 1/3% is reasonable.

For the iron oxide target data E_c was in the range of 10 to 20 kev with an error of about 9%. This again leads to an error of 1/3% in E_1.

In summary we have

Reaction energies accurate to 0.33%

Absolute cross section scale accurate to 10%

C. Extraction of Nuclear Parameters

1. Barrier Factors

The ratio of the partial width $\Gamma_{\lambda c}$ for break up of a compound state into channel c via level λ to the corresponding dimensionless reduced width $\theta^2_{\lambda c}$ will be called the barrier factor*. The nuclear effects are reflected in the quantity $\theta^2_{\lambda c}$; the barrier factor takes

*This barrier factor is not the same as the various penetration and transmission factors used in the current literature.

into account the Coulomb and centrifugal barrier and may be calculated. The barrier factors for the $O^{17}(p,\alpha)N^{14}$ reaction have been calculated for several values of relative orbital angular momentum near the observed resonance energies and also at several very low energies. The calculations are described in Appendix A and the results are given in Tables II and III. Several of these barrier factors will be needed in the analysis to follow.

2. Angular Distribution Factors

No angular distributions were measured in this experiment. All of the data were taken at a laboratory angle of 150° (θ = c.m. angle = 152°). It is of interest therefore to obtain some idea of the error that might be involved in computing the integrated cross section simply by multiplying the cross section per unit solid angle at $\theta = 152^{\circ}$ by 4π. An appropriate factor β which will measure the error in this assumption is

$$\beta = \frac{4\pi\sigma(152^{\circ})}{\int \sigma(\theta)\, d\Omega} \tag{29}$$

and β will be unity when no error is made. In fact to obtain the integrated cross section one should multiply the measured differential cross section by $4\pi/\beta$. The ground state spin and parity of O^{17} is $5/2^{+}$ and that of N^{14} is 1^{+} (Ajzenberg-Selove, 1959). Thus in terms of angular momentum we may write

$$\frac{5}{2}^{+} + \frac{1}{2}^{+} \xrightarrow{\ell} J^{\pi} \xrightarrow{\ell'} 1^{+} + 0^{+}$$

where ℓ is the relative orbital angular momentum in the $O^{17} + p$ system, ℓ' is the relative orbital angular momentum in the $N^{14} + \alpha$

system, and J^{π} is the total angular momentum and parity of the state in the compound nucleus F^{18} formed in the reaction. The incoming channel spin s can be either 3^+ or 2^+ and the outgoing channel spin s' is 1^+. In general the factor β depends on the channel spin mixture assumed in the incoming channel. Limits can be put on β, however, and these limits are given in Table IV. The quantity β_2 corresponds to pure s = 2 and β_3 corresponds to pure s = 3. The actual β must lie somewhere between these two values. Calculations were not made for some of the higher ℓ, ℓ' values for a given J^{π}. Note that a 0^+ level is completely forbidden to decay into $N^{14} + \alpha$. The calculation of β is discussed in Appendix B.

The results in Table IV indicate that in a few cases an error by as much as a factor of 2 would result from the assumption that $\beta = 1$. Thus if the spin and parity of a level are not known one would expect a maximum error of about a factor of 2 in assuming $\beta = 1$ but could reasonably expect this error to be less.

3. Broad Resonance Analysis

The data in the region $E_1 = 1.0$ to 1.5 Mev (Fig. 11) have been converted to c.m. quantities in the $O^{17} + p$ system. The results are plotted in Fig. 22. Here we describe how the resonance energies and widths of the high-yield broad resonance near E = 1200 kev and of the low-yield broad resonance near E = 1040 kev were determined. In this section the effects of the narrower anomalies at c.m. energies of 1040, 1177, and 1260 kev are neglected. The spin and parities of these broad levels are known to be 2^- and 1^- for the high-energy and low-energy levels respectively and both

are known to decay by p-wave alpha particles (Ajzenberg-Selove, 1959). It will be assumed in what follows that the protons also are p-wave. Since the levels do not have the same spin and parity the cross section integrated over solid angle would show no interference between the two levels. The cross section at a given angle however (this is all that was measured in the present experiment) will in general be expected to show interference effects, even between levels of different spin and parity (Lane, 1958). The correct general expression (which would include unknown phases) will not be used here. Instead it will be assumed that a simple sum of two single level contributions will suffice to determine the resonance energies and total widths to reasonable accuracy*. The energy variation of the level shift will also be neglected. The equation used to fit the two levels under discussion was thus taken to be

$$\sigma_{p\alpha}(152^{\circ})=\pi\lambda^{2}\left[\frac{\beta_1}{4\pi}\,g_1\,\frac{\Gamma_{\alpha 1}\,\Gamma_{p1}}{(E-E_{r1})^{2}+\frac{1}{4}(\Gamma_{\alpha 1}+\Gamma_{p1})^{2}}+\text{same term with } 1\rightarrow 2\right] \tag{30}$$

where 1 refers to the high-energy resonance and 2 refers to the low-energy resonance. Here g is the usual statistical weight, $g_1 = 5/12$ and $g_2 = 1/4$; λ is the reduced de Broglie wavelength; β has been defined in Eq. (29); E_r is the resonance energy; and the Γ's are the appropriate partial widths. The factors $\beta/4\pi$ were included in an

*It is to be expected that such a procedure will give good accuracy for the high-yield resonance parameters and relatively poorer accuracy for the low-yield resonance parameters. No estimate of the effect of neglecting the interference was made however.

attempt to obtain a reasonable normalization. The actual value of β which is chosen will strongly affect the values of the individual partial widths which are assumed but will have very little effect on the total widths or resonant energies. The values chosen were $\beta_1 = 1.00$ and $\beta_2 = 0.933$. The value for β_1 based on the observed isotropy in the $N^{14}(\alpha,p)O^{17}$ reaction for this level in F^{18} (Kashy, 1958), and the value of β_2 is that calculated for a pure $J^\pi = 1^-$, $\ell = \ell' = 1$ level (see Table IV and Appendix B). In using Eq. (30) the energy variation of the barrier factors Γ/θ^2 was included. Several values for these factors in the desired energy range are given in the column labeled $\ell = 1$ in Tables II and III. Polynomials of the form

$$\frac{\Gamma_p}{\theta_p^2} = \sum_{n=0}^{4} a_n E^n$$
$$\frac{\Gamma_\alpha}{\theta_\alpha^2} = \sum_{n=0}^{4} b_n E^n \qquad (31)$$

were fitted to these points. Figure 23 shows both the points taken from Tables II and III and curves calculated from Eq. (31). The coefficients appearing in Eq. (31) are listed in Table V, both Γ and E being measured in kev. Equation (31) was then used to obtain the barrier factors to be used in Eq. (30). The dimensionless reduced widths θ^2 and the resonance energies E_r were then varied and a "best fit" was determined by inspection of a graph on which both the experimental points and the cross section as calculated from Eq. (30) had been plotted. This "best fit" is shown as a dashed

curve in Fig. 22. The resonance energies and widths were found to be

$$E_{r1} = 1203 \pm 2 \text{ kev} \qquad E_{r2} = 1035 \pm 5 \text{ kev}$$

$$\Gamma_1 = 79 \pm 5 \text{ kev} \qquad \Gamma_2 = 85 \pm 5 \text{ kev}$$

where the errors are estimated from the analysis and do not include the errors in the energy scale as discussed in Section V-B. The energy scale errors are, however, included in Table VII, which gives a summary of all the level parameters as determined in this experiment.

The partial widths are not uniquely determined from the data. Even if one assumes that Eq. (30) holds exactly there is still an ambiguity as to whether or not it is the proton width or the alpha-particle width which is the largest. Table VI gives the partial widths which are consistent with Eq. (30) and the data. Group I are the values used to calculate the curve on Fig. 22. Group II could also have been used, however, as could a combination of I_a with II_b or I_b with II_a. This would result in only slight changes in the calculated cross section.

No analysis was performed on the resonance at E = 1260 kev. The other two narrow levels appearing on Fig. 22 are discussed in the next section.

4. Narrow Resonance Analysis

In Figs. 12 to 18 the alpha-particle yield from the narrow resonances is plotted vs proton bombarding energy. Most of these graphs have a full width at half maximum of about 5 kev. It is the purpose

of this section to determine the source of this width and to extract from the data as much information as possible about the level parameters for these resonances. Three sources of experimental width will be considered: magnetic spectrometer energy resolution, energy variation with angle, and energy straggling.

The thickness in energy units of the target lamina to the incoming protons due to spectrometer resolution is about 3.5 kev as calculated from Eq. (15). (The actual thickness at each resonance is listed as ξ_1 in Table IX.) It is clear then that additional contributions to the observed energy width are present.

Since the full spectrometer solid angle was used in the experiment it was decided to investigate the question of the energy spread introduced due to energy variations with reaction angle. The mean reaction angle was $\theta_{Lab} = 150^{o}$, however the actual reaction angle can vary somewhat about this mean due to the finite spectrometer acceptance angle. The formula for the energy width in a yield curve produced by a zero width resonance and observed by a spectrometer with infinite energy resolution but with an angular acceptance angle $\delta\theta$ has been calculated in Appendix C. The work of Bardin (1961) may also be used to derive the result. The resulting energy spread for the situation in this experiment is given in Table IX under the column labeled Δ_θ. These are all small--of the order of 1 kev--and would be expected to have only a small effect on the observed width. In fact if two rectangular distributions of widths 3.5 kev and 1.0 kev are folded together the result still has a full width at half maximum of 3.5 kev. It is quite reasonable to assume rectangular distributions for the spectrometer energy and angular resolution.

Finally we consider the effect of energy straggling on the observed yield width. Both the incoming protons and outgoing alpha particles will suffer from this. In Appendix D a formula is derived for the laboratory alpha-particle yield Y_L (E_{1B}) as a function of the proton bombarding energy E_{1B} for the case of a very narrow (δ-function) resonance in the cross section. In this formula the spectrometer energy resolution and particle straggling are taken into account [see Eq. (D.11)]. Angular effects are neglected. The Burroughs 220 computer was programmed to perform the necessary integral--the parameters used at each resonance are given in Table VIII. The resonance energies used in the calculation which were found to give the correct position of the peak of the yield were the same as those given by Eq. (13) to within a few tenths of a kev. The results of these calculations are shown as dashed curves in Figs. 12 to 18. It appears that in most cases the calculated energy spread is enough to account for the observed width. This would then imply a rather small width for the resonance involved. For the 1247-kev (Lab) resonance (Fig. 18), however, there is a definite contribution to the observed width from the natural width of the resonance and for the 747-kev (Lab) resonance (Fig. 14) there seems to be a much smaller, but observable, contribution.

One can notice a discrepancy between the calculated curves and the experimental data which occurs in the wings of the yield curves. In particular the high-energy experimental points lie higher than the calculated curve. This is due to the fact that Gaussian distributions were used for the straggling functions and can be explained

qualitatively in the following way. The actual straggling function is not Gaussian but has a higher low-energy tail than a Gaussian. Thus, at a high bombarding energy, more protons than calculated will slow down to the resonance energy by the time they reach the target lamina in which the main contribution to the spectrometer yield is produced. This would make the high-energy counts greater than those calculated--as observed. A quantitative explanation would require use of the correct straggling functions (Rossi, 1952).

It is quite easy to obtain the resonance energies from the data but very difficult to extract the widths with any degree of accuracy. The area under the yield curves, however, can be measured accurately and this area can be related to the resonance parameters. It is shown in Appendix D that for a δ-function cross section and Gaussian straggling functions the area under the yield curve is related to the area under the true cross section by the same formula one obtains if straggling is left out and a nonzero value is assumed for the natural width, Γ. It seems reasonable to assume that if the proper straggling functions are used and the cross section is allowed to have a small width then the same conclusion would hold. We then may write [see Appendix D Eqs. (D.21), (D.26)]

$$\int \frac{4\pi}{\beta} Y_L(E_{1B})\, dE_{1B} = \frac{2E_m(\max)}{R\epsilon_{1r}(\epsilon_{2r}/\epsilon_{1r} + \alpha)} (\pi\sigma_r \Gamma/2)_L \frac{n}{n_s} \qquad (32)$$

where $E_m(\max)$ is the spectrometer energy setting at the maximum of the yield curve, β is defined in Eq. (29), Y_L is the yield in alpha particles per proton-steradian as shown in Figs. 12 to 18, and $\alpha = \partial E_m / \partial E_{1B}$. The subscript r on the stopping cross sections denotes that they are to be evaluated at the resonance energy and the quantity

$(\sigma_r \Gamma \pi/2)_L$ is defined in Appendix D and is simply the total area under a single, narrow resonance in the laboratory system of coordinates. We may then calculate the quantity $\beta g \Gamma_\alpha \Gamma_p / \Gamma$ in the c.m. system by means of the following formula

$$\beta g \frac{\Gamma_\alpha \Gamma_p}{\Gamma} = \left(\frac{\Omega_L}{\Omega_{CM}}\right) \frac{2MM_0 E_r \epsilon_{1r} R(\epsilon_{2r}/\epsilon_{1r} + \alpha)}{\hbar^2 (M_1 + M_0) E_m(\max)} \int Y_L \, dE_{1B} \frac{n_s}{n} \tag{33}$$

with the statistical factor g given by

$$g = \frac{2J + 1}{12} \tag{34}$$

where J is the spin of the appropriate state in F^{18}, E_r is the resonance energy in the c.m. system, and Ω_L/Ω_{CM} is the solid angle ratio as computed from kinematics. This ratio varies from resonance to resonance but is assumed not to vary over a single narrow resonance. M is the reduced mass in the O^{17} + p channel, and M_1 and M_0 are the proton and O^{17} mass respectively.

The results obtained from applying Eq. (33) to the several narrow resonances are given in Table VII. The integral involved in Eq. (33) was evaluated with a planimeter. In Figs. 17 and 18 the dotted curves were used as the base line in evaluating the integrals.

In Table VII are also quoted estimates of the total widths. These were obtained by assuming that the spectrometer-straggling width, the small width due to the angular aperture of the spectrometer, and the resonance width combine as the square root of the sums of the squares to yield the measured width. The measured width was read from the graphs, and the spectrometer-straggling width was read from the dashed curves.

In between the narrow isolated resonances where the cross section was quite low the data allow an upper limit to be placed on the quantity $\beta g \Gamma_\alpha \Gamma_p/\Gamma$ for any unobserved narrow resonances.

$$\beta g \frac{\Gamma_\alpha \Gamma_p}{\Gamma} < 8 \text{ ev} \qquad \text{unobserved narrow resonances}$$

In fact below 1280 kev (Lab) the data were taken at small enough energy intervals so that this upper limit on unobserved narrow resonances is applicable from 490 to 1280 kev. Above 1280 kev the data were taken in larger energy steps so it is possible that in the range from 1280 to 1580 kev some narrow resonances with $\beta g \Gamma_\alpha \Gamma_p/\Gamma$ exceeding the above limit are present. It should be emphasized that even though actual cross section measurements are not shown in Fig. 11 in the region of very low cross sections, data were taken in these regions (for example, the off-resonance data shown in Fig. 4) which give the upper limit of 8 ev quoted above.

D. Discussion of Experimental Results

In the subsequent discussion all quoted excitation energies in F^{18} are based on the following mass differences (Everling, 1960)

$$O^{17} + H^1 - F^{18} = 5.597 \text{ Mev}$$

$$N^{14} + He^4 - F^{18} = 4.404 \text{ Mev}$$

All the levels observed in the present work have been previously reported except possibly the 747-kev level (E_{ex} = 6302 kev) (Ajzenberg-Selove, 1959). Hinds and Middleton (1959) in a study of $F^{19}(He^3, \alpha)F^{18}$ report a level at 6264 kev excitation. This could

possibly be the present 747-kev level since in their data the alpha-particle group for this level is not completely resolved from the group (about three times stronger) leading to the 6.232 level in F^{18}.

The upper limits found here for the widths of the narrow levels (Table VII) are all consistent with previously reported limits. Width limits for the levels at E_{ex} = 6376 and 6472 kev have not previously been reported. Also, the width of the level at E_{ex} = 6774 kev had not previously been measured.

There have been several discrepancies in the literature on the reported widths of the broad levels at E_{ex} = 6632 and 6800 kev (Fig. 22). The results of these previous measurements along with those of the present work are given in Table XI. Several of these discrepancies may easily be explained. It is clear from the papers of Ahnlund (1957), and Heydenburg and Temmer (1953) that their quoted widths for the 6800-kev level include the contribution from the higher energy 6857-kev level. It is fairly certain that this is also the case for the value quoted by Herring (1958b). In the work of Kashy et al. (1958) it is not clear whether or not their quoted value for the width of the 6800-kev level includes this extra contribution. They do not report a level at E_{ex} = 6857 kev. In any case their value for this width is in agreement with the present work. If the 6857-kev level contribution were added to the value obtained in the present work then a value of about 100 kev would be obtained (Fig. 22) in agreement with Heydenburg and Temmer (1953) and with Herring (1958b). The situation for

the 6632-kev level is somewhat puzzling. The value of 27 kev (Heydenburg, 1953) may be discarded since it is clear that the narrow level at E_{ex} = 6637 kev strongly influenced the data from which this width was derived. The present work agrees with the work of Herring (1958b) and not with Kashy et al. (1958). This seems odd since the situation was simply reversed for the 6800-kev level. No completely satisfactory explanation has been found for this situation. Kashy et al. carried out a detailed analysis, but only quote the resulting parameters; whereas Herring shows the fit which he obtained for the two broad resonances in question. Kashy et al. do not report the narrow level at E_{ex} = 6637 kev whereas Herring does--this suggests that this level may possibly have influenced the results of Kashy et al. It is felt safe to say that the present work is in agreement with that of Herring (1958b) provided that his width for the 6800-kev level is taken to include the contribution from the 6857-kev level.

In the region of excitation of F^{18} under investigation in the present experiment two levels have been reported in $N^{14}(\alpha, \alpha)N^{14}$ that were not seen in the present work. These are a level at E_{ex} = 6247 kev (Herring, 1958a, 1958b; Silverstein, 1960) and one at E_{ex} = 6556 kev (Herring, 1958a, 1958b). The 6247-kev level is known to be formed by s-wave alpha particles making $J^{\pi} = 1^{+}$. This would require d-wave or g-wave protons to form the state. Since Table II shows that Γ/θ^2 drops by a factor of 20 on going from p-wave to d-wave protons the absence of this level in the present experiment could perhaps be explained on

the basis of these angular momentum considerations. The 6556-kev level is thought to be formed through g-wave alpha particles giving $J^{\pi} = 3^+, 4^+,$ or 5^+ for the level. It is felt that the absence of this level in the present experiment is evidence for discarding the 3^+ possibility since a 3^+ level can be formed by s-wave protons whereas 4^+ and 5^+ levels require protons of d-wave or higher.

From the quantities $\beta g \Gamma_\alpha \Gamma_p / \Gamma$ listed in Table VII one can, if so desired, obtain a rough estimate of the minimum partial width involved at the level in question. Due to the fact that $\Gamma = \Gamma_\alpha + \Gamma_p$ (we neglect the radiative width) one can show that

$$\frac{\Gamma_\alpha \Gamma_p}{\Gamma} \leq \Gamma_{min} \leq 2 \frac{\Gamma_\alpha \Gamma_p}{\Gamma}$$

where Γ_{min} is the minimum of Γ_α, Γ_p. The equality on the left holds when one of the widths is much smaller than the other, i.e. when $\Gamma_{min} << \Gamma = \Gamma_{min} + \Gamma_{max}$. The equality on the right holds when the two widths are equal, i.e. when $\Gamma_{min} = \Gamma_{max} = \Gamma/2$. This then gives Γ_{min} to within a factor of 2 (assuming that β and g are known).

E. Summary of Experimental Results

To summarize we note that Fig. 11 shows the complete excitation curve for the $O^{17}(p,\alpha)N^{14}$ reaction as measured in the present work. Figures 21 and 22 show selected regions of this curve and Figs. 12 to 18 show the alpha-particle yield curves at the narrow resonances. Table VII summarizes the level parameters as determined from this investigation and Table VI lists

a consistent set of partial widths for the two broad resonances. Any unobserved narrow resonances below $E_1 = 1280$ kev have $\beta g \Gamma_\alpha \Gamma_p / \Gamma < 8$ ev.

VI. THE ASTROPHYSICAL PROBLEM

A. General Discussion

In a recent paper Fowler, Greenstein, and Hoyle (1961; referred to as FGH) propose that the relative abundance of several of the elements which were present in the original material from which the solar system condensed was modified by spallation processes and neutron interactions during the formation of the planets. Among their conclusions is that the O^{17} abundance was not modified appreciably by these processes and that therefore the ratio O^{17}/O^{16} present on the earth should be the same as for the primitive material. We use the symbols of the elements to stand for their relative abundances or the number of nuclei per cm^3, depending on the context. Following the notation of FGH we let β stand for the original production ratio of O^{16} relative to C^{12} in helium burning in red giant stars, and we let f represent the fraction of the C^{12} and O^{16} thus formed which has been processed to equilibrium in the CNO-cycle. If we add the O^{17} ratio to an equation given by FGH we find

$$C^{12}:N^{14}:O^{16}:O^{17} = [1 - f + 0.024f(1 + \beta)] : 0.95f(1+\beta) : [\beta(1 - f) + 0.02f(1 + \beta)] : \gamma f(1 + \beta) \qquad (36)$$

where the element symbols refer to the concentrations in the primitive material. This relation assumes that in the CNO-cycle the equilibrium abundance ratios are given by

$$C^{12}:N^{14}:O^{16}:O^{17} = 0.024 : 0.95 : 0.02 : \gamma \qquad (37)$$

The numbers in Eq. (37) come from assuming equilibrium in the CNO-cycle at a temperature of 35×10^6 °K. This rather high temperature comes from the assumption that the last CNO-cycle processing undergone by the O^{16} and C^{12} which were destined for the solar system took place in stars which were at a rather advanced stage of evolution. In these stars the hydrogen burning occurs in a thin high-temperature shell surrounding a helium core. We shall see below that the present calculation of the O^{17}/O^{16} ratio does not seem to agree with such a high temperature. FGH (1961) next assume that the present solar abundance ratio $C^{12}:N^{14}:O^{16} = 5.5 : 1 : 9.6$ represents the original ratio of these elements in the primitive material. This assumption, along with Eq. (36) then leads to the values

$$\beta = 1.75$$

$$f = 1/15$$

From Eq. (36) one then finds

$$\frac{O^{17}}{O^{16}} = \frac{\gamma f(1+\beta)}{\beta(1-f) + 0.02(1+\beta)f} = 0.11\gamma \qquad (38)$$

The observed terrestrial ratio is $O^{17}/O^{16} = 3.74 \times 10^{-4}$ (Nier, 1950) which leads to a value

$$\gamma = 3.4 \times 10^{-3}$$

The ratio at equilibrium in the CNO-cycle is then given by Eq. (37) to be

$$[O^{17}/O^{16}]_{CNO} = \gamma/0.02 = 0.17 \tag{39}$$

Here we assume that the only possible way of forming O^{17} is through the CNO-cycle. This is a rather high value for this ratio and would result from a rather low rate for the O^{17}-destroying reaction, $O^{17}(p,\alpha)N^{14}$.

In the remainder of this section we derive an expression for the low energy cross section for the $O^{17}(p,\alpha)N^{14}$ reaction and use this to calculate the ratio $[O^{17}/O^{16}]_{CNO}$ as a function of temperature. We then compare the results with the prediction of Eq. (39).

B. Cross Section Formula

The observation of the very narrow levels at low energy in the present experiment leads one to suppose that these levels will have very little effect at energies of interest in stellar reactions (around 30-kev c.m. energy in the O^{17} + p system or 5627-kev excitation in F^{18}). One is then interested only in the effect of F^{18} levels which occur near this stellar energy region. A look at the F^{18} level scheme (Ajzenberg-Selove, 1959) indicates that only two of the known levels might be of importance in determining the stellar cross section for $O^{17}(p,\alpha)N^{14}$. These two levels occur at E_{ex} = 5594 and 5662 kev (using the mass differences quoted in Section V-D).

The 5594-kev level has been investigated by means of the $N^{14}(\alpha,\gamma)F^{18}$ (Price, 1955; Phillips, 1958, Almqvist, 1958) and $N^{14}(\alpha,\alpha)N^{14}$ (Silverstein, 1960) reactions. All results point to

a spin and parity assignment of 1^- for this level. Silverstein (1960) reports that the alpha particles are p-wave and that the total width is about 200 ev.

The 5662-kev level has also been investigated by means of the $N^{14}(\alpha,\gamma)F^{18}$ (Price, 1955; Phillips, 1958) and $N^{14}(\alpha,\alpha)N^{14}$ (Silverstein, 1960) reactions. The evidence here also points to a 1^- assignment for the level. Silverstein (1960) again quotes a width of about 200 ev and assigns p-wave alpha particles to the level.

In order to calculate the $O^{17}(p,\alpha)N^{14}$ cross section at stellar energies we shall consider only the contribution of these two levels. Since they both have the same spin and parity the total cross section σ will exhibit interference between the two levels. We let 1 refer to the 5662-kev level and 2 refer to the 5594-kev level. The total cross section may then be written (Lane, 1958)

$$\sigma = \pi\lambda^2 g \left| \frac{(\Gamma_{p1}\Gamma_{\alpha 1})^{1/2}}{(E_{r1}-E) - i\Gamma_1/2} \pm \text{same term with } 1 \rightarrow 2 \right|^2 \qquad (40)$$

where the energy dependence of the level shift has been neglected and the approximation that the level widths Γ_1 and Γ_2 are much less than the level spacing $E_{r2} - E_{r1}$ has been made. This approximation is quite good in the present case. We have here defined $(\Gamma_p\Gamma_\alpha)^{1/2}$ to be positive and are allowing the $\pm$ in Eq. (40) to take care of the interference effects. For $J = 1$ we have $g = 1/4$.

For the O^{17} + p channel the energy E will be sufficiently low so that the approximation for the partial width given in Appendix A will be valid [see Eq. (A.15)]. The energy E + Q in the $N^{14} + \alpha$ channel is not low enough, however, to make use of this approximation. The p-wave barrier factors have been calculated in this

energy region and are given in Table III. A polynomial of the form

$$\frac{\Gamma_\alpha}{\theta_\alpha^2} = \sum_{n=0}^{2} c_n E^n \tag{41}$$

was fitted to these points. The calculated points, along with this fitted curve are shown in Fig. 25. The coefficients c_n are given in Table V.

It is convenient to define a quantity S(E), the cross section factor, by

$$S(E) = Ee^{2\pi\eta}\sigma(E) = E\sigma(E)\, e^{b\sqrt{E}} \tag{42}$$

with b given by Eq. (A.17). Combination of Eqs. (40), (A.15), and (42) then gives

$$S(E) = S_1(E) + S_2(E) \pm S_I(E) \tag{43}$$

with

$$S_1(E) = s(1 - \alpha_\ell E)\, \frac{\theta_{p1}^2 \Gamma_{\alpha 1}}{(E-E_{r1})^2 + \Gamma_1^2/4} \tag{44}$$

$S_2(E)$ is the same as $S_1(E)$ with 1 replaced by 2. The interference term $S_I(E)$ is given by

$$S_I(E) = s(1-\alpha_\ell E)\, \frac{2(\theta_{p1}^2 \theta_{p2}^2 \Gamma_{\alpha 1} \Gamma_{\alpha 2})^{1/2} [(E_{r1}-E)(E-E_{r2}) - \Gamma_1\Gamma_2/4]}{[(E-E_{r1})^2 + \Gamma_1^2/4][(E-E_{r2})^2 + \Gamma_2^2/4]} \tag{45}$$

In these equations s is given by

$$s = gEE_a(\pi\lambda)^2 \, K^2_{2\ell+1}(x) = g\pi^2\hbar^4/[\,2MaK_{2\ell+1}(x)]^2 \qquad (46)$$

The positive sign in Eq. (43) gives constructive interference between the levels and the minus sign gives destructive interference between the levels. From now on it will be assumed that only p-wave protons contribute to the reaction. We then find for the $O^{17}(p,\alpha)N^{14}$ reaction (see Appendix A)

$a = 5.000$ fermi $\qquad x = 3.24$

$K_3(x) = 0.0858 \qquad K_5(x) = 0.587$

$s = 6.543 \times 10^7$ kev^2-barns $\qquad \alpha_\ell = \alpha_1 = -2.095 \times 10^{-4}$ kev^{-1}

$b = 244.1$ kev$^{1/2}$

C. Choice of Reduced Widths

In order to obtain the cross section factor it is necessary to have an estimate of the dimensionless reduced widths θ_p^2 and θ_α^2 for the two levels in question. The total width of these levels is almost certainly due to the alpha-particle width and thus Γ_α is about 200 ev for the levels. On obtaining the barrier factor from Fig. 25 one finds that θ_α^2 would be about 0.10 for the upper level and about 0.18 for the lower level. We shall use*

$$\theta^2_{\alpha 1} = \theta^2_{\alpha 2} = 0.14$$

which gives $\Gamma_1 = 268$ ev and $\Gamma_2 = 154$ ev.

---

*For convenience in calculation, the reduced alpha-particle widths for the two levels are taken to be the same. The general shape of S(E) between the resonances is not strongly affected by such an assumption (refer to Fig. 26).

In order to obtain an estimate of θ_p^2 we shall assume that the two levels contributing to the stellar cross section have reduced widths similar to some of those found in the present experimental work on the $O^{17}(p,\alpha)N^{14}$ cross section. We shall now give rough estimates for the product $\theta_\alpha^2\theta_p^2$ on the basis of the present experimental work and other known properties of the appropriate F^{18} levels.

E_{ex} = 6086 kev: This state decays by f-wave alpha particles and Γ is about 200 ev (Silverstein, 1960). On the assumption of angular isotropy, $J^\pi = 3^-$, and p-wave protons, we find from Tables II, III, and VII that $\theta_p^2\theta_\alpha^2 = 1.9 \times 10^{-3}$.

E_{ex} = 6232 kev: This state decays by f-wave alpha particles and is known to have a total width less than 800 ev (Herring, 1958b; Phillips, 1958; Silverstein, 1960). If we assume angular isotropy, p-wave protons, and $J^\pi = 2^-$ we find, from Tables II, III, and VII, $\theta_p^2\theta_\alpha^2 < 1.06 \times 10^{-3}$. If we substitute the assumption $\theta_\alpha^2 = 0.14$ for the assumption $\Gamma < 800$ ev we find $\theta_p^2\theta_\alpha^2 = 0.74 \times 10^{-3}$.

E_{ex} = 6302 kev: An estimate is more difficult here. From Table VII we have $\beta g \Gamma_p \Gamma_\alpha = 0.465 \pm 0.210$ kev^2. If this state is similar to the previous two in that J = 3, and that f-wave alpha-particles and p-wave protons are involved, then setting $\beta = 1$ gives $\theta_p^2\theta_\alpha^2 = 4.3 \pm 1.9 \times 10^{-3}$.

The analysis of the remaining narrow levels would involve unjustified guessing as to the orbital angular momenta ℓ which were involved similar to that done in the case of the 6302-kev level. Thus this type of analysis will not be continued.

From Table VI we see that θ_α^2 for the two broad levels is not

very close to 0.14; therefore, we do not attempt to apply these reduced widths to the levels in the stellar energy region.

On the basis of the order-of-magnitude results from the preceding rough analysis the value

$$\theta_p^2 \theta_\alpha^2 = 1 \times 10^{-3}$$

will be assumed to apply to both of the levels in the stellar energy region. The cross section is proportional to this factor and any future revisions of this quantity will result in an appropriate scale correction to the present calculations.

The results of the S-factor calculations from Eqs. (43), (44), and (45) are shown in Fig. 26 for both the case of constructive and destructive interference between the resonances.

D. Calculation of Reaction Rates

Many authors (Burbidge, 1957, and references therein) have discussed the calculation of stellar reaction rates, so no detailed derivations will be given here. One assumes that the reacting nuclei are at equilibrium at absolute temperature T and possess a Maxwell-Boltzmann energy distribution. For charged particles one makes use of Eq. (42) and obtains

$$\frac{P}{XY} = \left[\frac{8}{M(kT)^3}\right]^{1/2} \int_0^\infty \Phi(E)\, dE \qquad (47)$$

where

$$\Phi(E) = S(E) \exp-(b/\sqrt{E} + E/kT) \qquad (48)$$

In these formulas X and Y represent the number of nuclei of type X and Y per cm^3, P is the reaction rate for X + Y in reactions per cm^3-sec, k is the Boltzmann constant, and M is the reduced mass of X and Y. For the $O^{17}(p,\alpha)N^{14}$ reaction we may write

$$\frac{P_{17}}{H^1 O^{17}} = \frac{2.008 \times 10^{-15}}{T_6^{3/2}} \int_0^\infty \Phi(E)\, dE \qquad (49)$$

In this expression T_6 is the absolute temperature expressed in units of 10^6 °K and the integral must be in units of kev^2-barns. We shall always measure S(E) in kev-barns and E in kev.

Two approximations are commonly made in performing the integral in Eq. (47). One is the resonant approximation (RA) in which the main energy variation in the integrand is assumed to be in S(E) (a resonance occurs at $E = E_r$). The exponential is evaluated at $E = E_r$ and a single level Breit-Wigner formula is used for S(E). The integral can be performed and this yields an analytic expression for the rate. The second approximation is the nonresonant approximation (NRA). In the NRA, S is assumed to vary slowly with energy, is evaluated at the energy E_0 at which the exponential is a maximum, and then is taken outside the integral sign. The exponential is then approximated by a Gaussian, and the integration may be carried out. Formulas for the rates in these two cases have been given by Burbidge et al. (1957). For a given reaction at a given temperature one generally uses the RA to obtain the effect on the rate of resonances in the cross section which occur near the stellar energy region and the NRA to obtain the effect on

the rate of the cross section away from the resonances. One effect usually predominates and the rate is quoted either as "resonant" or "nonresonant". In the present case it was suspected that at some temperatures the NRA may not be a very good way to obtain the nonresonant effect since S(E) would be changing rather rapidly. Also it was clear that for the case of destructive interference the NRA would give too low a rate at temperatures (around $T_6 = 15$) where the maximum of the exponential occurred near the minimum of S(E). For these reasons it was decided to perform the integral in Eq. (49) graphically.

In order to facilitate this graphical integration the effect of the resonance at $E_r = 65$ kev was subtracted out.* If this were not done then a plot of $\Phi(E)$ vs E would show a very high, very narrow spike at the higher temperatures. We thus write for the rate

$$P_{17} = P_r + P_c \tag{50}$$

where, for the case under consideration, P_r is given by the RA to be (Burbidge, 1957)

$$\frac{P_r}{H^1 O^{17}} = \frac{5.823 \times 10^{-9}}{T_6^{3/2}} e^{-\tau_r} \tag{51}$$

with

---

*This is the level referred to as number 1 in reference to Eq. (40). The lower resonance does not produce any difficulty since the exponential goes to zero at E = 0.

$$\tau_r = 30.28 + 754.7/T_6 \tag{52}$$

The correction term P_c is given by Eq. (49) with $\Phi(E)$ replaced by $\Phi_c(E)$ where

$$\Phi_c(E) = \Phi(E) - \Phi_r(E) \tag{53}$$

The integrand $\Phi_r(E)$ is simply that which is used in the RA and is given by

$$\Phi_r(E) = \frac{S_r \Gamma^2/4}{(E - E_r)^2 + \Gamma^2/4} \exp-(b/\sqrt{E_r} + E_r/kT) \tag{54}$$

where $S_r = S(E_r)$. In the present problem $E_r = 65$ kev and $\Gamma = 0.268$ kev.

The function $\Phi_c(E)$ was then calculated as a function of E. It was found that even this function exhibited a behavior which would make the graphical integration somewhat difficult. At energies just below E_r the function $\Phi_c(E)$ exhibits a sharp positive spike followed by a sharp negative spike just above E_r. This is because in the present case the function $\Phi_r(E)$ underestimates $\Phi(E)$ below E_r, and above E_r it overestimates $\Phi(E)$. This was handled by folding the negative spike back toward the low energy end and subtracting the absolute values of the ordinates. This effectively subtracts out the negative area produced by the negative spike and the resulting curve [called $\Phi_{cf}(E)$] is quite smooth. The net area under $\Phi_c(E)$ is equal to the area under $\Phi_{cf}(E)$ so we have

$$\frac{P_c}{H^1O^{17}} = \frac{2.008 \times 10^{-15}}{T_6^{3/2}} \int_0^\infty \Phi_{cf}(E)\, dE \tag{55}$$

The integrand $\Phi_{cf}(E)$ is shown in Figs. 27 to 30 for two temperatures. Both the case of constructive interference and the case of destructive interference are shown. The dashed curve in Figs. 28 to 30 shows a portion of the positive spike produced by $\Phi_c(E)$. The negative spike is not shown. After plotting $\Phi_{cf}(E)$ in this manner the area was obtained with a planimeter and the rate correction P_c was calculated from Eq. (55). The results of these calculations are given in the second and third columns of Table XII. The resonant rate P_r as calculated from Eq. (51) is shown in column four of this table. Above $T_6 = 25$ the resonant rate predominates so that P_c can be neglected. The total rate P_{17} obtained by adding P_c and P_r is given in columns five and six of Table XII.

It is of interest to compare the exact rate correction P_c to a rate P_0 obtained by using the formulas for the NRA (Burbidge, 1957). The expression for P_0 will not be written down here [it is similar in form to that given for P_{16} in Eq. (56) below], but the comparison in the form of log (P_c/P_0) vs T_6 is given in Fig. 32. It is seen that for the case of constructive interference P_0 is a good approximation to P_c but for the case of destructive interference a considerable error would be made in using P_0 above a temperature of about 13×10^6 °K.

It is now desired to obtain the rate P_{16} for the reaction $O^{16}(p,\gamma)F^{17}$ in order to check Eq. (39). The reaction is nonresonant with $S_0 = S(E_0) = 5$ kev-barns (Fowler, 1960). This gives

$$\frac{P_{16}}{H^1 O^{16}} = \frac{9.244 \times 10^{-15}}{T_6^{2/3}} \; e^{-\tau} \qquad (56)$$

with

$$\tau = 166.9/T_6^{1/3} \qquad (57)$$

The rate P_{16} obtained from Eqs. (56) and (57) is given in column seven of Table XII. The last two columns in this table give the quantity log $(O^{17}P_{16}/O^{16}P_{17})$. For $T_6 > 25$, P_r has been set equal to P_{17}. This quantity is also plotted vs temperature in Fig. 31. At equilibrium we have $P_{16} = P_{17}$, in which case the ordinate in Fig. 31 is just the logarithm of the ratio O^{17}/O^{16} in the CNO-cycle. The top horizontal dashed line corresponds to the value for this ratio given by Eq. (39).

E. Discussion of Results

If the case of constructive interference applies then a reduction of $\theta_\alpha^2\theta_p^2$ by a factor of 20 is necessary in order that $[O^{17}/O^{16}]_{CNO}$ reach the value given by Eq. (39). The case of destructive interference does reach the value of Eq. (39). If the present assumptions about the low energy cross section for $O^{17}(p,\alpha)N^{14}$ reaction made above are correct, then it appears from Fig. 31 that the terrestrial material which has been processed by the CNO-cycle underwent this processing at a considerably lower temperature than the 35 million degrees assumed in connection with Eq. (37). At this temperature only the 65-kev resonance will contribute to the reaction rate and the effect of the lower level can be neglected. A reduction of $\theta_\alpha^2\theta_p^2$ by a factor of over 2000 for the higher resonance would be required to obtain $[O^{17}/O^{16}]_{CNO} = 0.17$ at $T_6 = 35$. This is not impossible, but seems unlikely in view of the experimental results

of the present work. In order to be consistent one should now compute $[O^{17}/O^{16}]_{CNO}$ at this lower temperature rather than use Eq. (39) which was based on $T_6 = 35$. Fowler (1960) gives $C^{12}/N^{14} = 0.01$ and $O^{16}/N^{14} = 0.05$ at a temperature of about 15 million degrees. These values do not change f, β, or γ significantly, but $[O^{17}/O^{16}]_{CNO}$ is decreased to 0.072 (a factor of about 2.5). The bottom horizontal dashed line in Fig. 31 shows this ratio. It is seen that this results in a shift of only about one million degrees in the processing temperature for the destructive case. Thus Fig. 31 shows that for destructive interference a temperature of about 17 million degrees for the processing temperature in the CNO-cycle appears to be consistent with the present calculations* and that about the same temperature would result if the constructive case applied and $\theta_p^2\theta_\alpha^2$ were reduced by a factor of 10.

A rough estimate of remote-level contributions to S(E) gives an S-value of about 10 kev-barns in the stellar region. This would give a rate of the same order as that calculated for the destructive case and so would not greatly affect the above quoted processing temperature.

In summary we point out that the terrestrial O^{17}/O^{16} ratio can be obtained if

---

*Calculations by Burbidge et al. (1957) would indicate that at temperatures given by the low-temperature intersections of the rate curve with the horizontal dashed lines the mean life of O^{16} is quite long and thus one would not expect equilibrium to be reached in the participation of O^{16} in the cycle. No investigation of the CNO-cycle under nonequilibrium conditions has been carried out. Equilibrium conditions will almost certainly hold at high temperatures, however, so the present conclusion which excludes processing temperatures greater than 20 million degrees would seem to be a valid one.

(a) Constructive interference applies with $\theta_p^2\theta_\alpha^2 \approx 10^{-4}$. This results in a maximum processing temperature for terrestrial material produced in the CNO-cycle of about 20 million degrees.

(b) Destructive interference applies with $\theta_p^2\theta_\alpha^2 \approx 10^{-3}$. This gives a processing temperature of about 17 million degrees. A reduction of $\theta_p^2\theta_\alpha^2$ by a factor of 10 here would raise the temperature to about 20 million degrees.

(c) Either constructive or destructive interference applies and $\theta_p^2\theta_\alpha^2 \approx 10^{-6}$ with a processing temperature of about 35 million degrees.

It is felt that (c) is rather unlikely and that the best estimate of the processing temperature is about 17 million degrees. It is suggested that nonequilibrium conditions in the CNO-cycle should be investigated in order to determine this temperature more accurately, but it is expected that the temperature will not exceed 20 million degrees in any case.

APPENDIX A

Calculation of Barrier Factors

Much of the notation of Lane and Thomas (1958) will be used here. The partial width $\Gamma_{\lambda c}$ for the decay of a compound nucleus into channel c via level λ may be written

$$\Gamma_{\lambda c} = 2P_c \gamma_{\lambda c}^2 = \frac{2\hbar^2}{M_c a_c^2} P_c \theta_{\lambda c}^2 \qquad (A.1)$$

with

$$P_c = \left[\frac{\rho_c}{F_c^2 + G_c^2}\right]_{\rho_c = k_c a_c} \qquad (A.2)$$

and

$$k_c^2 = \frac{2M_c E_c}{\hbar^2} \qquad (A.3)$$

Here M_c is the reduced mass of the pair of particles in channel c, E_c is their energy of relative motion, a_c is the channel radius, $\gamma_{\lambda c}^2$ is the reduced width, $\theta_{\lambda c}^2$ is the dimensionless reduced width, and F_c and G_c are the regular and irregular Coulomb functions. F_c and G_c are functions of two parameters ρ_c and η_c where

$$\eta_c = \frac{Z_{1c} Z_{0c} e^2}{\hbar} \left(\frac{M_c}{2E_c}\right)^{1/2} \qquad (A.4)$$

Here Z_{1c} and Z_{0c} are the charge numbers of the two particles of the pair c. If we introduce the reduced mass number A, the mass numbers A_1 and A_0 of the pair c, and a characteristic energy E_a defined by

$$E_a = \frac{\hbar^2}{2M_c a_c^2} = \frac{20.9}{A a_c^2} \times 10^3 \text{ kev} \qquad a_c \text{ in fermis} \tag{A.5}$$

(1 fermi = 10^{-13} cm) then we may write

$$\Gamma_{\lambda c} = \theta^2_{\lambda c} \frac{4}{F_c^2 + G_c^2} (E_c E_a)^{1/2} \tag{A.6}$$

$$\rho_c = (E_c/E_a)^{1/2} \tag{A.7}$$

$$\eta_c = 4.98\, Z_1 Z_0 (A/E_c)^{1/2} \qquad E_c \text{ in kev} \tag{A.8}$$

The channel radius a_c will be taken to be

$$a_c = 1.40\,(A_1^{1/3} + A_0^{1/3}) \text{ fermi} \tag{A.9}$$

For the $O^{17}(p,\alpha)N^{14}$ reaction we consider two channels, the O^{17} + p channel and the N^{14} + α channel. We let the symbol E stand for the energy in the O^{17} + p channel; then E + Q is the energy in the N^{14} + α channel. We let ℓ denote the relative orbital angular momentum in units of $\hbar$ for the pair under consideration. We then have

$$\underline{O^{17} + p} \tag{A.10}$$

$A = 0.9517$ $\qquad$ $a = 5.000$ fermi

$E_a = 878$ kev $\qquad$ $\rho = \dfrac{E^{1/2}}{29.63}$ $\qquad$ E in kev

$$\eta = \frac{38.87}{E^{1/2}} \qquad \text{E in kev}$$

$$\frac{\Gamma_\ell}{\theta^2_\ell} = \frac{118.5\, E^{1/2}}{F_\ell^2 + G_\ell^2} \text{ kev} \qquad \text{E in kev}$$

$$\underline{N^{14} + \alpha} \qquad \text{(A.11)}$$

$A = 3.1138$ $\qquad a = 5.597$ fermi

$E_a = 214$ kev $\qquad \rho = \dfrac{(E+Q)^{1/2}}{14.63}$ $\qquad E, Q$ in kev

$$\eta = \frac{123}{(E+Q)^{1/2}} \qquad E, Q \text{ in kev}$$

$$\frac{\Gamma_\ell}{\theta_\ell^2} = \frac{58.52(E+Q)^{1/2}}{F_\ell^2 + G_\ell^2}$$

Interpolation in the graphs of Sharp, Gove, and Paul (1955) was used to obtain $F_\ell^2 + G_\ell^2$. The graphs can be read to an accuracy of about 3%. Tables II and III list the results of the computation of the ratio of the partial width Γ_ℓ to the reduced width θ_ℓ^2 (the barrier factor) for several energies and ℓ-values. Equations (A.10) and (A.11) were used in these computations.

In astrophysical calculations it is often necessary to obtain the barrier factors at very low energies where ρ is very small and η is large. This is the case, for example, for the O^{17} + p channel in the calculations carried out in Section VI. Such a formula has been given, in reference to astrophysical applications, in the paper by Burbidge, Burbidge, Fowler, and Hoyle (1957). The following brief discussion as to how one obtains the formula is based on a comprehensive article by Hull and Breit (1959).

For small ρ one has $G_\ell^2 >> F_\ell^2$ so that in computing $\Gamma_\ell/\theta_\ell^2$ we need only consider G_ℓ. One then writes

$$x^2 = 8\rho\eta = \begin{bmatrix} 10.49 & \text{for} & O^{17} + p \\ 67.26 & \text{for} & N^{14} + \alpha \end{bmatrix} \qquad (A.12)$$

and expands G_ℓ in an asymptotic series in $1/\eta^2$ while holding x^2 constant. When all but the first two terms in the expansion are dropped and $e^{2\pi\eta} >> 1$ one obtains

$$G_\ell^2 = \frac{e^{2\pi\eta}}{2\pi\eta}\, x^2 K_{2\ell+1}^2(x)\,(1 + \alpha_\ell E) \qquad (A.13)$$

with

$$\alpha_\ell = \frac{1}{3E_a}\left[\frac{1}{\ell+1}\left\{\frac{K_{2\ell+3}(x)}{K_{2\ell+1}(x)}\,(1 - 2\ell\,(\ell+1)(\tfrac{2}{x})^2) - 1\right\}\right.$$

$$\left. + 2\ell(\ell+1)\,(2\ell+1)\,(\tfrac{2}{x})^4\right] \qquad (A.14)$$

where E_a has been defined in Eq. (A.5) and $K_n(x)$ is the modified Bessel function of the second kind of order n. For Eq. (A.13) to be valid one should have $\alpha_\ell E << 1$, otherwise more terms in the asymptotic series should be kept. We now combine Eq. (A.6) with these results to find

$$\frac{\Gamma_\ell}{\theta_\ell^2} = \pi\,\frac{E_a e^{-b/\sqrt{E}}}{K_{2\ell+1}^2(x)}\,(1 - \alpha_\ell E) \qquad (A.15)$$

with Γ_ℓ having the same units as E_a. In comparing this with Burbidge, et al. (1957) one must note that their θ_ℓ^2 is to be multiplied by 1.5 to agree with the definition being used here. A convenient form for x is

$$x = 0.525\ (AZ_1Z_0a)^{1/2} \qquad a \text{ in fermis} \tag{A.16}$$

and the quantity b in the exponential in Eq. (A.15) is given by

$$b = 31.28\ Z_1Z_0A^{1/2} \tag{A.17}$$

APPENDIX B

Angular Distribution Factors

For the case where only a single level of spin and parity J^{π} contributes to the observed reaction and where a single orbital angular momentum ℓ is effective in forming the compound state and a single orbital angular momentum ℓ' occurs in the decay of the compound state, the general expression for the angular distribution of the reaction (Lane, 1958) reduces considerably. The energy dependence of the cross section factors out and the only remnants of the scattering matrix in the angular distribution function are amplitudes for formation of the states through the various channel spins involved in the reaction (Blatt, 1952). In the $O^{17}(p,\alpha)N^{14}$ reaction there are two channel spins involved in the O^{17} + p channel, s = 2 and s = 3; and there is one channel spin involved in the N^{14} + α channel, s' = 1. We define a quantity r by

$$\begin{aligned} &r = \text{probability to form compound state through } s = 3 \\ &1-r = \text{probability to form compound state through } s = 2 \end{aligned} \tag{B.1}$$

We then write the cross section proportional to an angular distribution function $w(\theta)$ and find

$$w(\theta) = \sum_{s} \sum_{L} (-1)^{s-1} [(1-r)\delta_{s2} + r\delta_{s3}] \, \overline{Z}(\ell J \ell J, sL) \, \overline{Z}(\ell' J \ell' J, 1L) P_L(\cos\theta) \tag{B.2}$$

where the P_L are Legendre polynomials, δ_{s2} and δ_{s3} are Kronecker δ symbols, s' has been set equal to unity, and the $\overline{Z}$ are defined by Lane and Thomas (1958). They are related to tabulated Z coefficients through

$$\overline{Z}(\ell_1 J_1 \ell_2 J_2, sL) = i^{\ell_1 - \ell_2 - L} Z(\ell_1 J_1 \ell_2 J_2, sL) \qquad (B.3)$$

In the calculation performed here the Z coefficients were taken from the tables of Sharp, Kennedy, Sears, and Hoyle (1954).

The distribution factor β is given by

$$\beta = \frac{4\pi w(152^\circ)}{\int_0^\pi 2\pi w(\theta) \sin\theta \, d\theta} \qquad (B.4)$$

On making use of the orthogonality of the P_L and the relation (Lane, 1958)

$$\overline{Z}(\ell_1 J_1 \ell_2 J_2, s0) = \delta_{\ell_1 J_1, \ell_2 J_2} (-1)^{J_1 - s} (2J_1 + 1)^{1/2} \qquad (B.5)$$

one finds

$$\beta = \frac{w(152^\circ)}{2J+1} \qquad (B.6)$$

The results for a variety of (J^π, ℓ, ℓ') are given below.

$(0^-, 3, 1)$: $\beta = 1$

$(1^+, 2, 0)$: $\beta = 1$

$(1^+, 2, 2)$: $\beta = 1 + (9r/14 - 1/2)P_2$

$(1^-, 1, 1)$: $\beta = 1 - (1/10)P_2$

$(1^-, 3, 1)$: $\beta = 1 + (9r/10 - 2/5)P_2$

$(2^+, 0, 2)$: $\beta = 1$

$(2^+, 2, 2)$: $\beta = 1 + (20/392)(5r+3)P_2 + (6/49)(5r-4)P_4$

$(2^-, 1, 1)$: $\beta = 1 + (1/10)(9r - 7)P_2$

$(2^-, 1, 3)$: $\beta = 1 + (4/35)(11r - 7)P_2$

$(3^+, 0, 2)$: $\beta = 1$

$(3^+, 2, 2)$: $\beta = 1 - (2/49)(17r-6)P_2 + (11/49)(5r-3)P_4$

$(3^-, 1, 3)$: $\beta = 1 - (21/140)(9r - 4)P_2$

$(4^+, 2, 4)$: $\beta = 1 + (1/196)(113r + 130)P_2 - (27/98)(3r-1)P_4$

$(4^-, 1, 3)$: $\beta = 1 + (55/84)P_2$

In the above the Legendre polynomials P_2 and P_4 are to be evaluated for $\theta = 152^\circ$. The factors β are linear functions of the probability r. Thus the limits on β are given by setting $r = 0$ and $r = 1$. These limits, called β_2 and β_3, are given in Table IV.

APPENDIX C

Energy Spread Introduced by Spectrometer Solid Angle

Suppose that a yield curve of counts vs bombarding energy E_{1B} is taken for a case where no reaction occurs except when the incoming particle has energy $E_1 = E_r$ and no counts are obtained unless the particle emerging from the target has energy $E_{20}=E_m-Z_2eV_t$ where E_m is the spectrometer setting. (We thus have a zero width resonance and a spectrometer with infinite energy resolution.) Refer to Fig. 24 in what follows. Suppose the apparatus is set so that

$$E_{1B} = E_r + \frac{n\epsilon_1 s}{\cos\theta_1} \tag{C.1}$$

and

$$E_{20} = E_2(E_r, \theta) - \frac{n\epsilon_2 s}{\cos\theta_2} \tag{C.2}$$

where n is the number of stopping atoms per cm^3 and s is the perpendicular distance from the target surface to the reaction position in the target. If so, then counts are being obtained. Now increase the bombarding energy to $E_{1B} + \Delta E_{1B}$. The position at which the resonance energy occurs in the target moves to $s + \Delta s$, thus

$$\Delta E_{1B} = \frac{n\Delta s\epsilon_1}{\cos\theta_1} \tag{C.3}$$

We assume that in taking the yield curve the magnet setting E_m is being changed linearly with E_e so that $\Delta E_m = \alpha \Delta E_e$ which guarantees that

$$\Delta E_{20} = \alpha \Delta E_{1B} \tag{C.4}$$

where α is a constant.

The energy E'_{20} of a particle produced at $s + \Delta s$ and emerging at an angle of $\theta + \Delta\theta$ is

$$E'_{20} = E_2(E_r, \theta + \Delta\theta) - \frac{n(s+\Delta s)\epsilon_2}{\cos(\theta_2 + \Delta\theta_2)} \tag{C.5}$$

Expanding and noting that $\Delta\theta = -\Delta\theta_2$ gives

$$E'_{20} = E_2(E_r, \theta) + \left(\frac{\partial E_2}{\partial \theta}\right)_{E_1} \Delta\theta - \frac{n\epsilon_2(s+\Delta s)}{\cos\theta_2} + \frac{n\epsilon_2 s \tan\theta_2}{\cos\theta_2}\Delta\theta \tag{C.6}$$

These particles will be counted if $\Delta\theta$ is such that $E_{20} + \Delta E_{20} = E'_{20}$. Applying this condition to Eqs. (C.2), (C.3), (C.4), and (C.6) gives

$$\frac{\Delta E_{1B}}{\Delta\theta} = \frac{\left(\frac{\partial E_2}{\partial\theta}\right)_{E_1} + \frac{n\epsilon_2 s}{\cos\theta_2}\tan\theta_2}{\alpha + \frac{\epsilon_2}{\epsilon_1}\frac{\cos\theta_1}{\cos\theta_2}} \tag{C.7}$$

Note that in deriving Eq. (C.7) energy variations in the stopping cross sections have been neglected--it being assumed that appropriate energies are chosen at which to evaluate them. Essentially the same relation as Eq. (C.7) may also be derived by using an expansion and partial derivatives given by Bardin (1961).

The maximum energy change allowable that will still produce counts is obtained by setting $\Delta\theta = \delta\theta$ where $\delta\theta$ is the angular opening of the spectrometer. $\delta\theta$ was calculated from

$$\delta\theta = (4\Omega/\pi)^{1/2} \quad \text{radians} \tag{C.8}$$

and amounts to 0.074 radians. The energy spreads ΔE_{1B} calculated from Eq. (C.7) are given in the column labeled Δ_θ in Table IX.

APPENDIX D

Energy Straggling

In this appendix we derive an expression for the spectrometer yield from a thick target when both energy straggling and spectrometer resolution are taken into account. The case where the bombarding energy E_{1B} is varied over the region of a very narrow resonance is considered. We then discuss the problem of the interpretation of the area under the yield curve. Finally the calculated full width at half maximum is compared with what one obtains when a square-root-of-the-sums-of-the-squares law (to be defined) is applied.

Let $P_1(E_{1B}, E_1; x)\, dE_1$ be the probability that the incoming particle having a bombarding energy E_{1B} will have an energy between E_1 and $E_1 + dE_1$ after penetrating a distance x into the target. Let $P_2(E_2, E_{2S}; x')\, dE_{2S}$ be the probability that the particle produced in the target at position x with energy $E_2 = E_2(E_1)$ (determined from kinematics) will have energy* between E_{2S} and $E_{2S} + dE_{2S}$ after passing a distance x' through the target. We shall consider the case where the target normal bisects the angle between the incoming proton beam and the spectrometer position; thus $x = x'$. If we let n be the number of reacting atoms per cm^3 then the number of particles produced per unit solid angle per incident proton in a region dx at x in the target is

---

*The present notation differs from that of Bardin (1961) in that he uses E_{20} to refer to the general energy of the emerging particles. We use E_{2S} since our E_{20} has already been defined by Eq. (12).

$$nP_1(E_{1B}, E_1; x)\sigma(E_1)\, dx\, dE_1$$

where $\sigma(E_1)$ is the laboratory reaction cross section per unit solid angle evaluated at the energy E_1. The energy of these particles is in the range E_2 to $E_2 + dE_2$ at the moment of production. By the time the particles have passed a distance x through the material and have emerged from the target this sharp energy distribution has been spread by the straggling. The number of these particles (per incident particle) having energy in the range E_{2S} to $E_{2S} + dE_{2S}$ is

$$nP_2(E_2, E_{2S}; x)P_1(E_{1B}, E_1; x)\sigma(E_1)\, dx\, dE_1\, dE_{2S}$$

An integration over E_1 gives the observed particle spectrum from a target lamina dx at x. A second integration, this time over x, gives the complete observed particle spectrum from the entire target. Finally, an integration of E_{2S} over the energy acceptance $\delta E_m = 2E_m/R$ of the spectrometer (we assume a rectangular distribution for the spectrometer energy acceptance) gives the laboratory yield $Y_L(E_{1B})$. Here E_m is the energy setting of the spectrometer and $R = p/\Delta p$ is the spectrometer momentum resolution. We thus have

$$Y_L(E_{1B}) = n \int_0^{E_{1B}} dE_1 \int_0^{X} dx \int_{E_{20}-E_m/R}^{E_{20}+E_m/R} dE_{2S}\; P_1(E_{1B}, E_1; x)P_2(E_2, E_{2S}; x)\sigma(E_1) \tag{D.1}$$

The normalization condition on the probabilities $P(E, w; x)$ is

$$\int_0^{E} P(E, w; x)\, dw = 1 \tag{D.2}$$

For the case of a very narrow resonance in the cross section we write

$$\sigma(E_1) = \frac{\pi}{2}\,\sigma_r\,\Gamma\,\delta(E_1 - E_r) \qquad (D.3)$$

where the area "under" the δ-function is written $\pi\sigma_r\Gamma/2$ since if σ_r is the cross section at the resonance and Γ is the total width this is just the area given by the single level formula for a narrow level. What is meant here by a very narrow resonance is that $\Gamma \to 0$ and $\sigma_r \to \infty$ in such a way that $\sigma_r\Gamma$ is constant. E_r in Eq. (D.3) is the resonance energy. The E_1 integral can then easily be performed. We prefer here not to use x as a variable but to measure depth into the target by means of the energy loss ξ to the incoming particles. It is a good approximation to neglect the energy variation of the stopping cross section. We then have

$$\xi = n_s \epsilon_{1r} x \qquad (D.4)$$

where the stopping cross section has been evaluated at the resonance energy and n_s is the number of stopping atoms per cm^3. Equation (D.1) then becomes

$$Y_L(E_{1B}) = \frac{\pi n \sigma_r \Gamma}{2 n_s \epsilon_{1r}} \int_0^{\Xi} d\xi \int_{E_{20}-E_m/R}^{E_{20}+E_m/R} dE_{2S}\; P_1(E_{1B}, E_r; \xi)\, P_2(E_{2r}, E_{2S}; \xi) \qquad (D.5)$$

where Ξ is the target thickness in energy units and $E_{2r} = E_2(E_r)$. Equation (D.5) assumes $E_{1B} > E_r$, otherwise the yield is zero. The next step is to assume that the straggling probabilities are given by Gaussian distributions with means given by $E_{1B} - \xi$ and

$E_{2r} - \epsilon_{2r}\xi/\epsilon_{1r}$ and with rms deviations Δ given by

$$\Delta^2 = z^2 \lambda_r \xi \tag{D.6}$$

with

$$\lambda_r = \frac{4\pi e^4}{\epsilon_{1r}} \sum_i Z_i \tag{D.7}$$

In the above expression for λ_r, ϵ_{1r} is the stopping cross section per molecule evaluated at E_r, and Z_i is the charge of the stopping atoms ($\sum Z_i = 36$ for NiO). This expression for the standard deviation was originally given by Bohr (1915). The condition for validity of the Gaussian approximation has been given by Rossi (1952) and is that the rms deviation Δ must be large compared with the maximum transferable energy in a single collision Q_{max} yet small compared to both the average energy at distance x and the energy loss. Q_{max} is given by

$$Q_{max} = \frac{4m}{M} E \tag{D.8}$$

where M and E are the mass and energy of the particle under consideration. In the present experiment it is found that the above criterion is fairly well satisfied for the alpha particles but only poorly satisfied for the protons. This is reflected in the discrepancy between the calculated and experimental yield curve at the high-energy end (Figs. 12 to 18).

The Gaussian assumption yields

$$P_1(E_{1B}, E_r; \xi) = \frac{1}{(2\pi\lambda_r \xi)^{1/2}} \exp\left[\frac{-(E_r - E_{1B} + \xi)^2}{2\lambda_r \xi}\right] \tag{D.9}$$

and

$$P_2(E_{2r}, E_{2S};\xi) = \frac{1}{(8\pi\lambda_r\xi)^{1/2}} \exp\left[\frac{-(E_{2S}-E_{2r}+\xi\epsilon_{2r}/\epsilon_{1r})^2}{8\lambda_r\xi}\right] \qquad (D.10)$$

On combining Eqs. (D.5), (D.9), and (D.10) one notices that the E_{2S} integral can be performed leading to error functions (erf). This gives

$$Y_L(E_{1B}) = \frac{n\sigma_r\Gamma}{4n_s\epsilon_{1r}} (\pi/2\lambda_r)^{1/2} I(E_{1B}) \qquad (D.11)$$

with

$$I(E_{1B}) = \int_0^{\bar{\xi}} \frac{d\xi}{\sqrt{\xi}} [\mathrm{erf}(L_+)-\mathrm{erf}(L_-)] \exp\left[\frac{-(E_r-E_{1B}+\xi)^2}{2\lambda_r\xi}\right] \qquad (D.12)$$

where

$$L_{\pm} = \frac{1}{(8\lambda_r\xi)^{1/2}} (E_{20} \pm E_m/R - E_{2r} + \xi\epsilon_{2r}/\epsilon_{1r}) \qquad (D.13)$$

The error function is defined by

$$\mathrm{erf}(x) = \frac{2}{\sqrt{\pi}} \int_0^x e^{-t^2} dt \qquad (D.14)$$

The Burroughs 220 computer was programmed to do the integral $I(E_{1B})$ [Eq. (D.12)] for the seven narrow resonances. The spectrometer setting E_m was changed as the analyzer energy E_e was changed. The relation between these quantities was very closely linear so we write [see also Eq. (C.4)]

$$E_m = \alpha E_e + \beta \qquad (D.15)$$

The parameters used for each resonance are listed in Table VIII.

The resonance energies were chosen so that the peak of the calculated integral and the peak of the experimental points fell at the same value of E_{1B}. These resonance energies are equal to those calculated from Eq. (13) to within a few tenths of a kev. The integrand in Eq. (D.12) was found to fall to very small values before ξ reached the actual target thickness. A value Ξ = 20 kev was found sufficient and was used in all the calculations.

After the integral had been calculated as a function of E_{1B} use was made of Eq. (D.11) to obtain the yield. A value of $\sigma_r \Gamma$ was chosen that normalized the calculated yield to the experimental yield at the maximum value. These calculated results are shown as dashed curves in Figs. 12 to 18.

We next discuss the problem of the relationship of the area A_Y under the yield curve to the level parameters. A_Y is defined by

$$A_Y = \int Y_L (E_{1B})\, dE_{1B} \tag{D.16}$$

A somewhat different area A'_Y is obtained if one writes the yield as a function of the reaction energy E_1 instead of the bombarding energy. We have

$$A'_Y = \int Y_L(E_1)\, dE_1 \tag{D.17}$$

The relationship between the two areas can be found from Eq. (13), and is

$$A_Y = \frac{\epsilon_{2r}/\epsilon_{1r} + \partial E_2/\partial E_1}{\epsilon_{2r}/\epsilon_{1r} + \alpha} A'_Y \tag{D.18}$$

where α is defined in Eq. (D.15).

The area under the calculated yield curve was also computed on the Burroughs 220. The quantity $A_Y/(\sigma_r \Gamma \pi/2)$ resulting from this computation is given in the second column of Table X.

We now obtain the corresponding relations for the case of no straggling, using lower case symbols for this case. We let

$$\sigma(E) = \frac{\sigma_r \Gamma^2/4}{(E - E_r)^2 + \Gamma^2/4} \tag{D.19}$$

If we then substitute Eq. (D.19) and δ-functions for the straggling probabilities into Eq. (D.1) one obtains

$$Y_L(E_1) = \frac{n\Gamma\sigma_r}{2\epsilon_{1r} n_s} \tan^{-1} \frac{\xi_1 \Gamma/2}{(E_1 - E_r)^2 + (\Gamma^2 - \xi_1^2)/4} \tag{D.20}$$

This result has also been given by Fowler et al. (1948). The quantity ξ_1 is given in Eq. (15) and is a function of E_1 through Eqs. (D.15) and (13). We define the areas a_y and a'_y by

$$a_y = \int y_L(E_{1B})\, dE_{1B} \tag{D.21}$$

and

$$a'_y = \int y_L(E_1)\, dE_1 \tag{D.22}$$

The relation

$$a_y = \frac{\epsilon_{2r}/\epsilon_{1r} + \partial E_2/\partial E_1}{\epsilon_{2r}/\epsilon_{1r} + \alpha}\, a'_y \tag{D.23}$$

also holds here. If one then writes ξ_1 explicitly as a function of E_1 the integral a'_y can be performed giving

$$a'_y = \frac{n\pi\sigma_r \Gamma E_m(\max)}{n_s \epsilon_{1r} R(\epsilon_{2r}/\epsilon_{1r} + \partial E_2/\partial E_1)} \frac{1}{1 - G^2/4} \qquad \text{(D. 24)}$$

with

$$G = \frac{2\alpha}{R(\epsilon_{2r}/\epsilon_{1r} + \alpha)} \qquad \text{(D. 25)}$$

G is quite small in the present experiment so the correction term in Eq. (D. 24) which involves G will be neglected from now on. Application of Eq. (D. 23) then gives

$$\frac{a_y}{\pi\sigma_r \Gamma/2} = \frac{2nE_m(\max)}{n_s \epsilon_{1r} R(\epsilon_{2r}/\epsilon_{1r} + \alpha)} \qquad \text{(D. 26)}$$

The results of applying Eq. (D. 26) to the resonances are also listed in Table X. The fact that the numbers in the two columns are so nearly equal shows that as far as the yield area is concerned straggling can be neglected. This fact is used in the discussion in Section V-C4.

Brief mention should also be made of the fact that if one does not restrict the E_{2S} integration in Eq. (D.1), but requires that one observe the entire outgoing particle spectrum, then the E_{2S} integral gives unity by virtue of Eq. (D. 2). The situation then reduces to that considered by Gove (1959) in which he shows that the area is independent of energy spread in the beam or straggling of the incoming particles.

As a final topic in this appendix we briefly investigate the problem of compounding experimental widths from several sources into a total width. A rule for compounding experimental widths that

has been used in the past (Cohen, 1949) is to approximate the various distribution functions with Gaussians having the means and rms deviations of the true distributions. The result of folding these Gaussians together then yields a Gaussian with an rms deviation equal to the square root of the sums of the squares of the rms deviations of the individual distributions. This type of rule can be checked against the present exact calculation. We let ΔE_p and ΔE_α stand for the straggling widths of the protons and alpha particles respectively. We use Eq. (D.6) evaluated at the value of ξ which gives the maximum yield. We thus take

$$\Delta E_p^2 = \Delta E_\alpha^2/4 = \lambda_r [\, E_{1B}(\max) - E_r \,] \qquad (D.27)$$

Note that ΔE_p and ΔE_α are not necessarily the direct contributions to the spread in $Y_L(E_{1B})$ from straggling. The direct contributions, denoted by σ_p and σ_α must be calculated, and depend in part on the rate at which the spectrometer setting is varied with respect to bombarding energy.

We first note that the contribution Δ_m to the width of $Y_L(E_{1B})$ from the spectrometer window may be found from ξ_1, as given in Eq. (15), and from Eq. (13). ξ_1 is just the width of $Y_L(E_1)$ due to the spectrometer window. We thus have

$$\Delta_m = \frac{\epsilon_{2r}/\epsilon_{1r} + \partial E_2/\partial E_1}{\epsilon_{2r}/\epsilon_{1r} + \alpha} \; \xi_1 \qquad (D.28)$$

The values of Δ_m are listed in Table IX. The spectrometer resolution function is assumed to be rectangular so that

$$\sigma_m^{\,2} = \Delta_m^2/12 \qquad (D.29)$$

where σ_m is the rms deviation contribution to the width of the yield curve from the spectrometer energy window.

We next compute σ_p by assuming that proton straggling is the only source of width. Monoenergetic protons are incident on the target surface and pass into the target. Let the mean energy at a distance x_r in the target be the resonance energy E_r. At this distance the protons have an energy spread ΔE_p due to straggling; however, we consider the cross section to have zero width, and therefore only protons with energy E_r will produce alpha particles. At a slightly different distance in the target, say at $x_r + dx$, the mean proton energy is not E_r, but due to the spread ΔE_p there are protons at $x_r + dx$ which have energy E_r, and which will thus initiate a reaction. It can be seen, therefore, that along a length Δx at x_r there are present protons of energy E_r, which can produce alpha particles of energy E_{2r}. The length Δx is related to the width ΔE_p through

$$\Delta x = \Delta E_p / n\epsilon_{1r} \tag{D.30}$$

The energy E_{2S} of an alpha particle emerging from the target and having been produced at a distance x in the target is given by $E_{2S} = E_{2r} - nx\epsilon_{2r}$, and the energy spread ΔE_{2S} of these alpha particles is given by $\Delta E_{2S} = n\epsilon_{2r}\Delta x$. On using Eq. (D.30) one then finds

$$\Delta E_{2S} = \epsilon_{2r}\Delta E_p / \epsilon_{1r} \tag{D.31}$$

which gives the spread in alpha particle energy due to proton straggling at a bombarding energy E_{1B}. Suppose, then, that the spectrometer is set to detect the alpha-particle energy at the edge of this spread, i.e. suppose we have

$$E_{20} = E_{2r} - (E_{1B}-E_r)\,\epsilon_{2r}/\epsilon_{1r} - \Delta E_{2S}/2 \qquad (D.32)$$

Then let us increase E_{1B} by ΔE_{1B} and E_{20} by $\Delta E_{20} = \Delta E_m = \alpha \Delta E_{1B}$ so that we have

$$E_{20} + \Delta E_{20} = E_{2r} - (E_{1B}+\Delta E_{1B} - E_r)\epsilon_{2r}/\epsilon_{1r} + \Delta E_{2S}/2 \qquad (D.33)$$

Equations (D.32) and (D.33) guarantee that the change ΔE_{1B} in the proton bombarding energy just covers the spread ΔE_{2S} in the alpha particle spectrum. On subtracting the two equations and using Eq. (D.31) one obtains

$$\sigma_p = \frac{\Delta E_p\, \epsilon_{2r}/\epsilon_{1r}}{\epsilon_{2r}/\epsilon_{1r} + \alpha} \qquad (D.34)$$

We have set $\sigma_p = \Delta E_{1B}$, by definition of σ_p. The quantities σ_p^2 are given in Table IX.

A similar calculation yields σ_α. Here we assume that the only width comes from the alpha-particle straggling. The alpha particles produced in the target with energy E_{2r} emerge with a spread ΔE_α. Equations (D.32) and (D.33) then hold with ΔE_{2S} replaced by ΔE_α. If we set $\Delta E_{1B} = \sigma_\alpha$ and use Eq. (D.27) we find

$$\sigma_\alpha = \frac{2\Delta E_p}{\epsilon_{2r}/\epsilon_{1r}+\alpha} \qquad (D.35)$$

The quantities σ_α^2 are listed in Table IX.

We define

$$\Delta_{sum} = 2.35\,[\sigma_p^2 + \sigma_m^2 + \sigma_\alpha^2]^{1/2} \qquad (D.36)$$

and compare this full width at half maximum with the true value Δ_t. The factor 2.35 is the ratio of the full width at half maximum to the rms deviation for a Gaussian. The values of Δ_{sum} are given in Table IX along with the values of Δ_t, which were determined from Figs. 12 to 18. The agreement is quite good.

REFERENCES

K. Ahnlund, 1957, Phys. Rev. 106, 124.

F. Ajzenberg-Selove and T. Lauritsen, 1959, Nuclear Physics 11, 1.

S. K. Allison, 1958, Revs. Modern Phys. 30, 1137.

E. Almqvist, D. A. Bromley, and J. A. Kuehner, 1958, Bull. Am. Phys. Soc. 3, 27.

R. K. Bardin, 1961, Ph.D. Thesis, California Institute of Technology.

S. Bashkin, R. R. Carlson, R. A. Douglas, and J. A. Jacobs, 1958, Phys. Rev. 109, 434.

J. M. Blatt and L. C. Biedenharn, 1952, Revs. Modern Phys. 24, 258.

N. Bohr, 1915, Phil. Mag. 30, 581.

R. O. Bondelid and C. A. Kennedy, 1959, Phys. Rev. 115, 1601.

A. B. Brown, C. W. Snyder, W. A. Fowler, and C. C. Lauritsen, 1951, Phys. Rev. 82, 159.

E. M. Burbidge, G. R. Burbidge, W. A. Fowler, and F. Hoyle, 1957, Revs. Modern Phys. 29, 547.

R. R. Carlson, C. C. Kim, J. A. Jacobs, and A. C. L. Barnard, 1961, Phys. Rev. 122, 607.

E. R. Cohen, 1949, Ph.D. Thesis, California Institute of Technology.

G. A. Dissanaike, 1953, Phil. Mag. 7, 44, 1051.

J. P. Elliott and B. H. Flowers, 1955, Proc. Roy. Soc. (London) A229, 536.

J. P. Elliott, 1958a, Proc. Roy. Soc. (London) A245, 128.

J. P. Elliott, 1958b, Proc. Roy. Soc. (London) A245, 562.

F. Everling, L. A. Konig, J. E. Mattauch, and A. H. Wapstra, 1960, Nuclear Physics 18, 529.

W. A. Fowler, C. C. Lauritsen, and T. Lauritsen, 1948, Revs. Modern Phys. 20, 236.

W. A. Fowler, 1960, Memoire Soc. Roy. Sciences de Liege 16, 207.

W. A. Fowler, J. L. Greenstein, and F. Hoyle, 1961 (to be published). This article is referred to by the abbreviation FGH.

H. E. Gove, 1959, "Resonance Reactions, Experimental," in P. M. Endt and M. Demeur, Editors, Nuclear Reactions (Interscience Inc., New York), Chap. VI, p. 259.

L. H. Gray, 1943, Proc. Cambridge Phil. Soc. 40, 72.

D. F. Herring, R. Chiba, B. R. Gasten, and H. T. Richards, 1958a, Phys. Rev. 112, 1210.

D. F. Herring, 1958b, Phys. Rev. 112, 1217.

N. P. Heydenburg and G. M. Temmer, 1953, Phys. Rev. 92, 89.

S. Hinds and R. Middleton, 1959, Proc. Phys. Soc. (London) 73, 721.

M. H. Hull, Jr. and G. Breit, 1959, "Coulomb Wave Functions," Handbuch der Physik (Springer-Verlag, Berlin), vol. XLI/1, p. 408.

E. Kashy, P. D. Miller, and J. R. Risser, 1958, Phys. Rev. 112, 547.

A. M. Lane and R. G. Thomas, 1958, Revs. Modern Phys. 30, 257.

J. B. Marion, 1961, Revs. Modern Phys. 33, 139.

E. A. Milne, 1953, Ph. D. Thesis, California Institute of Technology.

F. S. Mozer, 1956, Ph. D. Thesis, California Institute of Technology.

A. O. Nier, 1950, Phys. Rev. 77, 789.

W. R. Phillips, 1958, Phys. Rev. 110, 1408.

R. L. Platzman, 1952, "Influences of Details of Electronic Binding on Penetration Phenomena, and the Penetration of Energetic Charged Particles through Liquid Water," in J. J. Nickson, Editor, Symposium on Radiobiology (John Wiley and Sons, Inc., New York), Chap. 9, p. 139.

P. C. Price, 1955, Proc. Phys. Soc. (London) A68, 553.

M. G. Redlich, 1954, Phys. Rev. 95, 448.

M. G. Redlich, 1958, Phys. Rev. 110, 468.

H. K. Reynolds, D. N. F. Dunbar, W. A. Wenzel, and W. Whaling, 1953, Phys. Rev. 92, 742.

B. Rossi, 1952, High-Energy Particles (Prentice-Hall, Inc., New York).

W. T. Sharp, J. M. Kennedy, B. J. Sears, and M. G. Hoyle, 1954, Atomic Energy of Canada Ltd., AECL-97.

W. T. Sharp, H. E. Gove, and E. B. Paul, 1955, Atomic Energy of Canada Ltd., AECL-268, 2nd edition.

E.A. Silverstein, G. Hardie, L. Oppliger, and S. Salisburg, 1960, Bull. Am. Phys. Soc. 5, 405.

C. W. Snyder, S. Rubin, W. A. Fowler, and C. C. Lauritsen, 1950, Rev. Sci. Instr. 21, 852.

W. Whaling, 1958, "The Energy Loss of Charged Particles in Matter," Handbuch der Physik (Springer-Verlag, Berlin), Vol. XXXIV, p. 193.

Table I. Contributions to error in cross section. The quantities needed to obtain the absolute cross section are given along with their estimated rms deviations in percent. These quantities appear in Eqs. (21) and (22). For a discussion of these errors see text p. 31 ff.

Table I

Contributions to Error in Cross Section

Quantity	Error (percent)
$F_{2\infty}$	2.6
O^{17} concentration	1.0
Q	0.4
Ω/R	3.6
kinematics	0.0
E_m	0.2
ϵ (p in NiO)	3.0
ϵ (α in NiO)	10.0
$\epsilon_1 \partial E_2/\partial E_1 + \epsilon_2$	9.0
cross section	10.0

Table II. Barrier factors for the O^{17} + p channel. The barrier factors $\Gamma_\ell^2/\theta_\ell^2$ are given in kev for various ℓ-values. The proton energy E_p in the laboratory and the c.m. energy E in the O^{17} + p channel are also given in kev. The calculation of these factors is described in Appendix A. See text pp. 35, 38, 46, 55, 66.

Table II

Barrier Factors, $O^{17} + p$

E_p	E	$\ell = 0$	$\ell = 1$	$\ell = 2$	$\ell = 3$	$\ell = 4$
1350.6	1275.0		407			
1274.0	1202.7	924	333	31.1	1.70	0.0457
1246.7	1176.9	865	308	27.5	1.54	0.0395
1101.3	1039.7	622	195	15.9	0.843	0.0176
927.1	875.2	361	101	7.15	0.294	0.00538
825.0	778.8	241	60.2	4.06	0.153	0.00258
747.2	705.4	173	37.4	2.56	0.0841	0.00121
672.4	634.8	110	23.3	1.42	0.0406	5.68×10^{-4}
518.5	489.5	37.2	5.82	0.377	0.00675	8.35×10^{-5}

Table III. Barrier factors for the $N^{14} + \alpha$ channel. The barrier factors $\Gamma_\ell^2/\theta_\ell^2$ are given in kev for various ℓ-values. The energies listed are those for the $O^{17} + p$ channel, E_p being the proton energy in the laboratory and E being the c.m. energy. Both of these energies are given in kev. The c.m. energy in the $N^{14} + \alpha$ channel is given by E + Q. The calculation of these factors is described in Appendix A. See text pp. 35, 38, 53, 55, 66.

Table III

Barrier Factors, $N^{14} + \alpha$

E_p	E	$\ell = 0$	$\ell = 1$	$\ell = 2$	$\ell = 3$	$\ell = 4$
1350.6	1275.0		280			
1274.0	1202.7	372	242	102	28.6	4.90
1246.7	1176.9	354	230	99.3	25.9	4.52
1101.3	1039.7	271	177	67.4	17.1	2.82
927.1	875.2	185	114	40.8	9.47	1.36
825.0	778.8	140	85.2	29.4	6.54	0.887
747.2	705.4	115	68.0	23.6	5.00	0.644
672.4	634.8	86.4	47.7	16.6	3.34	0.400
518.5	489.5	49.0	25.3	8.52	1.55	0.185
	92.0		2.32			
	40.1		1.58			
	-10.7		1.02			

Table IV. Angular distribution factors β_2, β_3 for isolated levels in the reaction $O^{17}(p,\alpha)N^{14}$. J^{π} refers to the total angular momentum and parity of the state in F^{18}. The orbital angular momentum in the O^{17} + p channel is denoted by ℓ and that in the N^{14} + α channel is denoted by ℓ'. The quantities β_2 and β_3 are for formation of the compound state through channel spins 2 and 3 respectively. The actual β for the level must lie between these two values. In the cases where only one channel spin is possible, β is unique and is given in the appropriate column. The calculation of these factors is described in Appendix B. See text pp. 36, 38, 71.

Table IV

Angular Distribution Factors

J^{π}	ℓ	ℓ'	β_2	β_3
0^+	2	forbidden		
0^-	3	1		1.00
1^+	2	0	1.00	1.00
1^+	2	2	0.66	1.10
1^-	1	1	0.93	
1^-	3	1	0.73	1.34
2^+	0	2	1.00	
2^+	2	2	0.84	0.74
2^-	1	1	0.54	1.13
2^-	1	3	0.46	1.31
3^+	0	2		1.00
3^+	2	2	1.09	0.75
3^-	1	3	1.40	0.50
4^+	2	4	0.53	1.00
4^-	1	3		1.45

Table V. Barrier factor coefficients. The coefficients a_n, b_n, and c_n have been used to fit polynomials in E to the barrier factors in two energy regions. See text pp. 38, 53.

Table V

Barrier Factor Coefficients

n	a_n	b_n	c_n
0	-4.974×10^{3}	-4.586×10^{3}	1.126
1	1.902×10^{1}	1.564×10^{1}	1.011×10^{-2}
2	-2.723×10^{-2}	-1.957×10^{-2}	3.093×10^{-5}
3	1.735×10^{-5}	1.088×10^{-5}	
4	-4.001×10^{-9}	-2.197×10^{-9}	

Table VI. Partial widths for the two broad resonances occurring at c.m. energies of 1035 and 1203 kev (lab energies of 1096 and 1274 kev) as determined by the fitting of a simple sum of two Breit-Wigner expressions to the experimental data. The c.m. resonance energies E_r and the partial widths Γ_p and Γ_α are given in kev. The widths in Group I were those used in obtaining the dashed curve shown in Fig. 22. Group II or a combination of I_a with II_b or I_b with II_a could also have been used without destroying the fit. See text pp. 39, 47, 55.

Table VI

Partial Widths

Group	E_r	θ_p^2	θ_α^2	Γ_p	Γ_α
I_a	1035	0.013	0.470	2.5	82.5
I_b	1203	0.194	0.060	64.5	14.5
II_a	1035	0.430	0.015	82.4	2.6
II_b	1203	0.044	0.267	14.5	64.5

Table VII. Summary of level parameters as determined in the present experiment. The quantity $\beta g \Gamma_\alpha \Gamma_p / \Gamma$ is given in ev and all other quantities are expressed in kev. See text pp. 39, 43, 45, 47, 55.

Table VII

Summary of Level Parameters

E_r(Lab)	E_r(c.m.)	E_{ex}	$\beta g \frac{\Gamma_\alpha \Gamma_p}{\Gamma}$	Γ(c.m.)
518 ± 2	489 ± 2	6086	50 ± 5	<2.0
672 ± 2	635 ± 2	6232	43 ± 4	<2.0
747 ± 3	705 ± 3	6302	100 ± 10	3.1 ± 1.4
825 ± 3	779 ± 3	6376	23 ± 2	<4.5
927 ± 3	875 ± 3	6472	39 ± 4	<1.2
1096 ± 6	1035 ± 6	6632		85 ± 5
1101 ± 4	1040 ± 4	6637	36 ± 4	<3.0
1247 ± 5	1177 ± 5	6774	150 ± 16	10 ± 3
1274 ± 5	1203 ± 5	6800		79 ± 5
1335 ± 10	1260 ± 10	6857		

Table VIII. Straggling-integral parameters needed in the calculation described in Appendix D. E_r, E_{2r}, λ_r, and β are expressed in kev. ϵ_{1r} is given in 10^{-5} ev-cm^2, and $\epsilon_{1r}/\epsilon_{2r}$ and α are dimensionless. See text pp. 41, 78.

Table VIII

Straggling-Integral Parameters

E_r(Lab)	ϵ_{1r}	$\epsilon_{2r}/\epsilon_{1r}$	λ_r	α	β	E_{2r}
518.5	26.03	4.950	0.3613	0.6429	783.9	1155.7
672.4	22.51	5.664	0.4176	0.6870	731.2	1239.9
747.2	21.20	5.981	0.4434	0.7137	676.0	1281.3
825.0	19.99	6.298	0.4703	0.6101	761.9	1324.5
927.1	18.72	6.661	0.5022	0.5070	880.3	1381.5
1101.3	16.92	7.228	0.5556	0.5234	819.1	1479.3
1246.7	15.70	7.643	0.5987	0.5061	869.9	1561.3

Table IX. Width contributions to the yield curves given in Figs. 12 to 18. σ_p^2 and σ_α^2 are given in kev^2 and the remaining quantities are expressed in kev. The calculation of several of these width contributions is described in Appendix D. See text pp. 40, 73, 83 ff.

Table IX

Width Contributions

E_r(Lab)	Δ_θ	ξ_1	Δ_m	σ_p^2	σ_α^2	Δ_{sum}	Δ_t
518	0.95	3.79	3.72	1.90	0.31	4.3	4.5
672	0.98	3.57	3.49	2.39	0.31	4.5	4.6
747	0.95	3.47	3.38	3.02	0.35	4.9	4.9
825	1.0	3.41	3.38	3.32	0.33	5.0	5.1
927	1.1	3.48	3.51	1.78	0.16	4.0	4.1
1101	1.0	3.29	3.31	5.17	0.22	5.9	5.9
1247	1.1	3.37	3.39	3.79	0.25	5.3	5.2

Table X. Calculated area of narrow resonances. The resonance energy E_r is given in kev. The other two quantities are given in cm^{-2} and are proportional to the area under a yield curve for a narrow resonance. Both the case of straggling of the incident and outgoing particle and of no straggling are given. The calculation of these quantities is described in Appendix D.

See text p. 80f.

Table X

Calculated Area of Narrow Resonances

E_r (Lab)	$\frac{A_Y}{\pi \sigma_r \Gamma/2}$ (straggling)	$\frac{a_y}{\pi \sigma_r \Gamma/2}$ (no straggling)
518.5	0.5695×10^{16}	0.5699×10^{16}
672.4	0.6205	0.6201
747.2	0.6387	0.6391
825.0	0.6809	0.6808
927.1	0.7470	0.7458
1101.3	0.7890	0.7905
1246.7	0.8705	0.8701

Table XI. Reported c.m. widths of the F^{18} levels at E_{ex} = 6632 and 6800 kev. Previous determinations of these widths are compared with those of the present work. Widths are given in kev. See text p. 45.

Table XI

Reported C. M. Widths of the F^{18} Levels at E_{ex} = 6632 and 6800 kev

Source	6632-kev Width	6800-kev Width
(Heydenburg, 1953)	27 ± 4	93 ± 8
(Ahnlund, 1957)		90
(Herring, 1958b)	93 ± 5	101 ± 5
(Kashy, 1958)	59 ± 8	74 ± 8
Present work	85 ± 5	79 ± 5

Table XII. Stellar reaction rates. Various reaction rates as a function of temperature in millions of degrees are given. The calculations are described in Section VI. See text p. 60f.

Table XII

Stellar Reaction Rates

T_6	$\log \frac{P_c}{H^1 O^{17}}$ (cons.)	$\log \frac{P_c}{H^1 O^{17}}$ (dest.)	$\log \frac{P_r}{H^1 O^{17}}$	$\log \frac{P_{17}}{H^1 O^{17}}$ (cons.)	$\log \frac{P_{17}}{H^1 O^{17}}$ (dest.)	$\log \frac{P_{16}}{H^1 O^{16}}$	$\log \frac{O^{17} P_{16}}{O^{16} P_{17}}$ (cons.)	$\log \frac{O^{17} P_{16}}{O^{16} P_{17}}$ (dest.)
5.0	-54.770	-55.397	-87.981	-54.770	-55.397	-56.901	-2.130	-1.504
10.0	-46.387	-47.524	-55.659	-46.387	-47.524	-48.355	-1.968	-0.831
12.5	-44.051	-45.521	-49.249	-44.051	-45.521	-46.007	-1.955	-0.486
15.0	-42.272	-43.828	-44.998	-42.271	-43.797	-44.219	-1.947	-0.421
20.0	-39.555	-40.514	-39.723	-39.330	-39.658	-41.613	-2.282	-1.954
25.0	-37.550	-38.222	-36.591	-36.546	-36.574	-39.763	-3.216	-3.188
30.0			-34.525			-38.353	-3.828	-3.828
35.0			-33.065			-37.229	-4.164	-4.164
40.0			-31.981			-36.302	-4.321	-4.321
45.0			-31.148			-35.521	-4.373	-4.373

Figure 1. Proton counts vs fluxmeter setting V_m for the elastic scattering of protons by Ni. The figure compares a clean Ni target with an oxided Ni target. The proton bombarding energy E_{1B} was 1.005 Mev. See text pp. 8, 10f.

Figure 2. α vs μ as determined from data in Fig. 1. α and μ are defined in Eqs. (3) and (4). See text p. 10f.

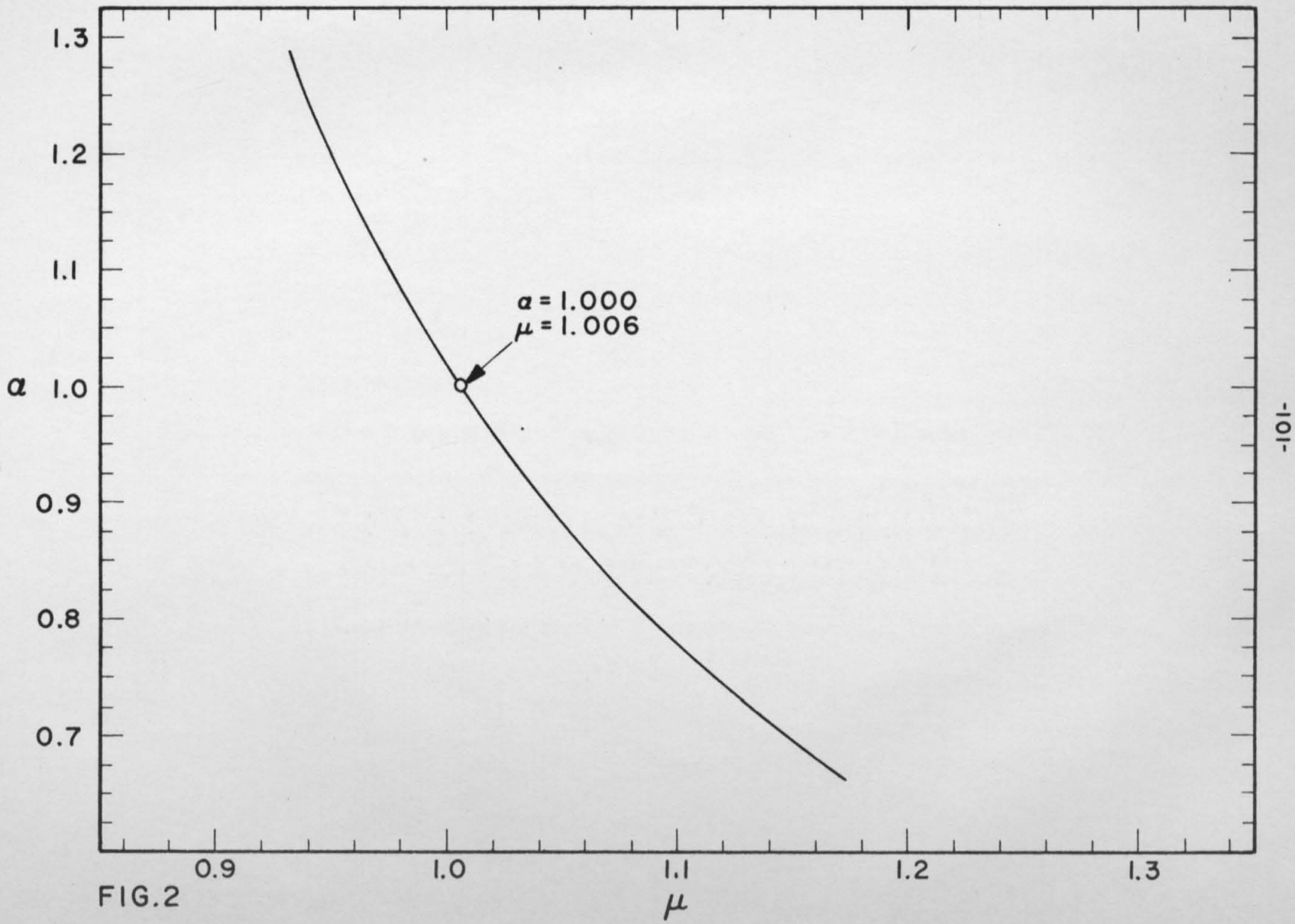

FIG.2

Figure 3. Alpha-particle pulse height spectrum for protons on NiO. The solid histogram is that obtained with a target enriched in O^{17} and the dashed histogram is that obtained with a target made with natural oxygen. For this spectrum E_{1B} = 1.342 Mev, V_m = 498.6 mv, and Q = 276 μcoul. See text p. 17.

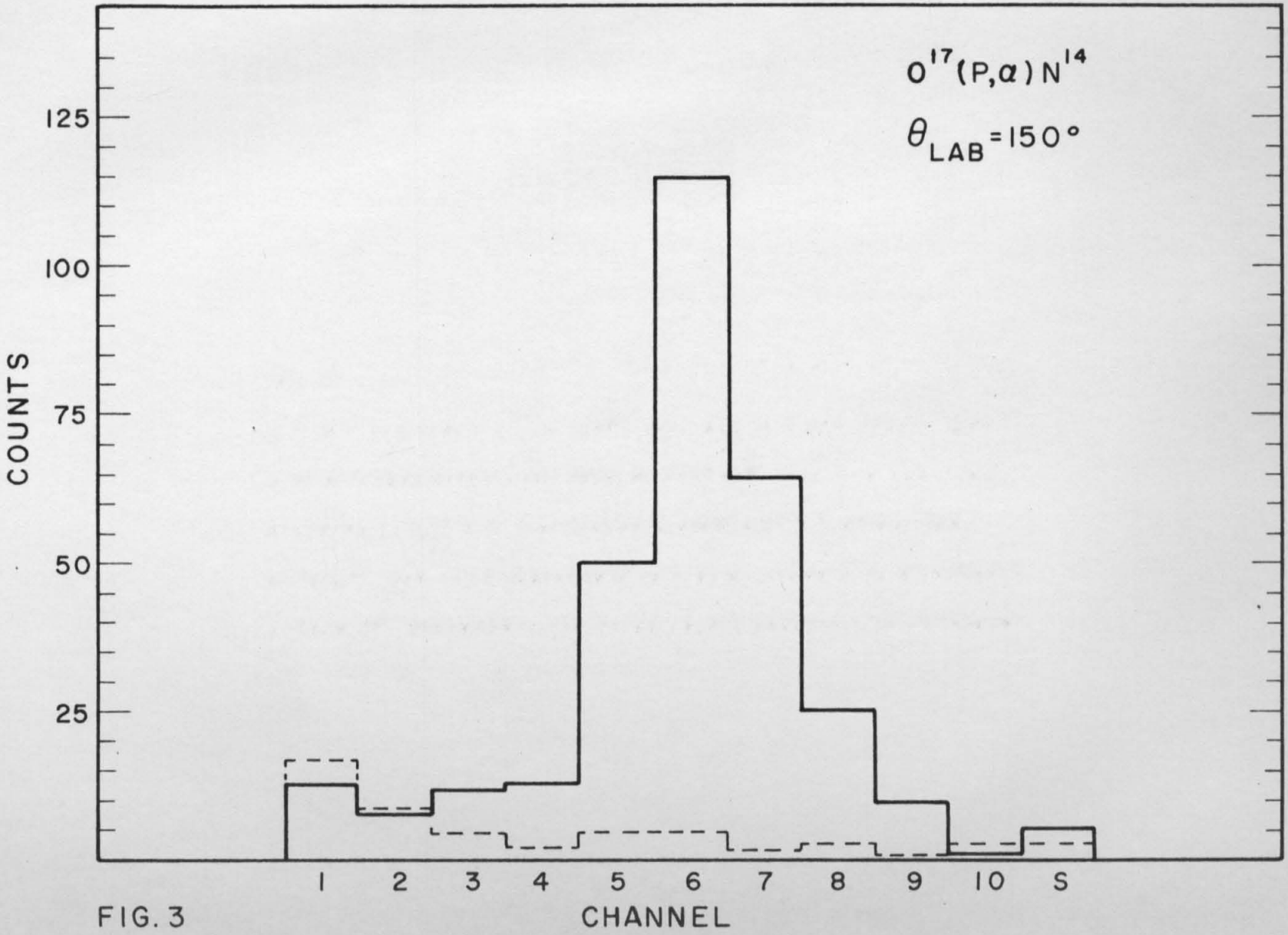
$O^{17}(P,\alpha)N^{14}$
$\theta_{LAB}=150°$
COUNTS
125
100
75
50
25
1
2
3
4
5
6
7
8
9
10
S
CHANNEL

FIG. 3

Figure 4. Uncorrected data taken at the 672-kev resonance showing counts per integration vs analyzer potentiometer setting V_e. Data from both the enriched target and natural target are shown. These data were used to obtain the yield curve of Fig. 13. See text pp. 18, 44.

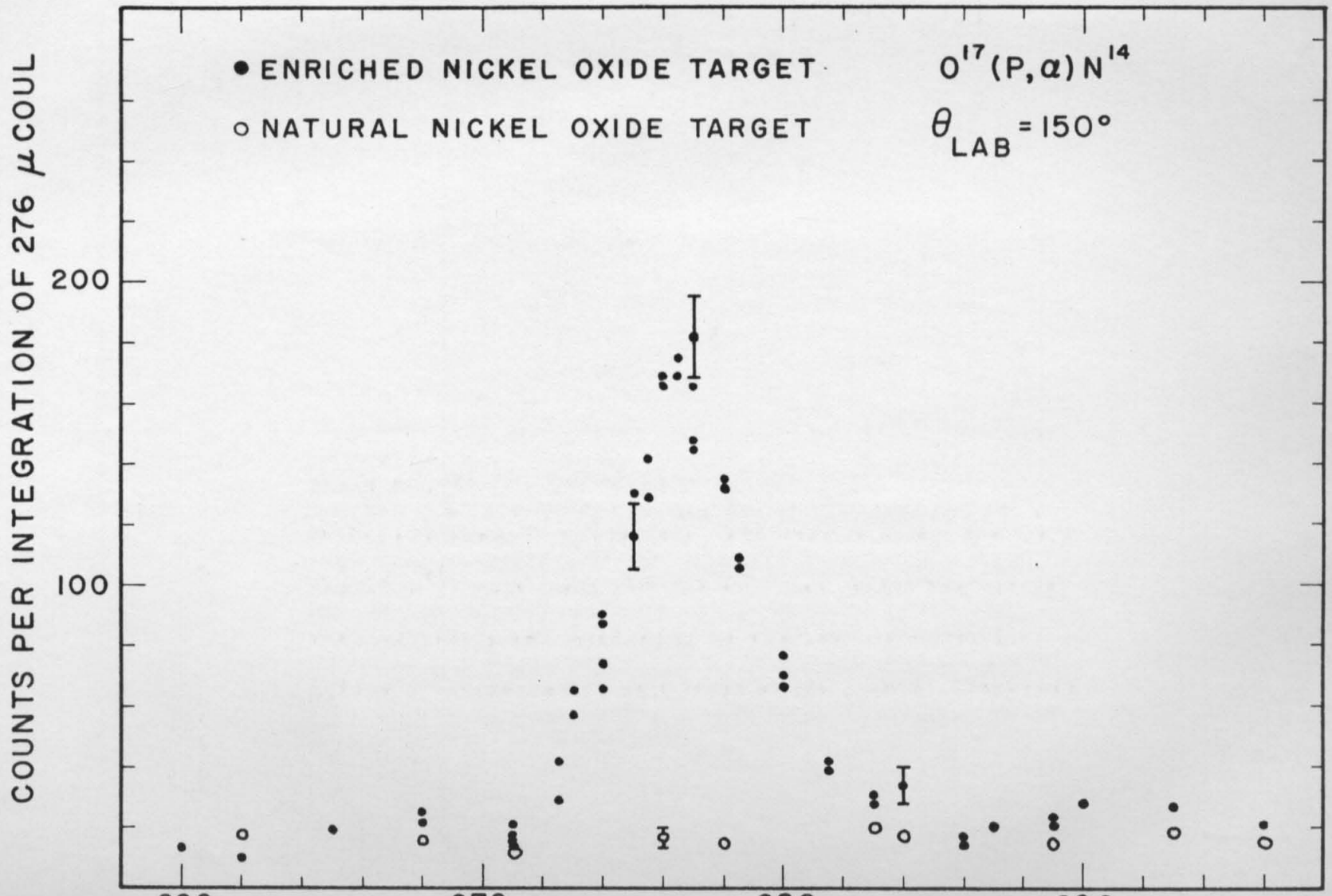
● ENRICHED NICKEL OXIDE TARGET
○ NATURAL NICKEL OXIDE TARGET
$O^{17}(P,\alpha)N^{14}$
$\theta_{LAB} = 150°$
COUNTS PER INTEGRATION OF 276 μ COUL
200
100
.660
.670
.680
.690
ELECTROSTATIC ANALYZER POTENTIOMETER SETTING (DECI V.)

FIG. 4

Figure 5. Iron oxide target profile showing alpha-particle counts vs fluxmeter setting V_m. Data from both the target back and the oxided target front are shown. These data were used to obtain Fig. 19. For this profile $E_{1B} = 1.280$ Mev and Q = 88.6 μcoul for each point. See text pp. 19, 22, 30.

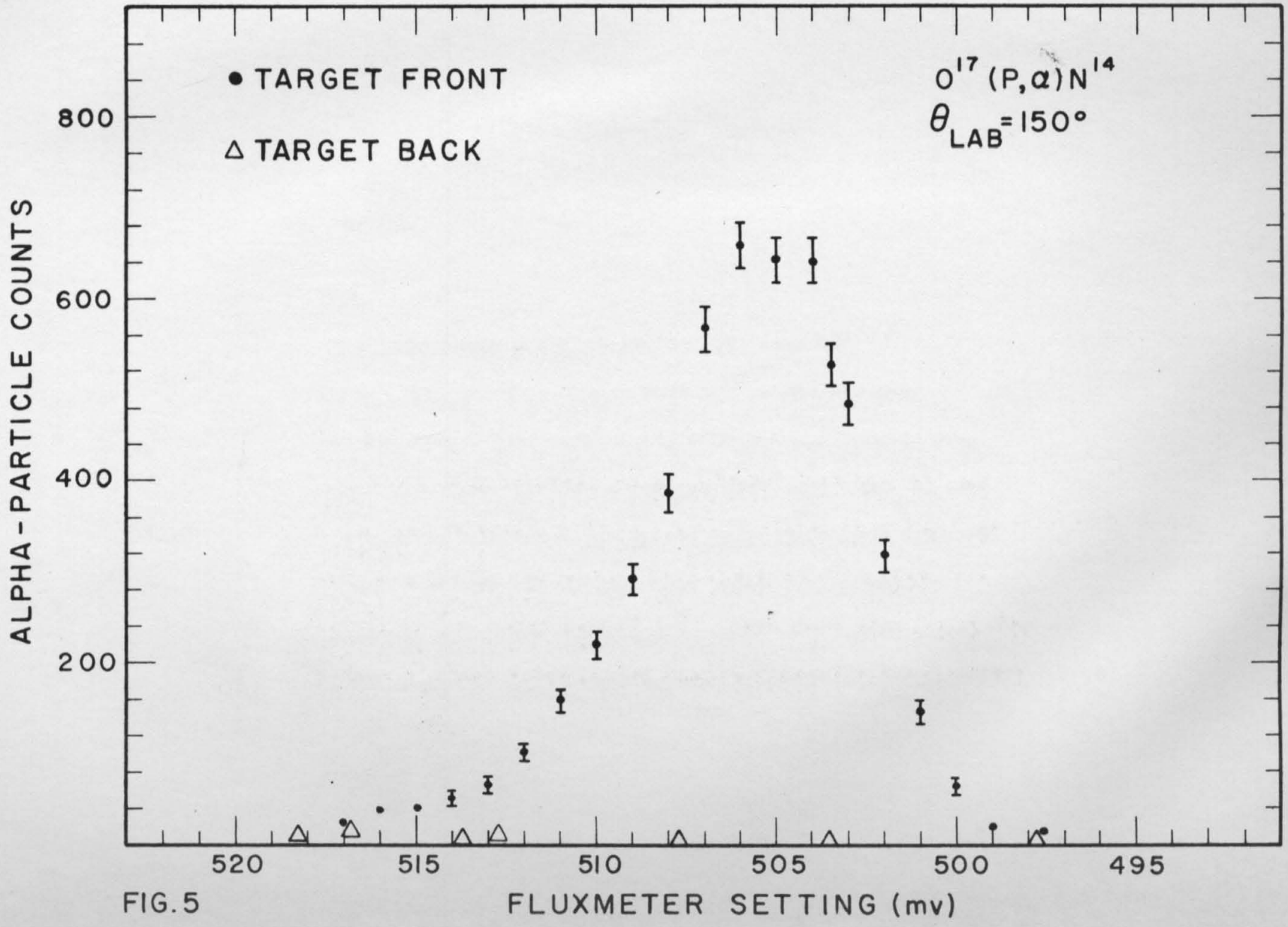
● TARGET FRONT
△ TARGET BACK
$O^{17}(P,\alpha)N^{14}$
$\theta_{LAB}=150°$
ALPHA-PARTICLE COUNTS
800
600
400
200
520
515
510
505
500
495
FLUXMETER SETTING (mv)

FIG. 5

Figure 6. Iron oxide target profile showing alpha-particle counts vs fluxmeter setting V_m. The circles, triangles, and square are data taken with different reference profiles. The error bars have been omitted from the data obtained when the back of the target was bombarded. The data in this figure were used to obtain Fig. 20. For this profile E_{1B} = 854 kev and Q = 2850 μcoul for each point. See text pp. 20, 22, 31.

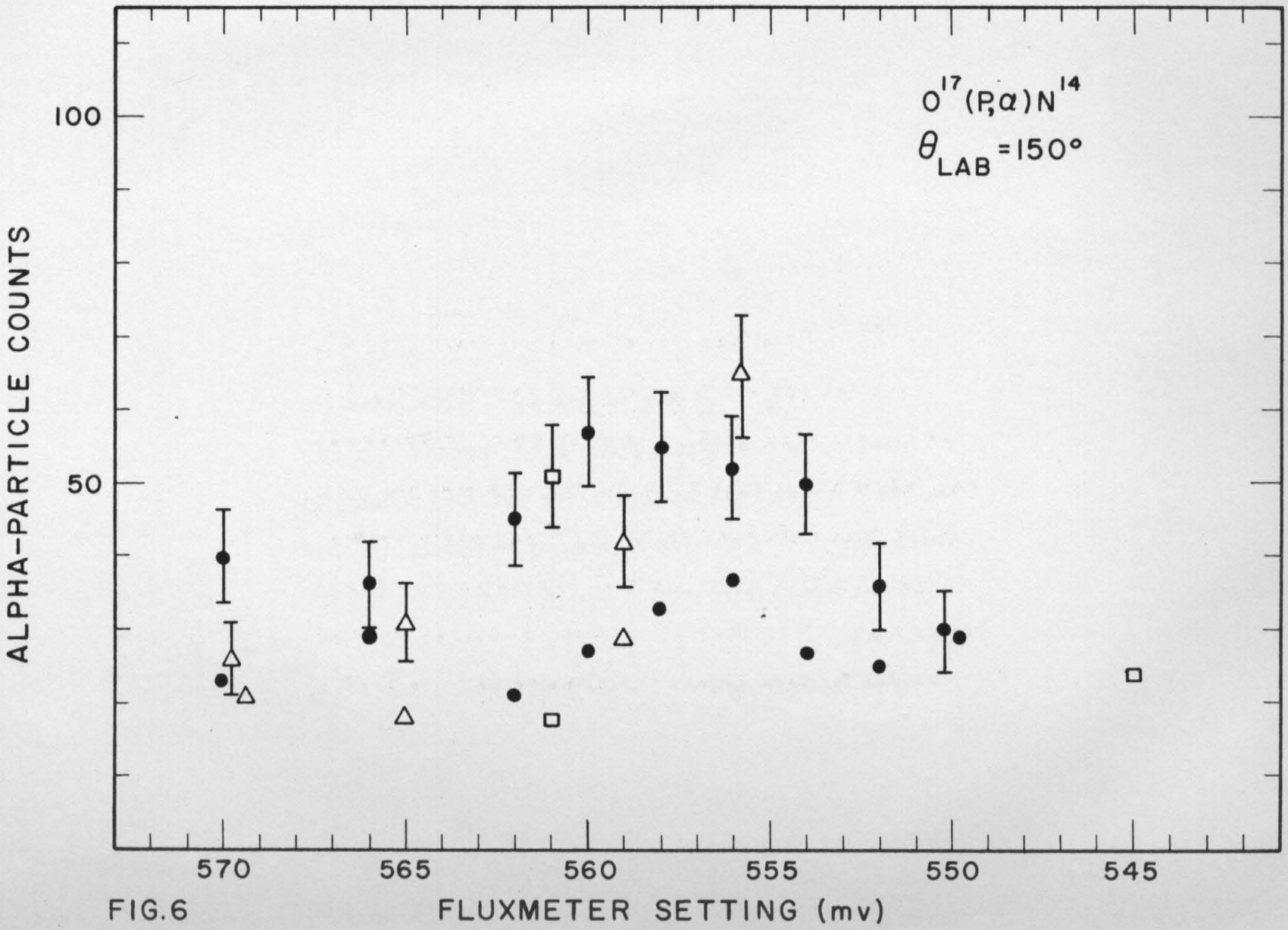
$O^{17}(P,\alpha)N^{14}$
$\theta_{LAB}=150°$
ALPHA-PARTICLE COUNTS
100
50
570
565
560
555
550
545
FLUXMETER SETTING (mv)

FIG.6

Figure 7. Iron oxide target profile showing alpha-particle counts vs fluxmeter setting V_m. Data from the target back and the oxided target front are shown. For this profile E_{1B} = 1.005 Mev and Q = 713 μcoul for each point. See text p. 20f.

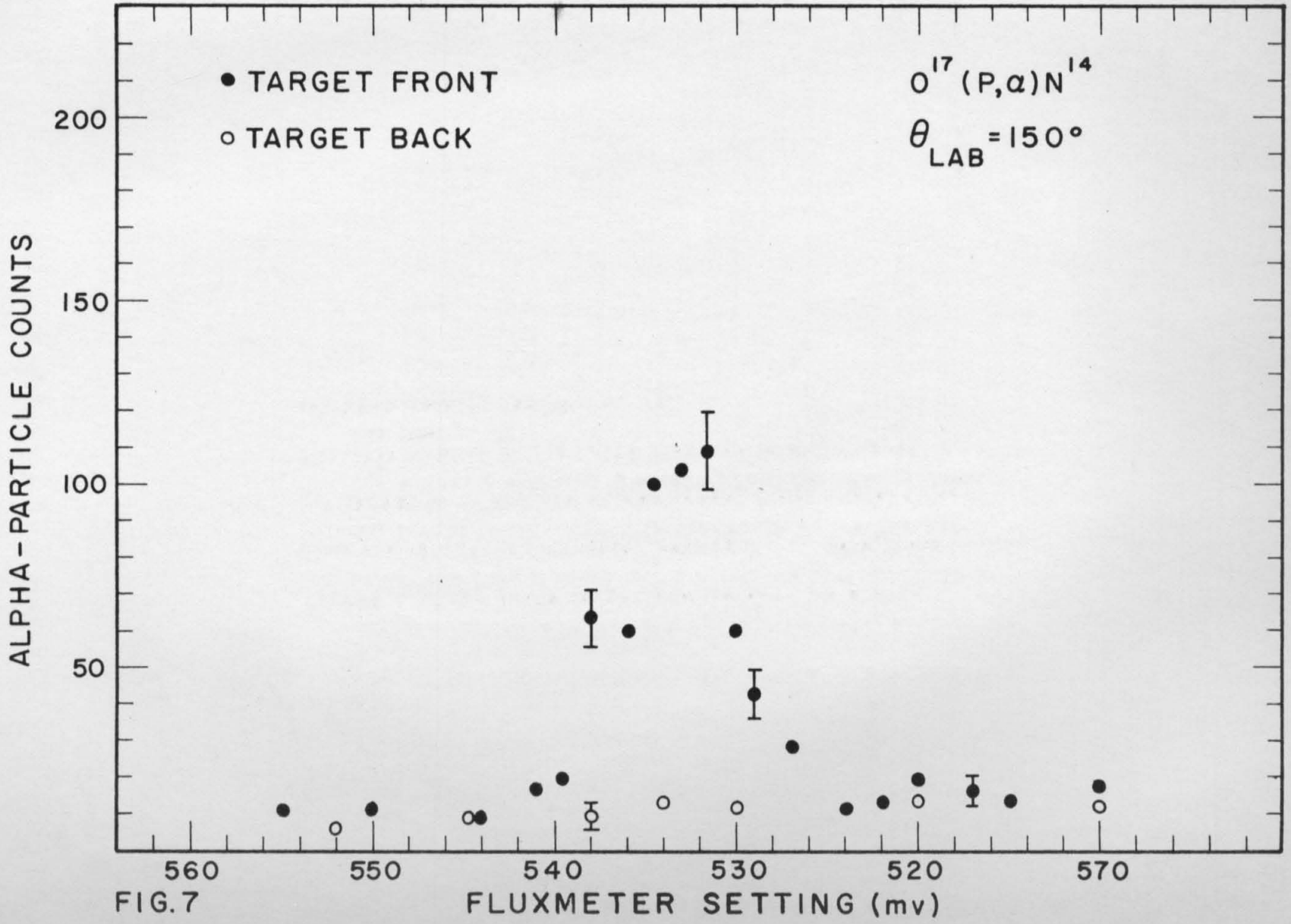
● TARGET FRONT
○ TARGET BACK
$O^{17}(P,\alpha)N^{14}$
θ_{LAB} = 150°
ALPHA-PARTICLE COUNTS
200
150
100
50
560
550
540
530
520
570
FLUXMETER SETTING (mv)

FIG. 7

Figure 8. Alpha-particle pulse height spectrum for protons on the iron oxide target. The solid histogram is for the target front and the dashed histogram is for the target back. For this spectrum E_{1B} = 955 kev, V_m = 544.0 mv, and Q = 1430 μcoul for each point.

See text p. 22.

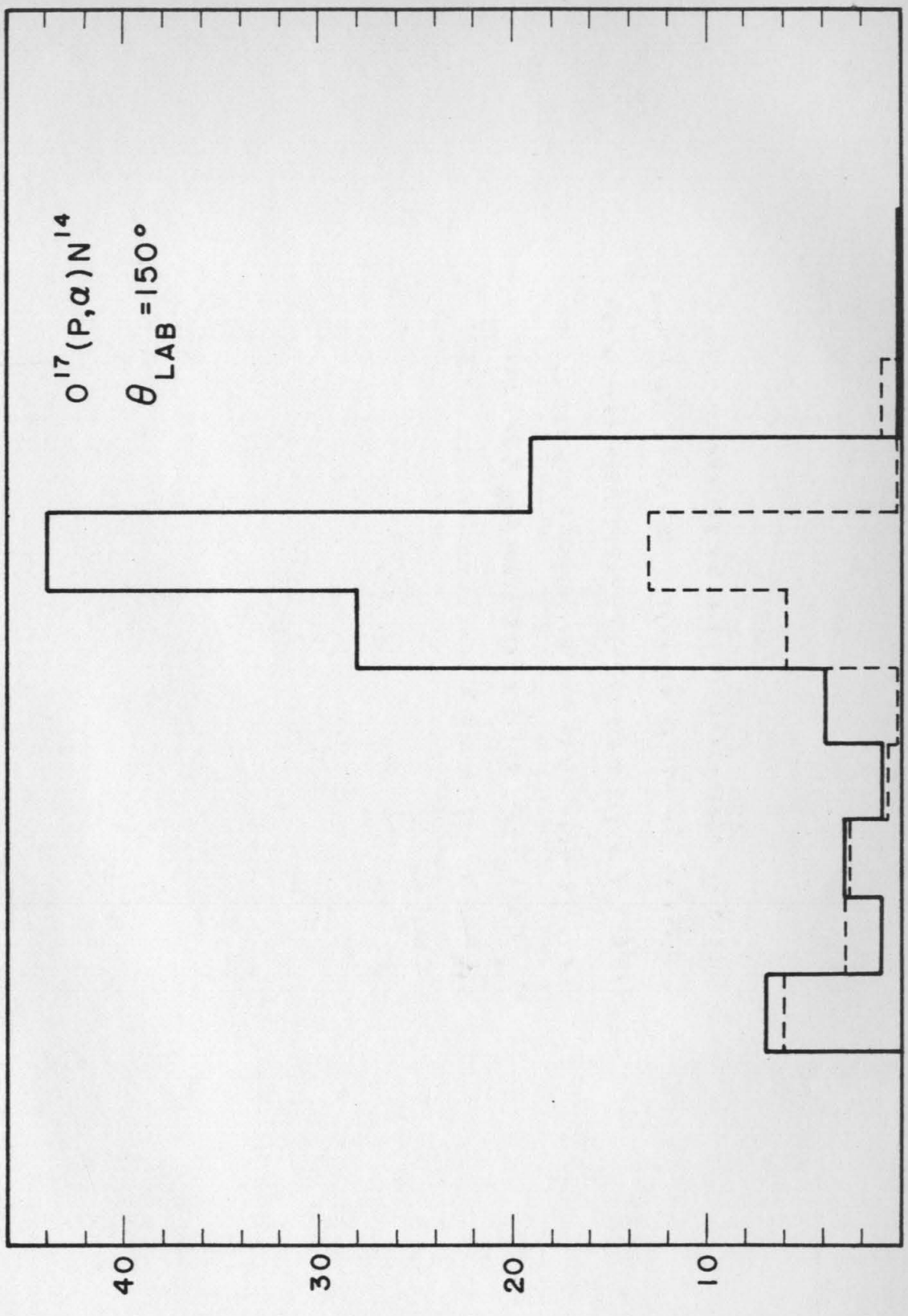
$O^{17}(P,\alpha)N^{14}$
$\theta_{LAB}=150°$
COUNTS
10
20
30
40
CHANNEL
1
2
3
4
5
6
7
8
9
10
S

FIG. 8

Figure 9. Alpha-particle pulse height spectrum for protons on the iron oxide target. The solid histogram is for the target front and the dashed histogram is for the target back. For this spectrum E_{1B} = 854 kev, V_m = 560.0 mv, and Q = 2850 μcoul for each point.

See text p. 22.

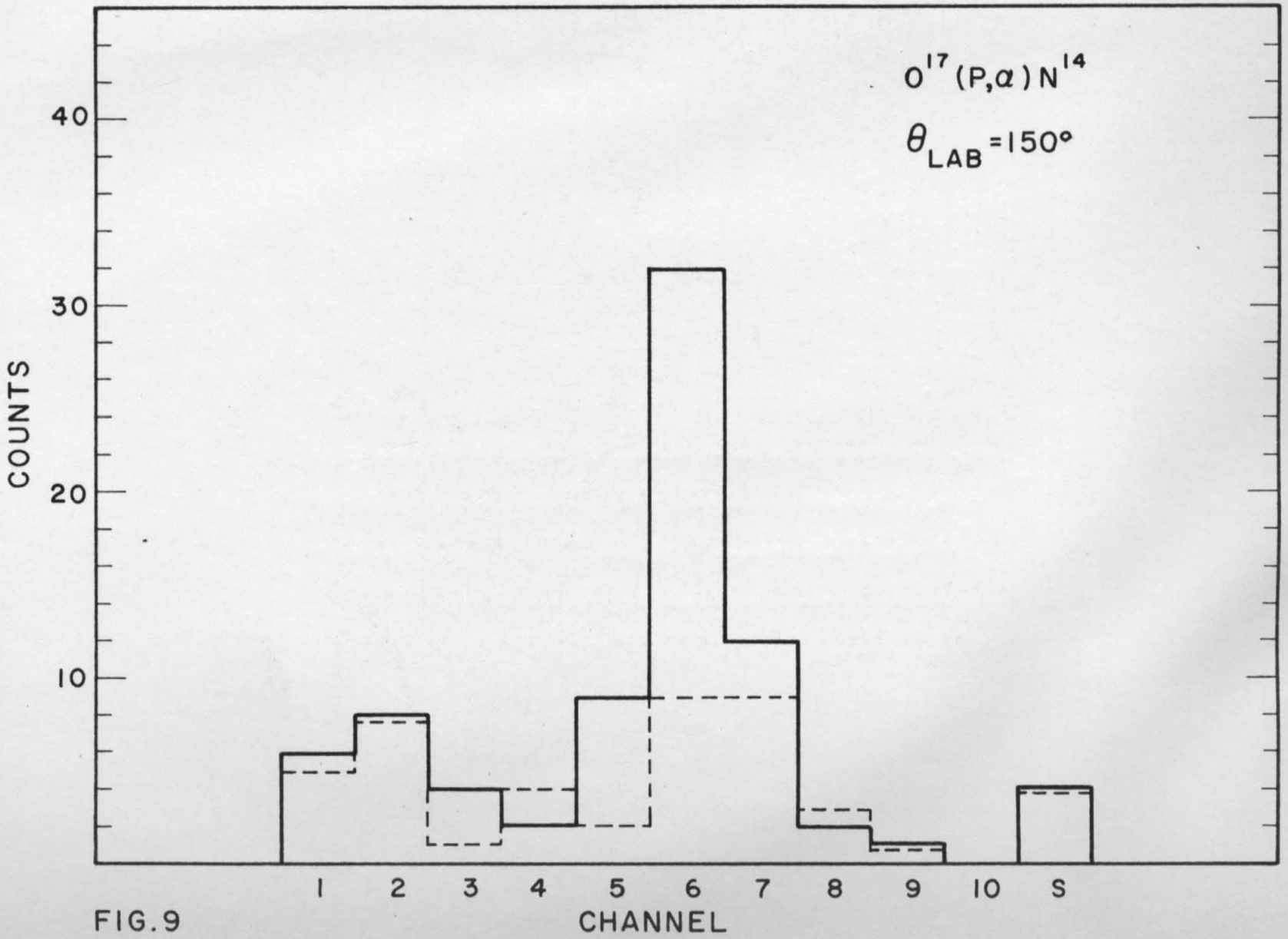
$O^{17}(P,\alpha)N^{14}$
$\theta_{LAB}=150°$
COUNTS
40
30
20
10
1
2
3
4
5
6
7
8
9
10
S
CHANNEL

FIG. 9

Figure 10. Alpha-particle charge equilibrium fraction in solids. $F_{2\infty}$, $F_{1\infty}$, and $F_{0\infty}$ are the equilibrium fractions of He^{++}, He^{+}, and He respectively. Data are from the review by Allison (1958). See text p. 26.

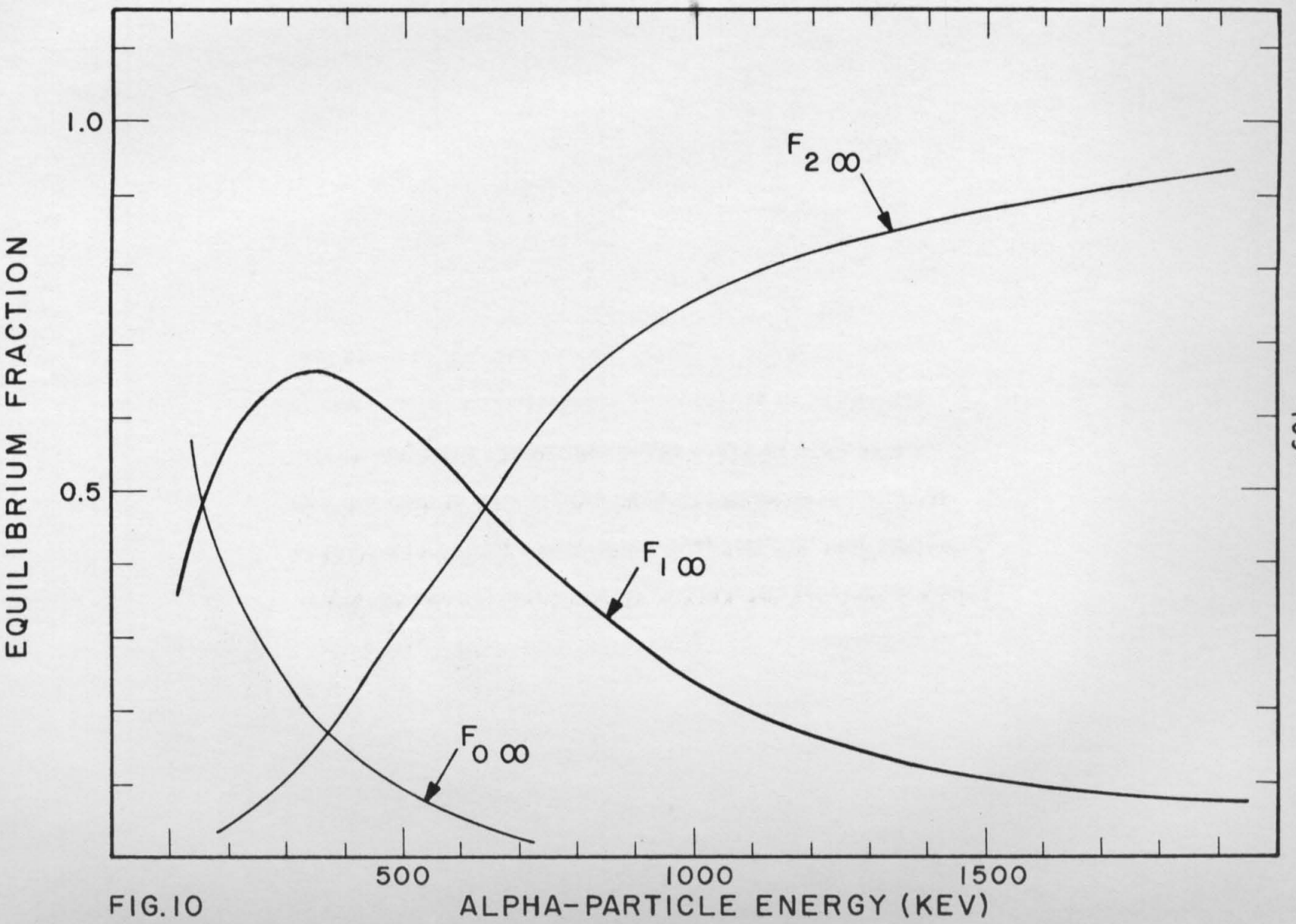
EQUILIBRIUM FRACTION
1.0
0.5
$F_{2\infty}$
$F_{1\infty}$
$F_{0\infty}$
500
1000
1500
ALPHA-PARTICLE ENERGY (KEV)

FIG. 10

Figure 11. Laboratory differential cross section $\sigma_L(\theta_L)$ vs proton energy E_1. The experimental resolution was about 5 kev due to spectrometer resolution and straggling, and the data in this figure have not been corrected for this resolution. Data from both types of targets are shown. The ordinate scale is accurate to 10%. See text pp. 24, 29, 31, 36, 44, 47.

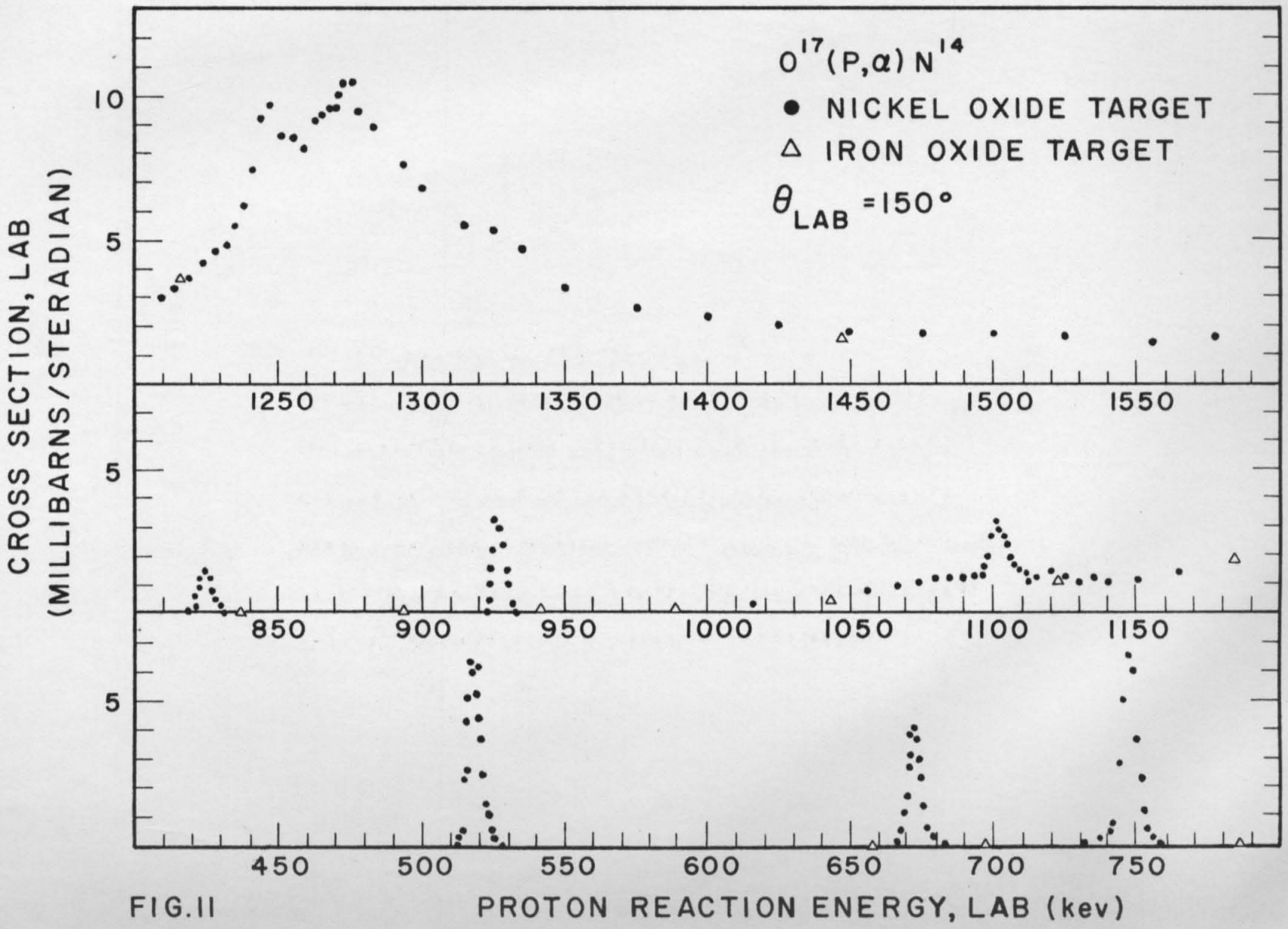
$O^{17}(P,\alpha)N^{14}$
● NICKEL OXIDE TARGET
△ IRON OXIDE TARGET
θ_{LAB} =150°
CROSS SECTION, LAB
(MILLIBARNS/STERADIAN)
10
5
5
5
1250
1300
1350
1400
1450
1500
1550
850
900
950
1000
1050
1100
1150
450
500
550
600
650
700
750
PROTON REACTION ENERGY, LAB (kev)

FIG.11

Figure 12. Laboratory alpha-particle yield Y_L vs proton bombarding energy E_{1B} near the 518-kev resonance. The error bars indicate statistical errors only. The dashed curve has been calculated from the theory given in Appendix D. See text pp. 29, 31, 39, 41f., 47, 77, 79, 84.

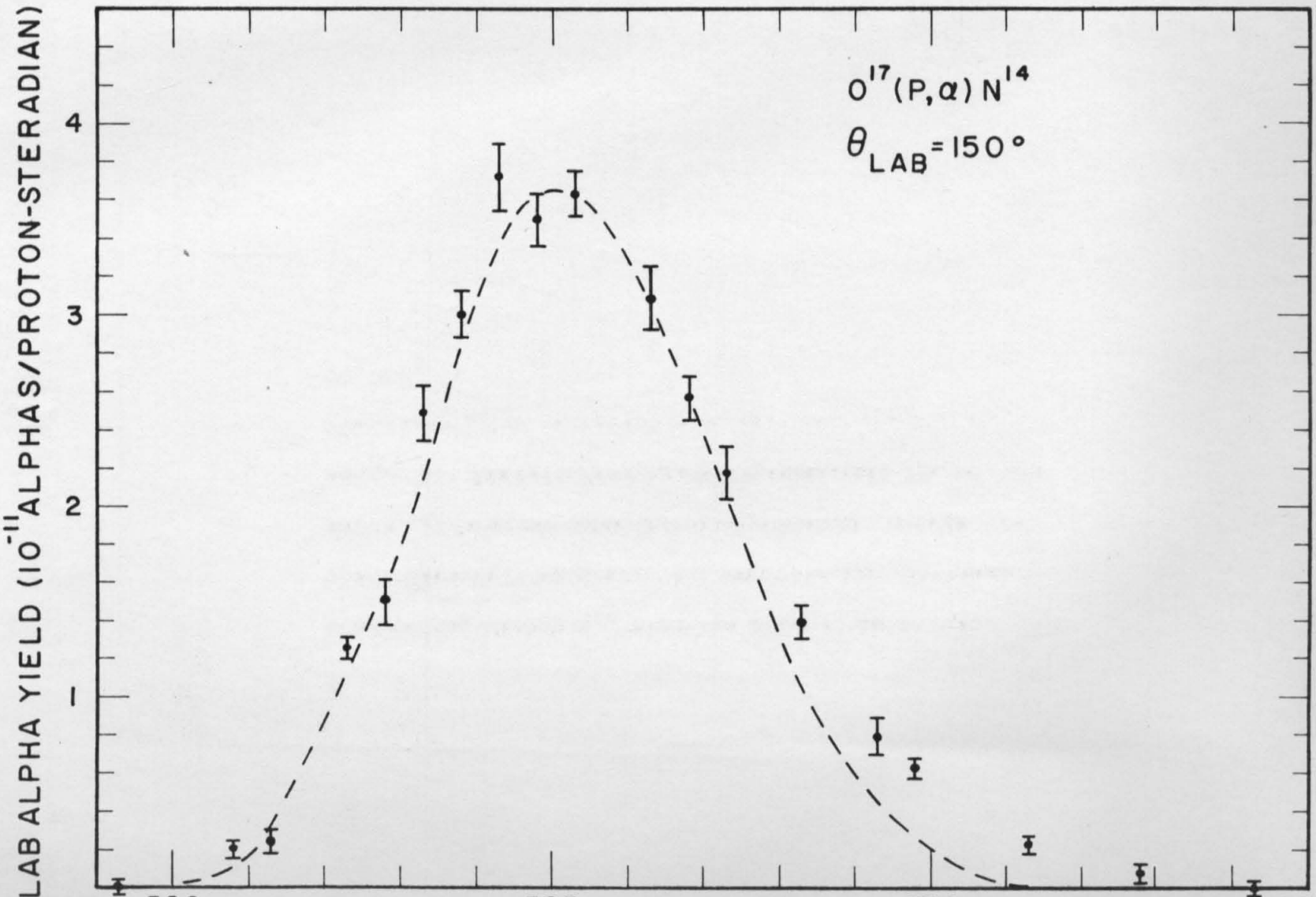
$O^{17}(P,\alpha)N^{14}$
$\theta_{LAB}=150°$
LAB ALPHA YIELD (10^{-11} ALPHAS/PROTON-STERADIAN)
4
3
2
1
520
525
530
535
PROTON BOMBARDING ENERGY, LAB (kev)

FIG.12

Figure 13. Laboratory alpha-particle yield Y_L vs proton bombarding energy E_{1B} near the 672-kev resonance. The error bars indicate statistical errors only. The dashed curve has been calculated from the theory given in Appendix D. See text pp. 29, 31, 39, 41f., 47, 77, 79, 84.

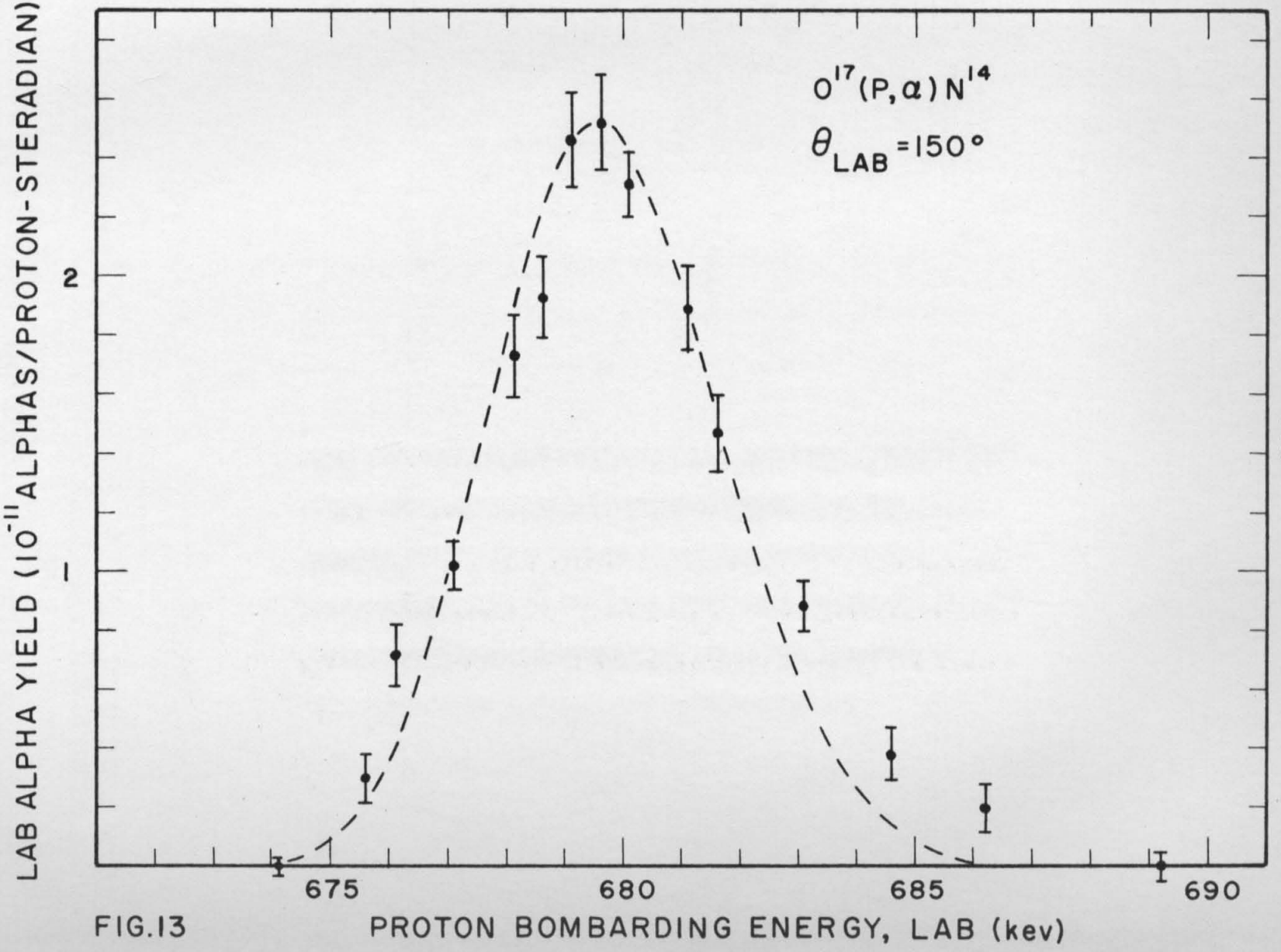
LAB ALPHA YIELD (10^{-11} ALPHAS/PROTON-STERADIAN)
2
1
$O^{17}(P,\alpha)N^{14}$
θ_{LAB} = 150°
675
680
685
690
PROTON BOMBARDING ENERGY, LAB (kev)

FIG.13

Figure 14. Laboratory alpha-particle yield Y_L vs proton bombarding energy E_{1B} near the 747-kev resonance. The error bars indicate statistical errors only. The dashed curve has been calculated from the theory given in Appendix D. See text pp. 29, 31, 39, 41f., 47, 77, 79, 84.

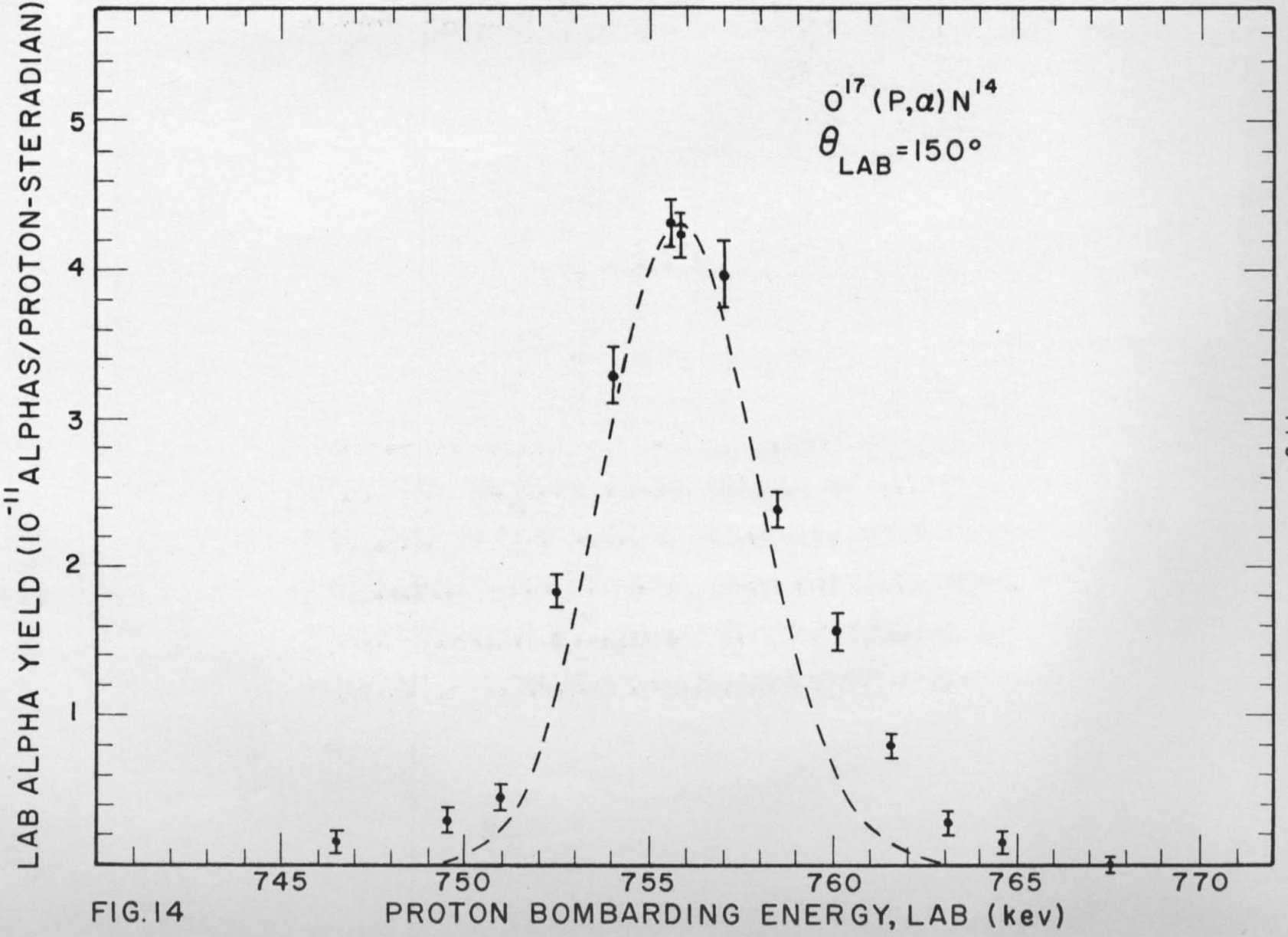
$O^{17}(P,\alpha)N^{14}$
$\theta_{LAB}=150°$
LAB ALPHA YIELD (10^{-11} ALPHAS/PROTON-STERADIAN)
1
2
3
4
5
745
750
755
760
765
770
PROTON BOMBARDING ENERGY, LAB (kev)

FIG. 14

Figure 15. Laboratory alpha-particle yield Y_L vs proton bombarding energy E_{1B} near the 825-kev resonance. The errors bars indicate statistical errors only. The dashed curve has been calculated from the theory given in Appendix D. See text pp. 29, 31, 39, 41f., 47, 77, 79, 84.

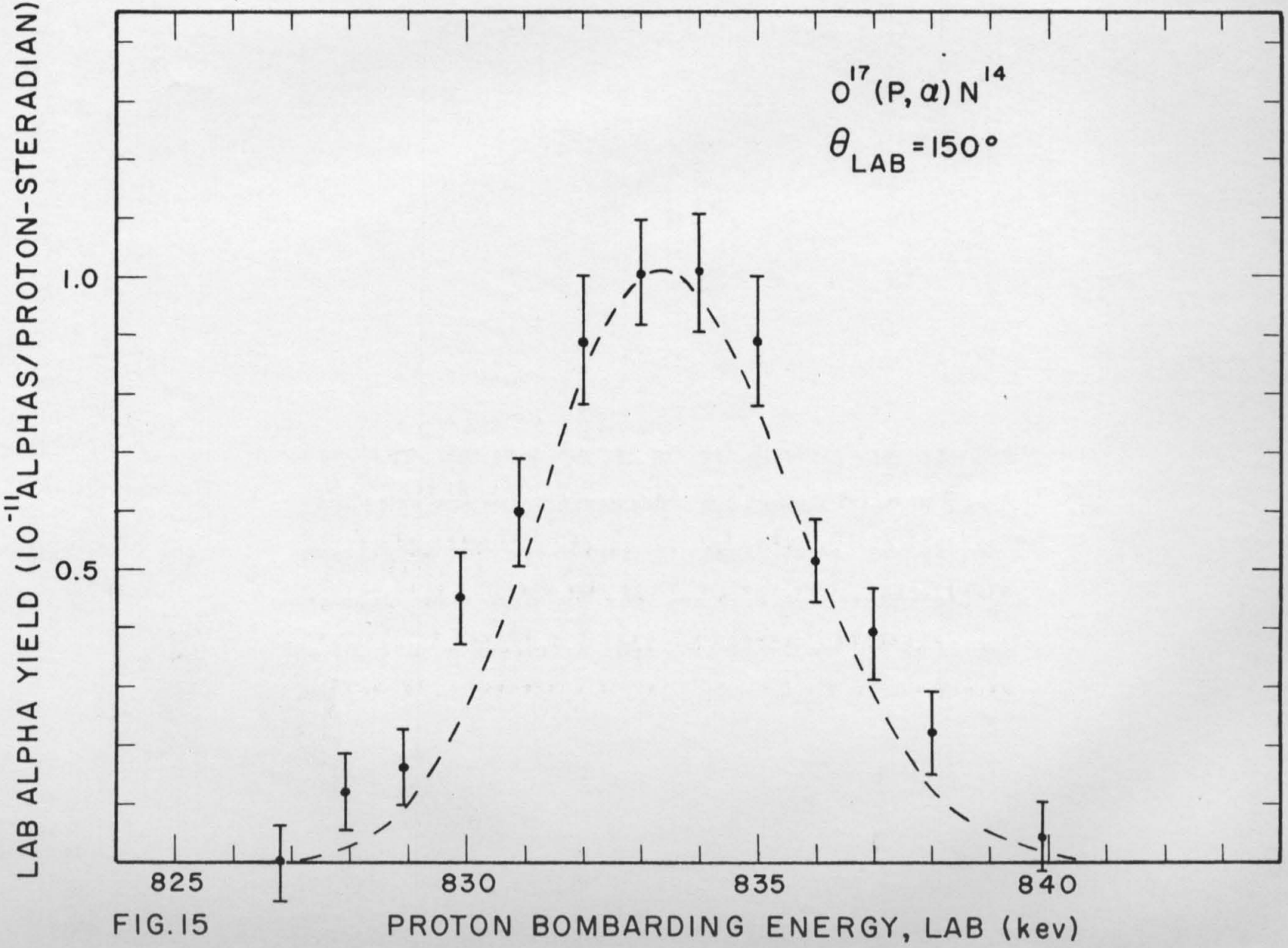
LAB ALPHA YIELD (10^{-11} ALPHAS/PROTON-STERADIAN)
1.0
0.5
$O^{17}(P,\alpha)N^{14}$
$\theta_{LAB} = 150°$
825
830
835
840
PROTON BOMBARDING ENERGY, LAB (kev)

FIG. 15

Figure 16. Laboratory alpha-particle yield Y_L vs proton bombarding energy E_{1B} near the 927-kev resonance. The error bars indicate statistical errors only. The dashed curve has been calculated from the theory given in Appendix D. See text pp. 29, 31, 39, 41f., 47, 77, 79, 84.

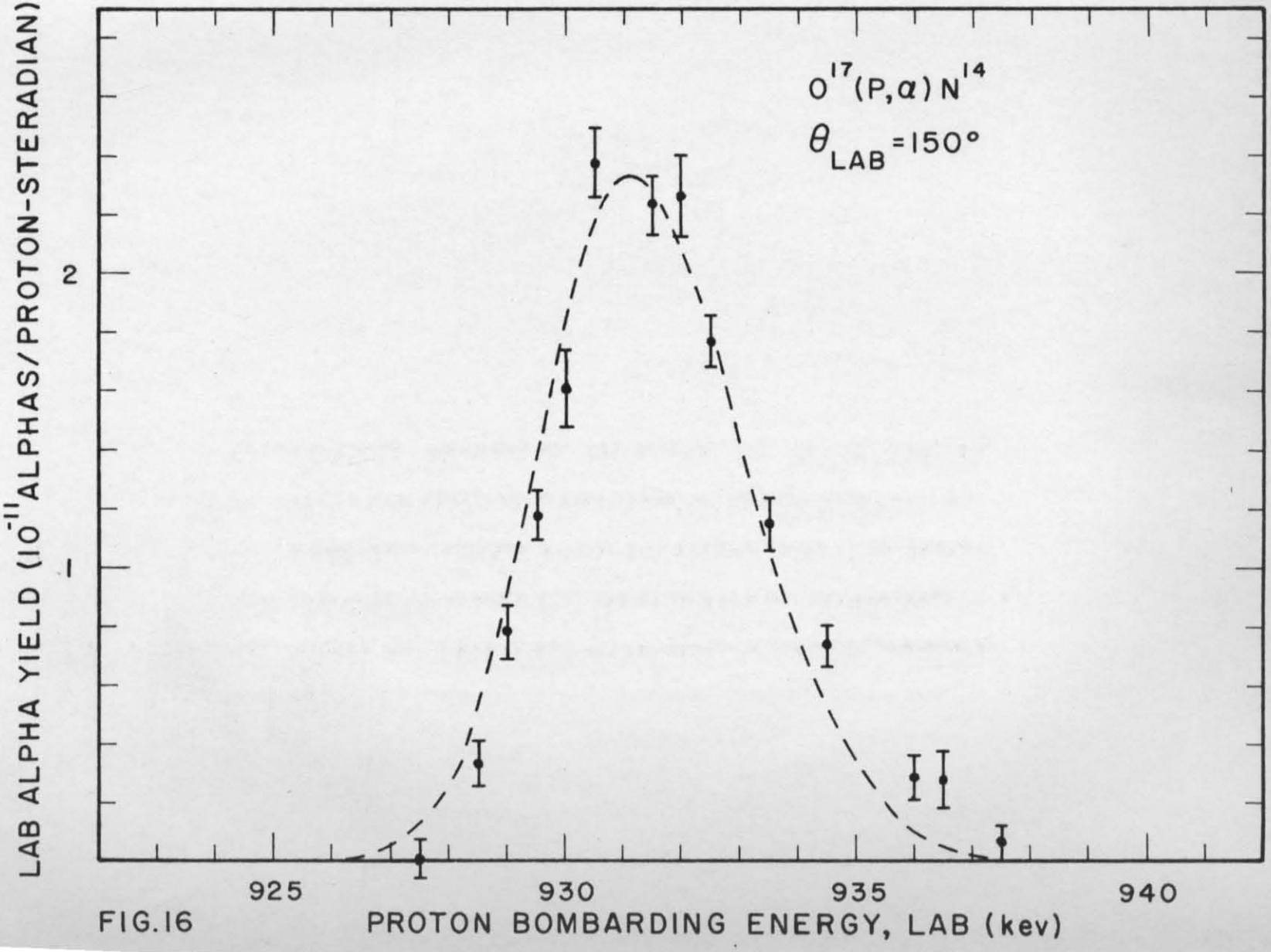
$O^{17}(P,\alpha)N^{14}$
$\theta_{LAB}=150°$
LAB ALPHA YIELD (10^{-11} ALPHAS/PROTON-STERADIAN)
2
1
925
930
935
940
PROTON BOMBARDING ENERGY, LAB (kev)

FIG.16

Figure 17. Laboratory alpha-particle yield Y_L vs proton bombarding energy E_{1B} near the 1101-kev narrow resonance. The error bars indicate statistical errors only. The dashed curve has been calculated from the theory given in Appendix D, and the dotted curve is the assumed background from the broad 1096-kev resonance. See text pp. 29, 31, 37, 41ff., 47, 77, 79, 84.

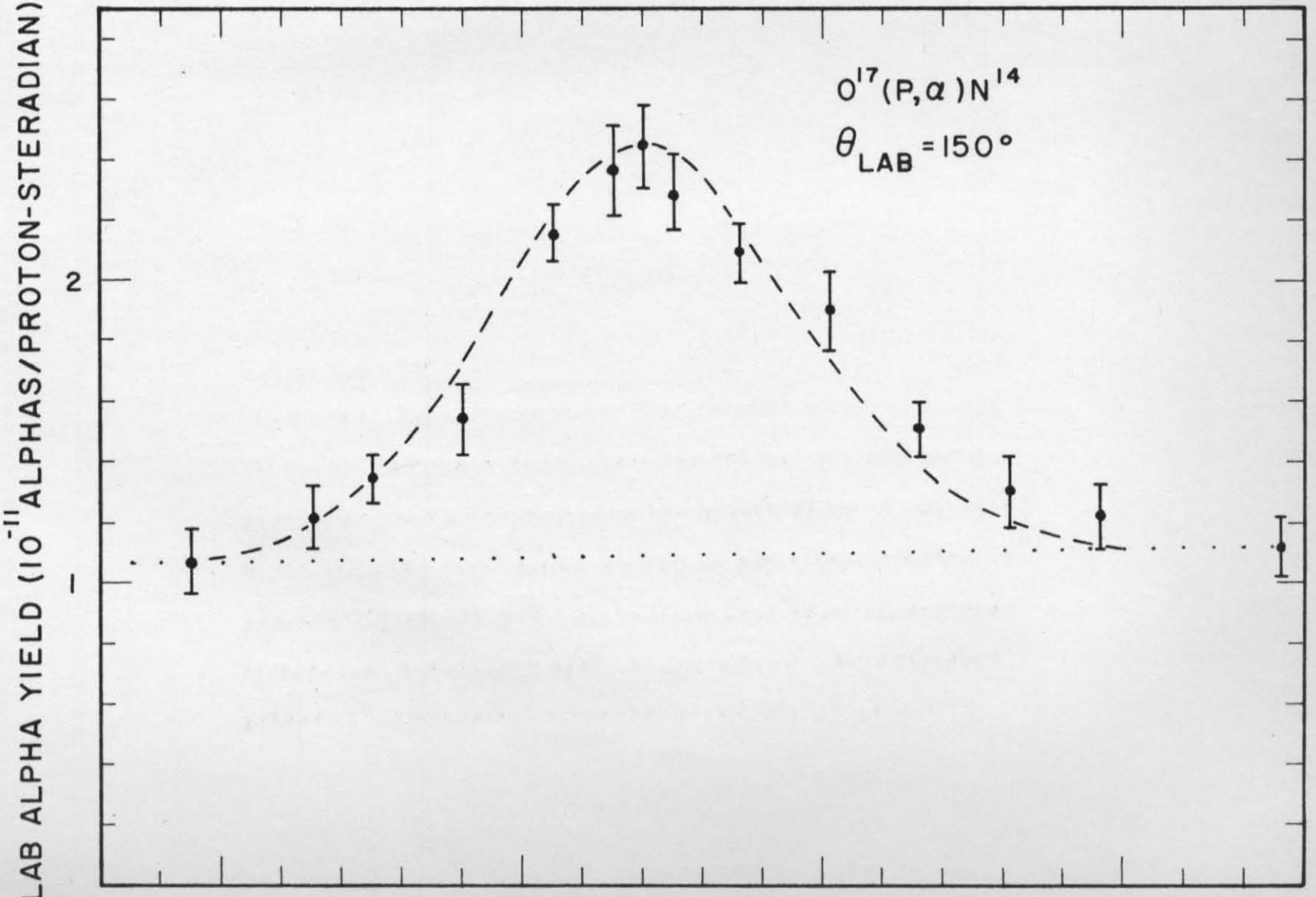
$O^{17}(P,\alpha)N^{14}$
$\theta_{LAB} = 150°$
LAB ALPHA YIELD (10^{-11} ALPHAS/PROTON-STERADIAN)
2
1
1105
1110
1115
1120
PROTON BOMBARDING ENERGY, LAB (kev)

FIG.17

Figure 18. Laboratory alpha-particle yield Y_L vs proton bombarding energy E_{1B} near the 1247-kev resonance. The error bars indicate statistical errors only. The dashed curve has been calculated from the theory given in Appendix D, and the dotted curve is the assumed background from the 1274-kev resonance. See text pp. 29, 31, 39, 41ff., 47, 77, 79, 84.

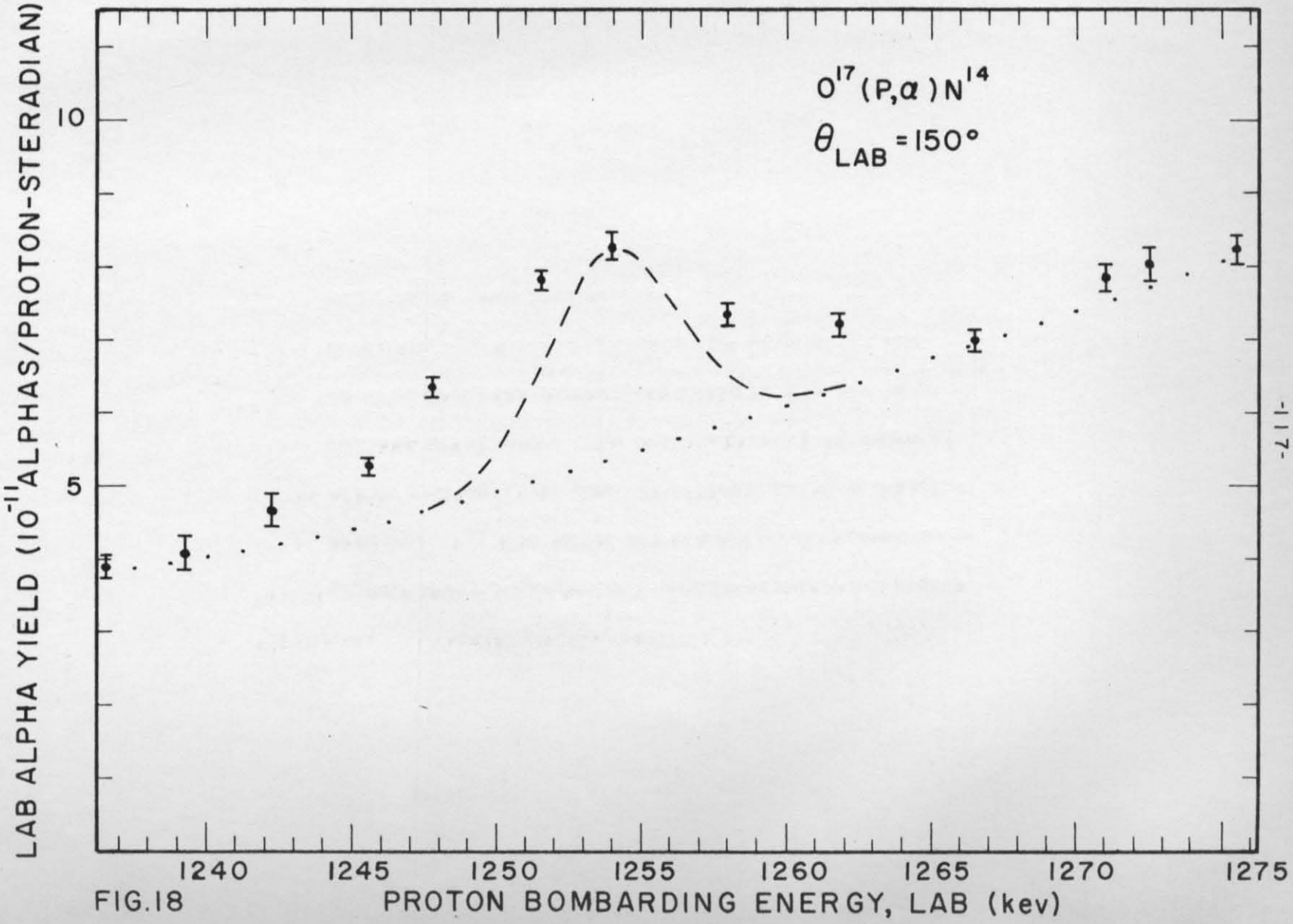
$O^{17}(P,\alpha)N^{14}$
$\theta_{LAB} = 150°$
LAB ALPHA YIELD (10^{-11} ALPHAS/PROTON-STERADIAN)
10
5
1240
1245
1250
1255
1260
1265
1270
1275
PROTON BOMBARDING ENERGY, LAB (kev)

FIG.18

Figure 19. Alpha-particle counts per unit fluxmeter setting N/V_m corrected for charge exchange vs fluxmeter setting V_m. The error bars indicate the statistical error only. The data in this figure were derived from the uncorrected data in Fig. 5. For this data E_{1B} = 1.280 Mev and Q = 88.6 μcoul for each point. See text p. 30.

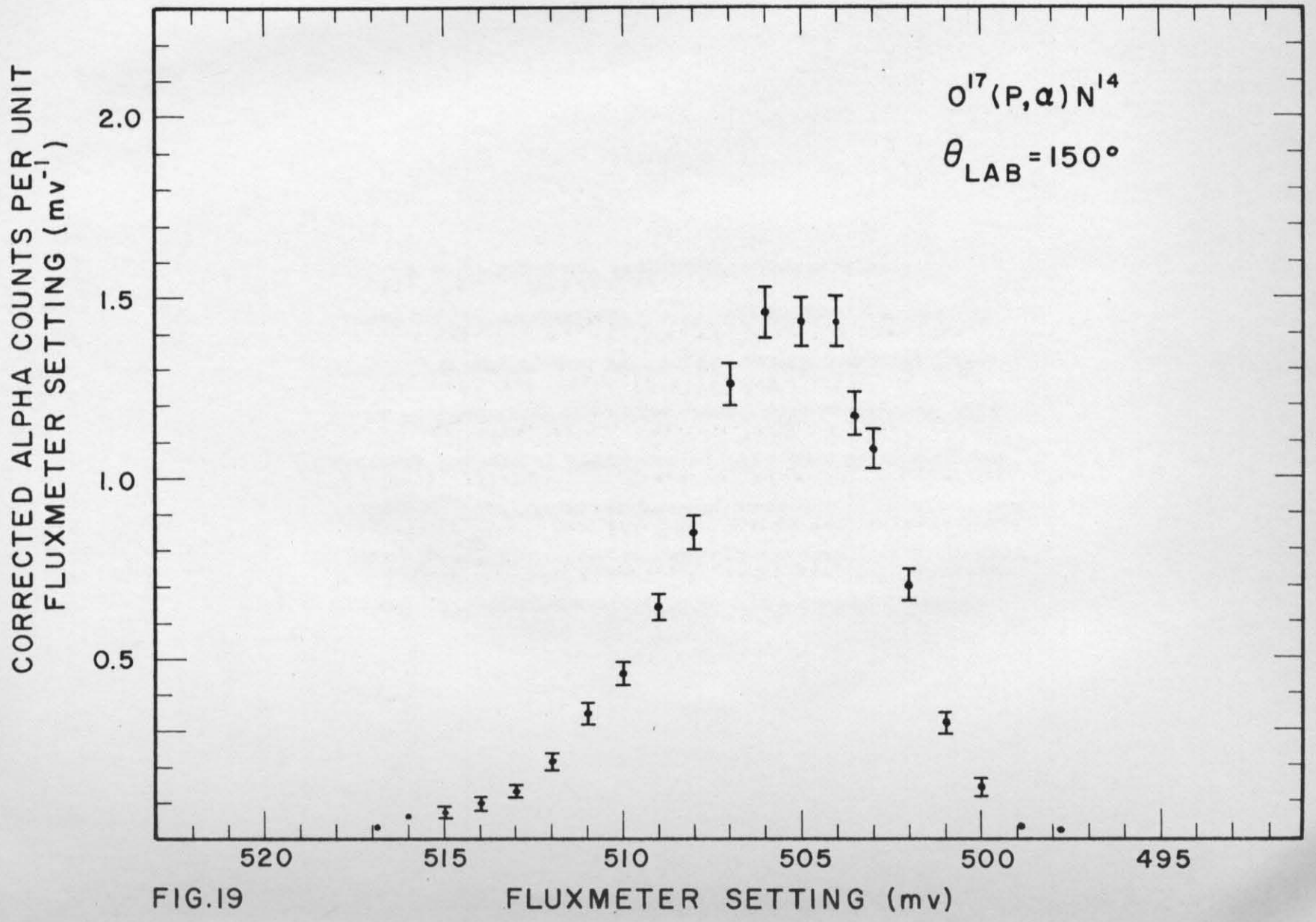
$O^{17}(P,\alpha)N^{14}$
$\theta_{LAB} = 150°$
CORRECTED ALPHA COUNTS PER UNIT FLUXMETER SETTING (mv^{-1})
2.0
1.5
1.0
0.5
520
515
510
505
500
495
FLUXMETER SETTING (mv)

FIG.19

Figure 20. Alpha-particle counts per unit fluxmeter setting N/V_m corrected for charge exchange vs fluxmeter setting V_m corrected for carbon build up. The error bars indicate statistical errors only. The data in this figure were derived from the uncorrected data in Fig. 6. The circles, triangle, and square are data taken with different reference profiles. For this data E_{1B} = 854 kev and Q = 2850 μcoul for each point. See text p. 31.

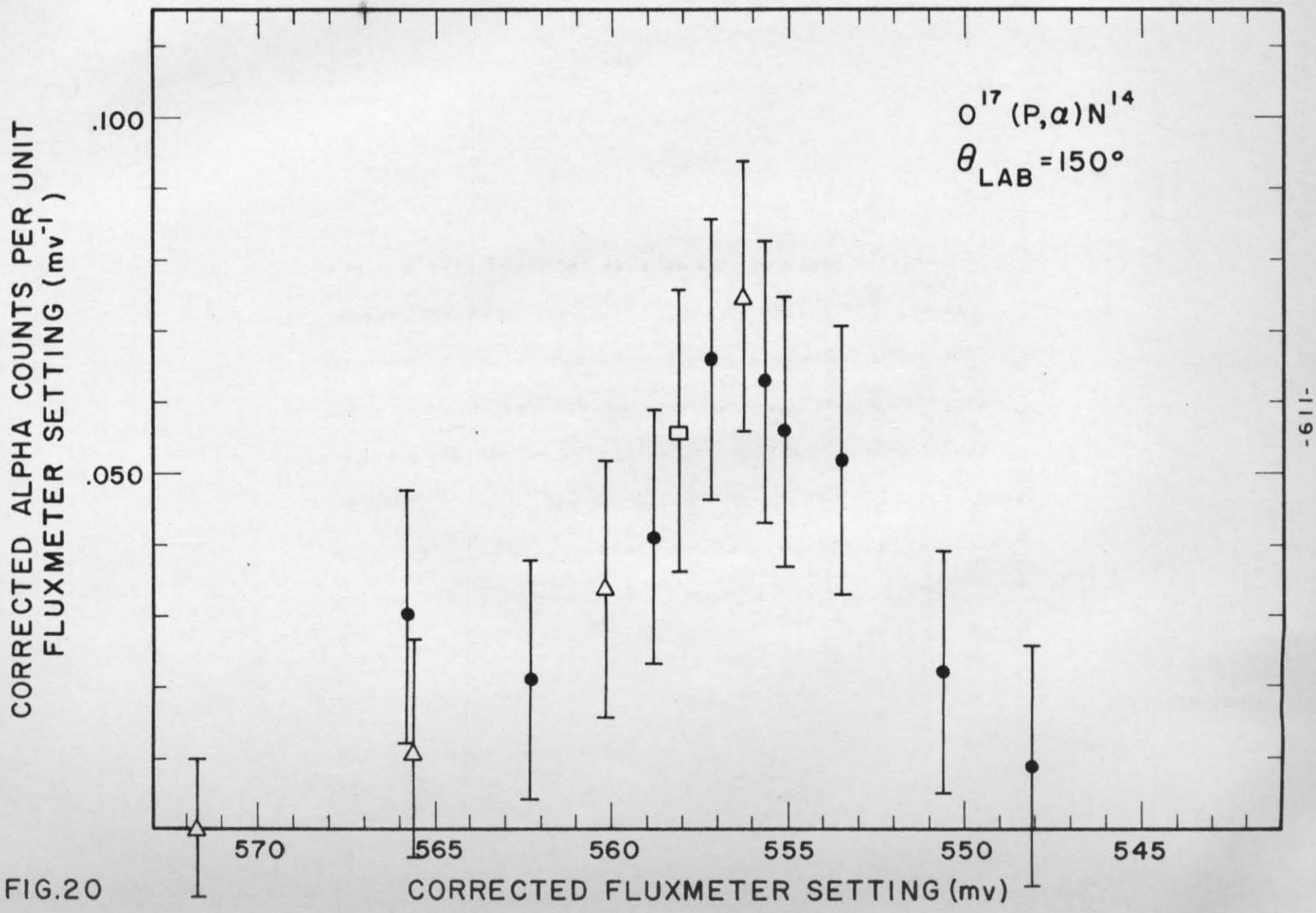
$O^{17}(P,\alpha)N^{14}$
$\theta_{LAB} = 150°$
CORRECTED ALPHA COUNTS PER UNIT FLUXMETER SETTING (mv^{-1})
.100
.050
570
565
560
555
550
545
CORRECTED FLUXMETER SETTING (mv)

FIG.20

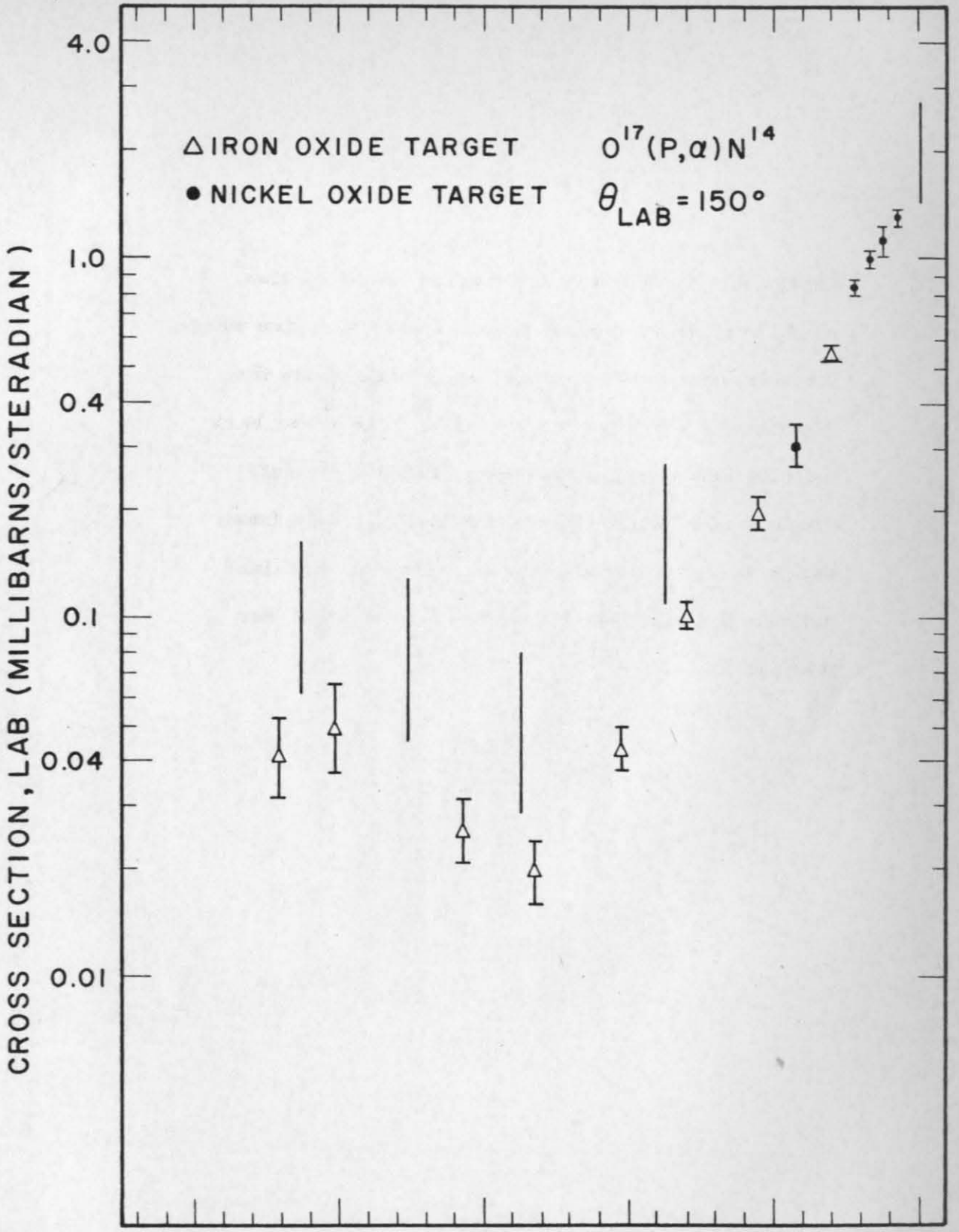
4.0
1.0
0.4
0.1
0.04
0.01
△IRON OXIDE TARGET
● NICKEL OXIDE TARGET
$O^{17}(P,\alpha)N^{14}$
$\theta_{LAB} = 150°$
CROSS SECTION, LAB (MILLIBARNS/STERADIAN)
600
700
800
900
1000
1100
PROTON REACTION ENERGY, LAB (kev)

FIG. 21

Figure 21. Laboratory differential cross section $\sigma_L(\theta_L)$ vs proton energy E_1 in the energy region where the measured cross section was lowest. Note the logarithmic scale for the ordinate. The error bars indicate statistical errors only, and the absolute cross section scale is accurate to 10%. Data from both types of target are shown. The vertical lines indicate the positions of narrow resonances. See text pp. 31, 47.

Figure 22. Differential cross section $\sigma(\theta)$ in the c.m. system vs. c.m. energy E in the O^{17} + p system. The figure shows the experimental results near the two broad resonances at c.m. energies of 1203 and 1035 kev (lab energies of 1274 and 1096 kev). The error bars indicate statistical errors only. The dashed curve is that computed by summing two single level formulas, one for each of the two broad resonances. See text pp. 24, 31, 36, 39, 45, 47.

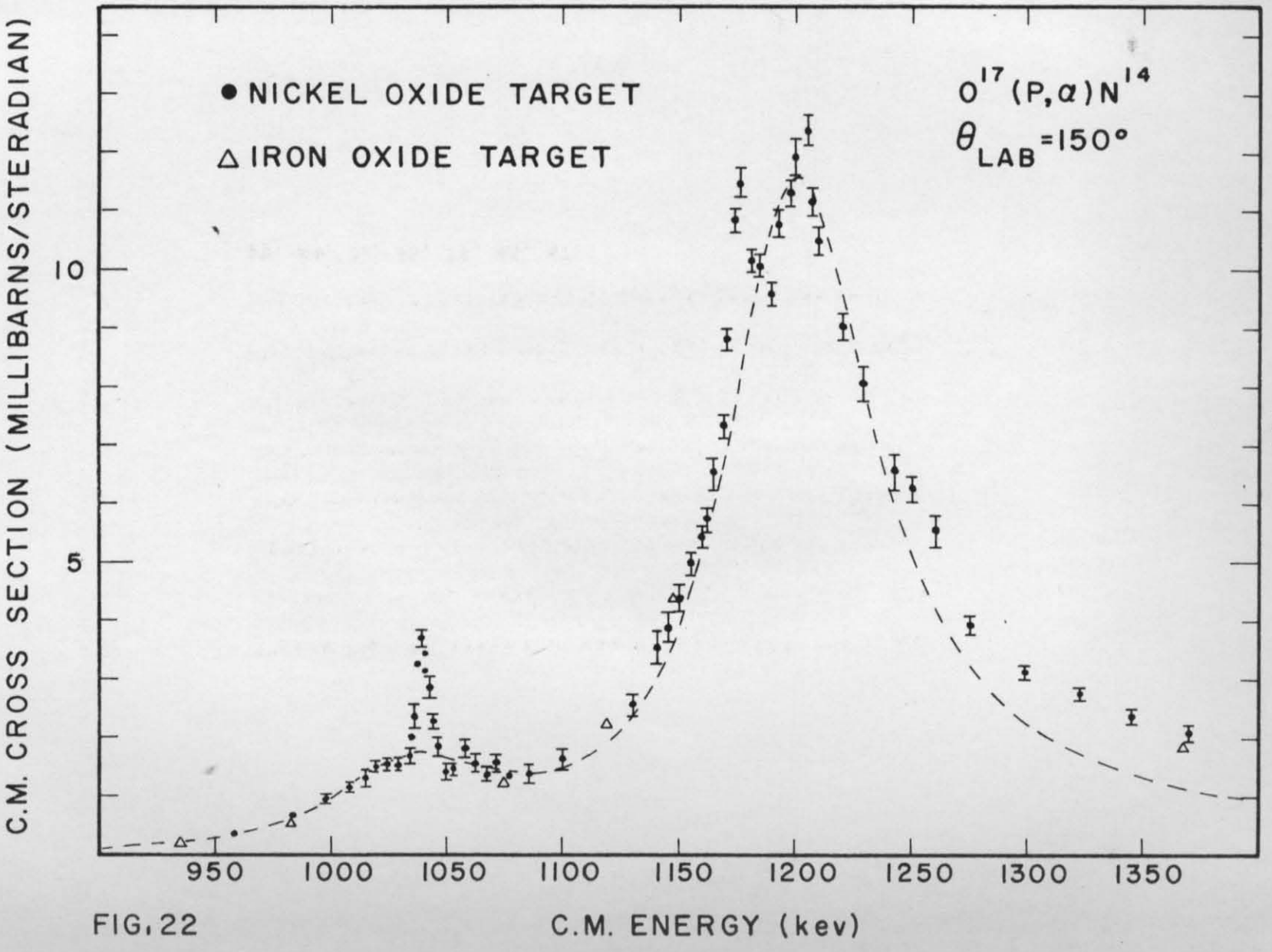
● NICKEL OXIDE TARGET
△ IRON OXIDE TARGET
$O^{17}(P,\alpha)N^{14}$
$\theta_{LAB}=150°$
C.M. CROSS SECTION (MILLIBARNS/STERADIAN)
10
5
950
1000
1050
1100
1150
1200
1250
1300
1350
C.M. ENERGY (kev)

FIG. 22

Figure 23. p-wave barrier factors Γ/θ^2 for both incoming and outgoing channels vs c.m. energy E in the O^{17} + p channel. Points are taken from Tables II and III, and the dashed curves are polynomials fitted to these points. See text p. 38.

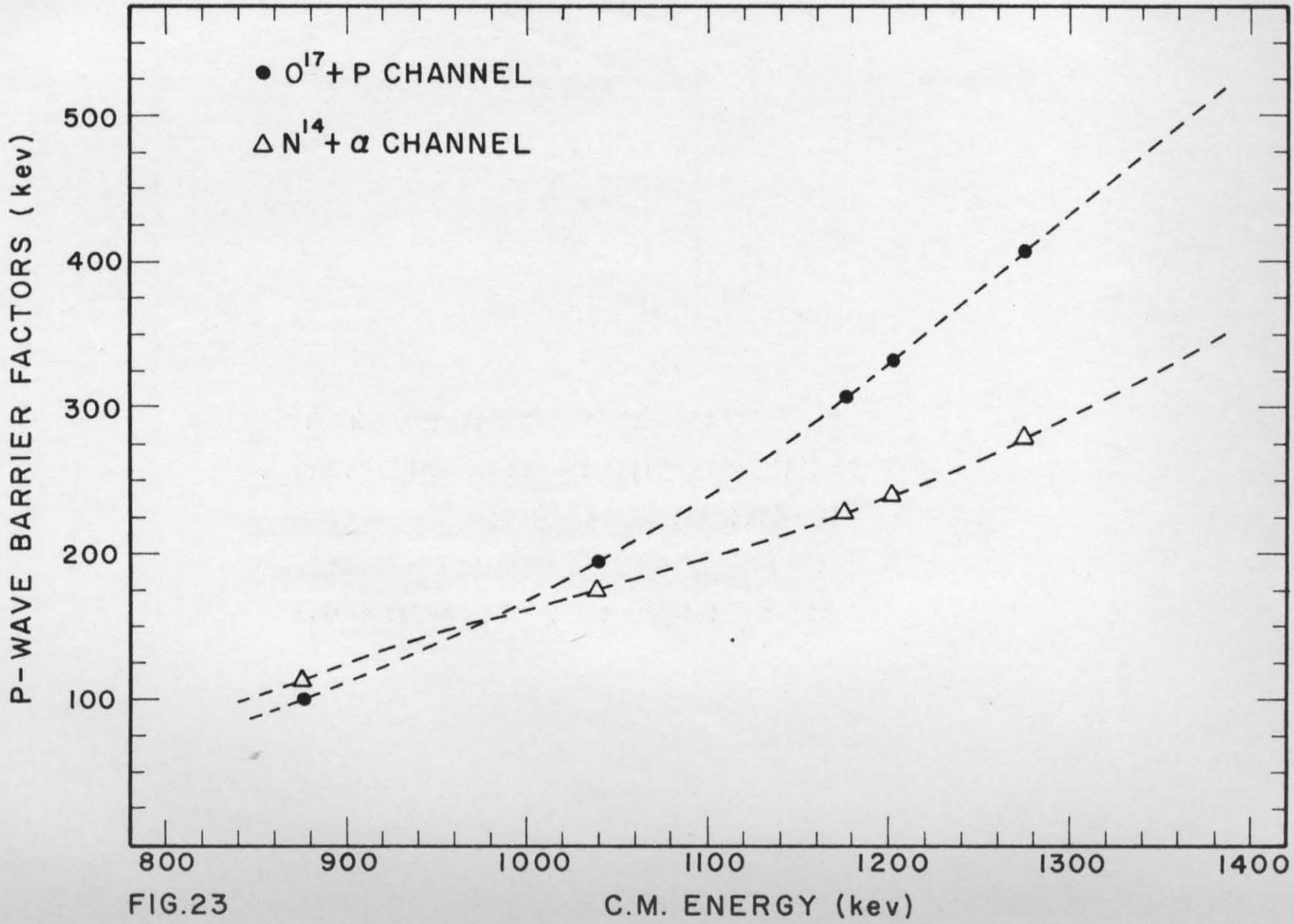
● O^{17} + P CHANNEL
△ N^{14} + α CHANNEL
P-WAVE BARRIER FACTORS (kev)
100
200
300
400
500
800
900
1000
1100
1200
1300
1400
C.M. ENERGY (kev)

FIG.23

Figure 24. Energy relations in the target used in calculating the energy spread due to the angular acceptance of the spectrometer. See Appendix C, p. 72.

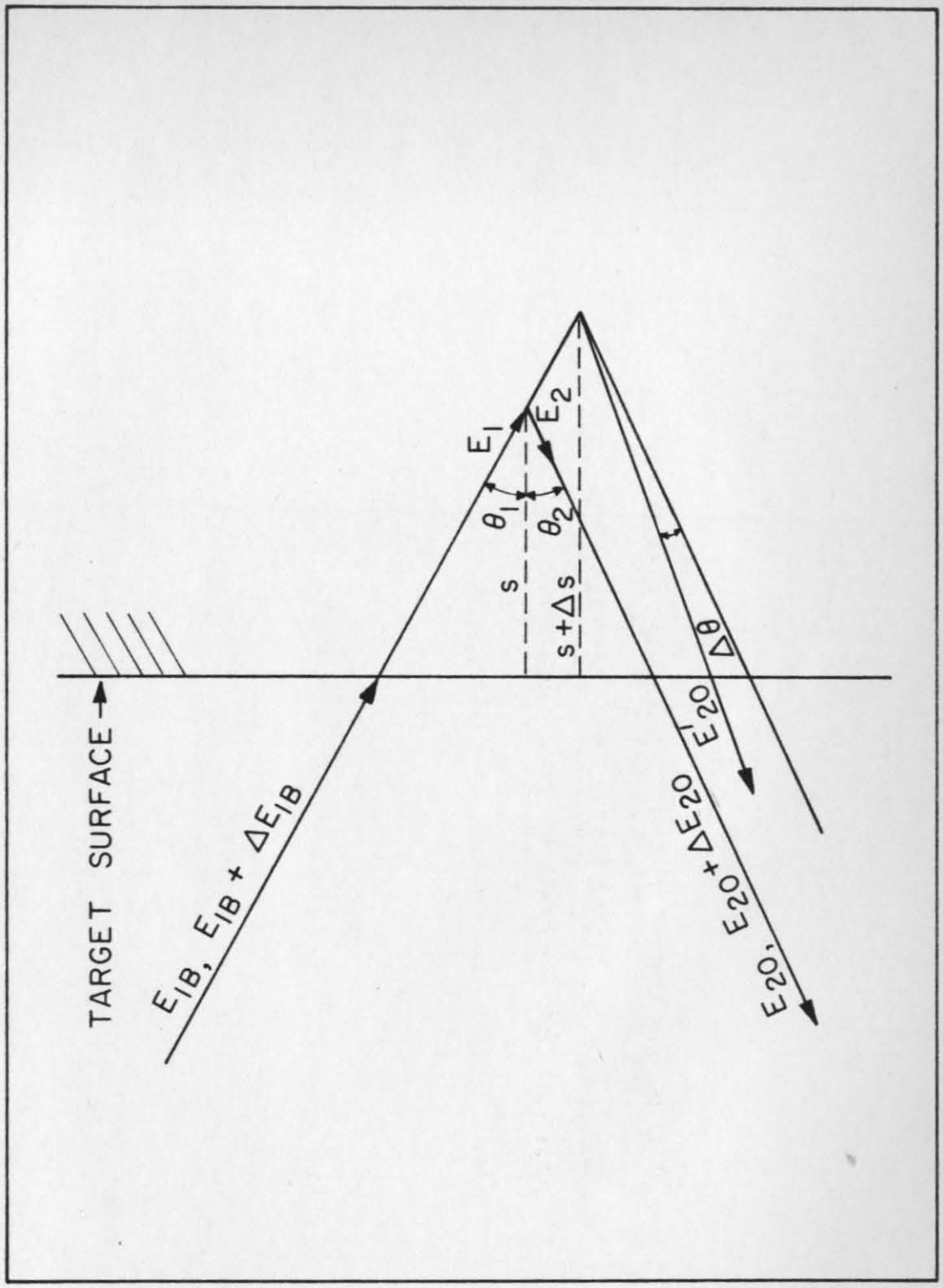
TARGET SURFACE
E_{1B}, $E_{1B} + \Delta E_{1B}$
E_1
E_2
θ_1
θ_2
s
s+Δs
Δθ
E_{20}, $E_{20} + \Delta E_{20}$
E'_{20}

FIG. 24

Figure 25. p-wave barrier factor Γ/θ^2 for the $N^{14} + \alpha$ channel vs c.m. energy E in the O^{17} + p channel. Points are taken from Table III and the dashed curve is a polynomial fitted to those points. See text p. 53f.

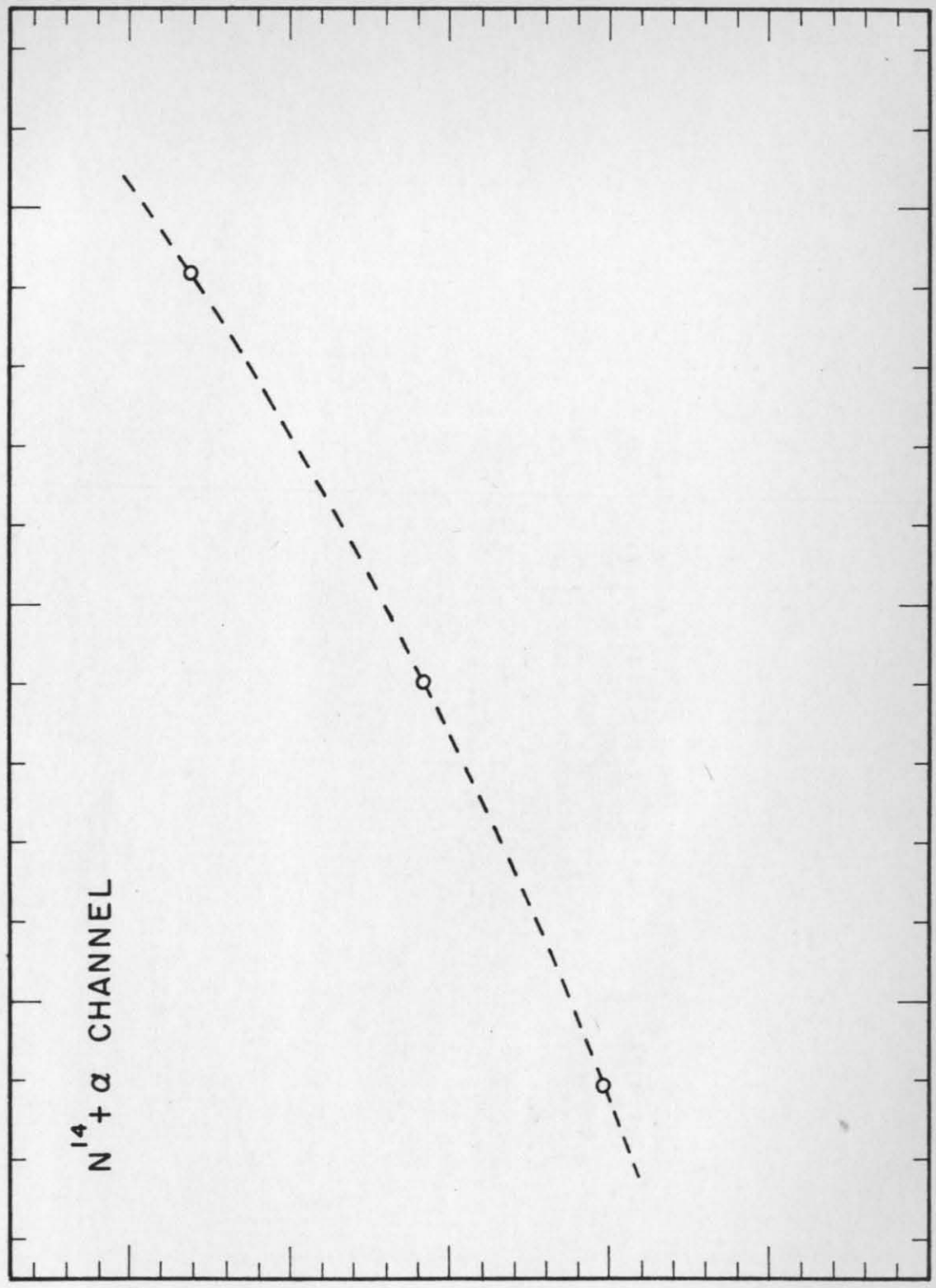
$N^{14} + \alpha$ CHANNEL
p- WAVE BARRIER FACTOR (kev)
2.5
2.0
1.5
1.0
0.5
0
50
100
C.M. ENERGY (kev)

FIG.25

Figure 26. Cross section factor S(E) vs c.m. energy E in the O^{17} + p system at the stellar energy region. Both the case of constructive interference and of destructive interference between the levels are shown. At the high energy resonance S rises to 6.88×10^{6} kev-barns. See text pp. 54, 56.

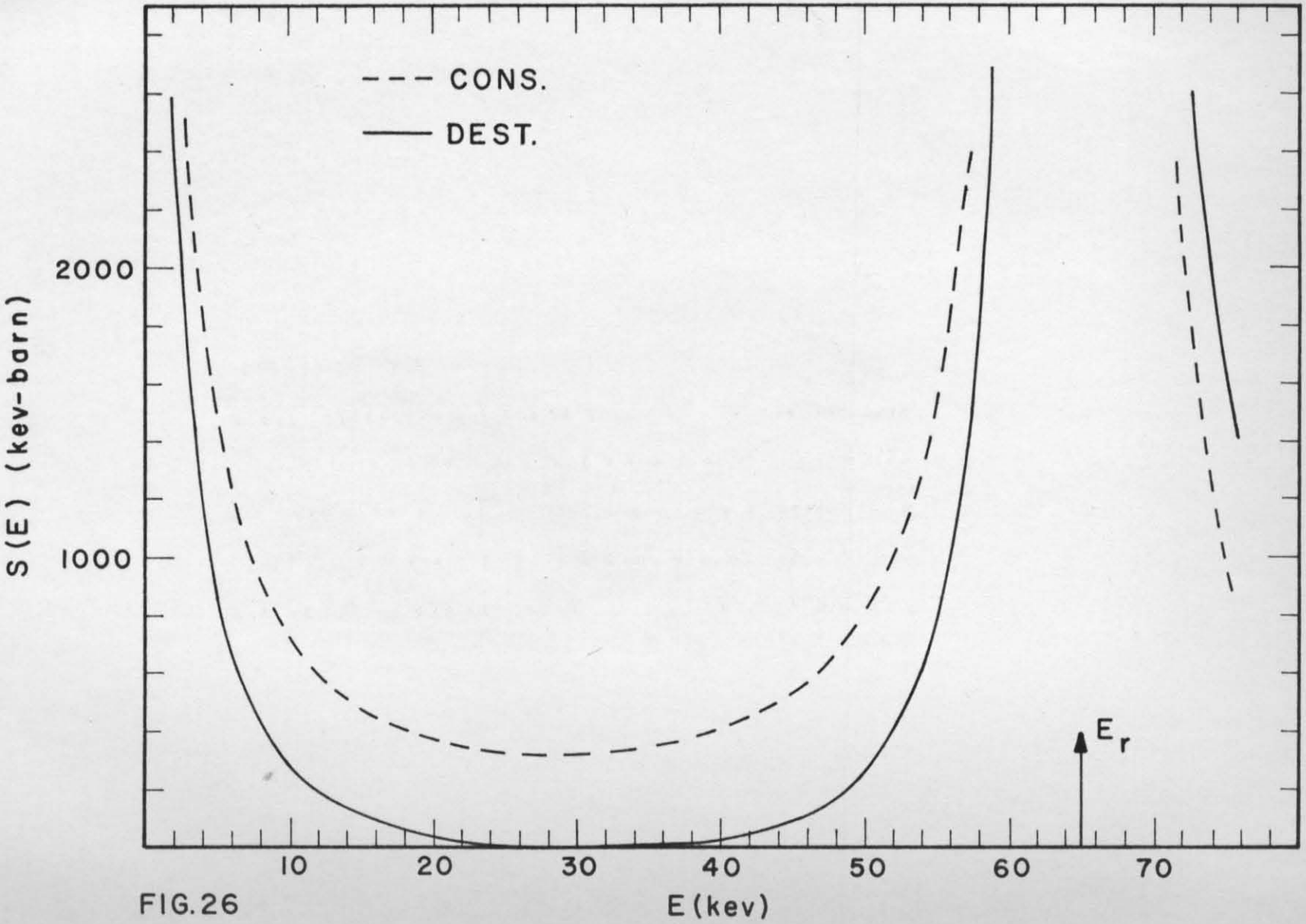

FIG. 26

Figure 27. Folded rate integrand $\Phi_{cf}(E)$ vs c.m. energy E in the O^{17} + p system. The area under this curve is proportional to the $O^{17}(p,\alpha)N^{14}$ reaction rate at a temperature of 15 million degrees. This curve is for constructive interference between the two levels which contribute to the stellar cross section. See text p. 60.

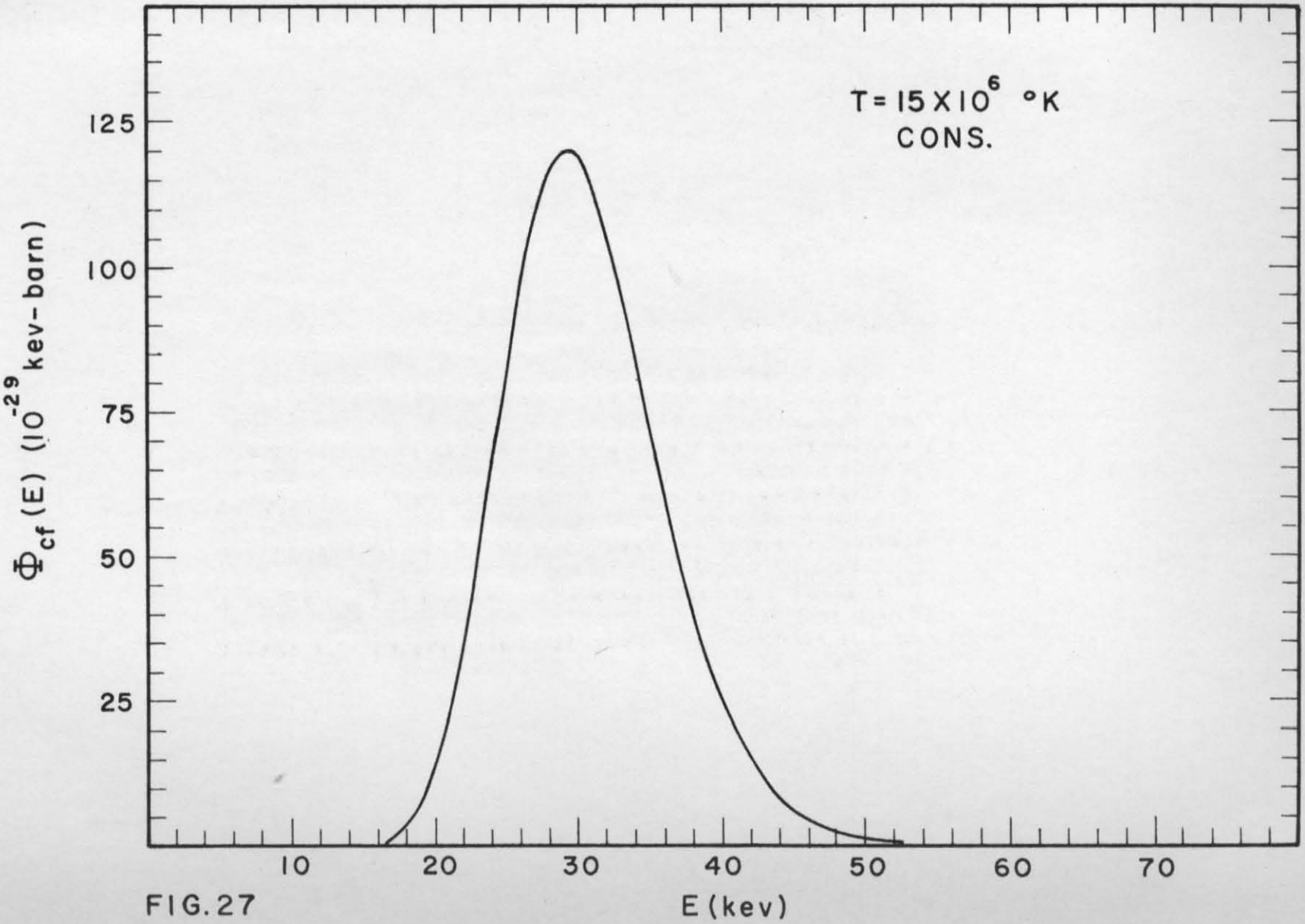
T = 15 X 10^6 °K
CONS.
125
100
75
50
25
Φcf (E) (10^-29 kev-barn)
10
20
30
40
50
60
70
E (kev)

FIG. 27

Figure 28. Folded rate integrand $\Phi_{cf}(E)$ vs c.m. energy E in the O^{17} + p system. Part of the unfolded integrand $\Phi_c(E)$ is shown as a dashed curve. The area under this curve is proportional to the $O^{17}(p,\alpha)N^{14}$ reaction rate at a temperature of 15 million degrees. This curve is for destructive interference between the two levels which contribute to the stellar cross section. See text p. 60.

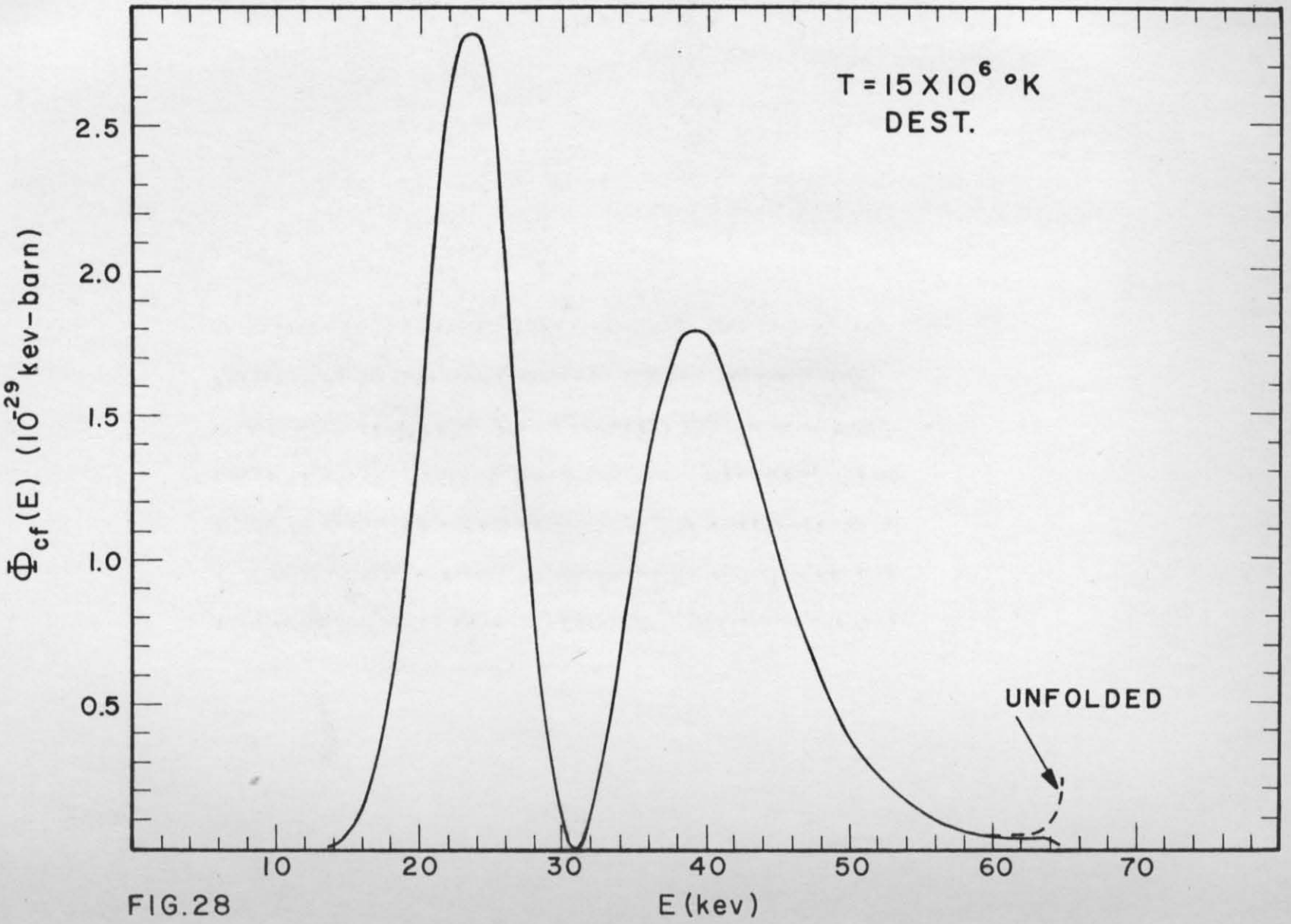
T = 15 X 10^6 °K
DEST.
UNFOLDED
$\Phi_{cf}(E)$ (10^{-29} kev-barn)
2.5
2.0
1.5
1.0
0.5
10
20
30
40
50
60
70
E (kev)

FIG. 28

Figure 29. Folded rate integrand $\Phi_{cf}(E)$ vs c.m. energy E in the O^{17} + p system. Part of the unfolded integrand $\Phi_c(E)$ is shown as a dashed curve. The area under this curve is proportional to the $O^{17}(p, \alpha)N^{14}$ reaction rate at a temperature of 20 million degrees. This curve is for constructive interference between the two levels which contribute to the stellar cross section. See text p. 60.

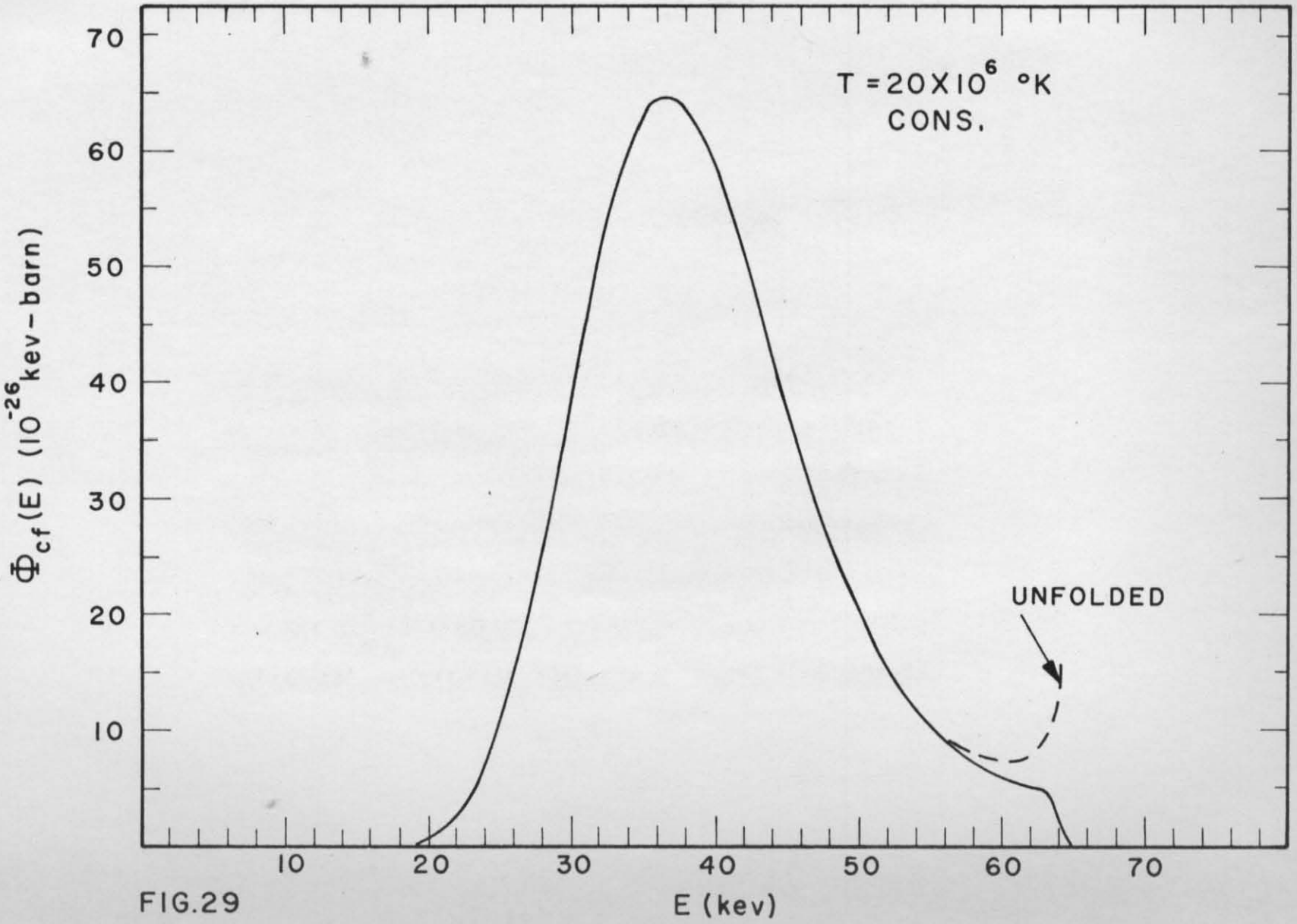
T = 20X10^6 °K
CONS.
UNFOLDED
$\Phi_{cf}(E)$ (10^{-26} kev-barn)
E (kev)
10
20
30
40
50
60
70

FIG.29

Figure 30. Folded rate integrand $\Phi_{cf}(E)$ vs c.m. energy E in the O^{17} + p system. Part of the unfolded integrand $\Phi_c(E)$ is shown as a dashed curve. The area under this curve is proportional to the $O^{17}(p, \alpha)N^{14}$ reaction rate at a temperature of 20 million degrees. This curve is for destructive interference between the two levels which contribute to the stellar cross section. See text p. 60.

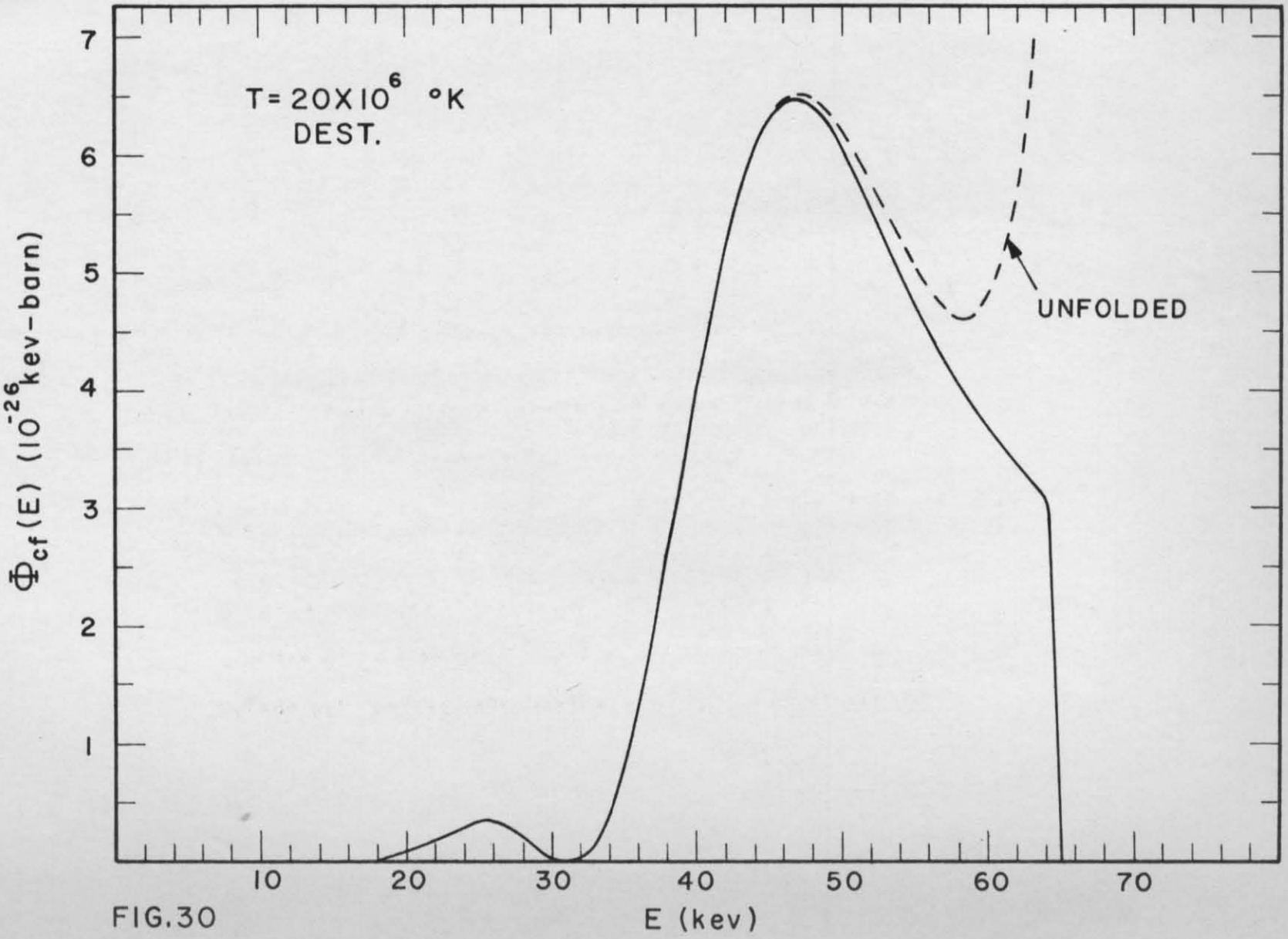
T= 20X10^6 °K
DEST.
UNFOLDED
$\Phi_{cf}(E)$ (10^{-26} kev-barn)
E (kev)
1
2
3
4
5
6
7
10
20
30
40
50
60
70

FIG.30

Figure 31. Log($O^{17}P_{16}/O^{16}P_{17}$) vs temperature T as calculated in the text and given in Table XII. Both the case of constructive and of destructive interference are shown. The dashed curve is what one obtains on assuming the entire $O^{17}(p,\alpha)N^{14}$ rate is given by the resonant formula Eq. (51). At equilibrium we have $P_{16} = P_{17}$, and the ordinate then gives the logarithm of the concentration ratio. See text p. 61f.

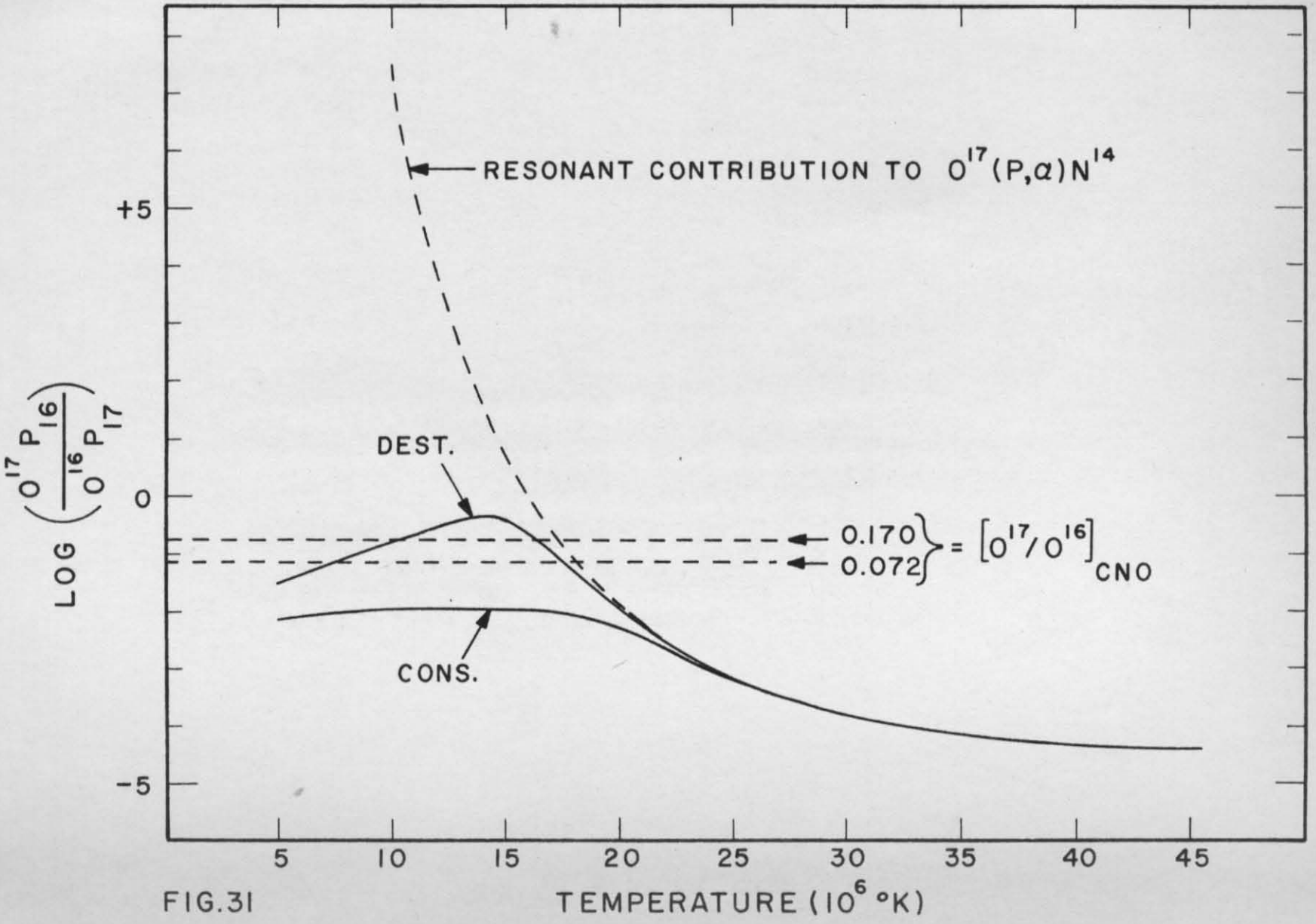
RESONANT CONTRIBUTION TO $O^{17}(P,\alpha)N^{14}$
DEST.
CONS.
0.170
0.072
$= [O^{17}/O^{16}]_{CNO}$
$\text{LOG}\left(\frac{O^{17}P_{16}}{O^{16}P_{17}}\right)$
+5
0
-5
5
10
15
20
25
30
35
40
45
TEMPERATURE (10^6 °K)

FIG.31

Figure 32. A comparison of the true rate correction P_c with the rate P_0 as calculated by the nonresonant approximation (NRA) vs temperature. Both constructive and destructive interference are shown. The vertical arrow indicates the temperature at which $P_0 = 0$. See text p. 60.

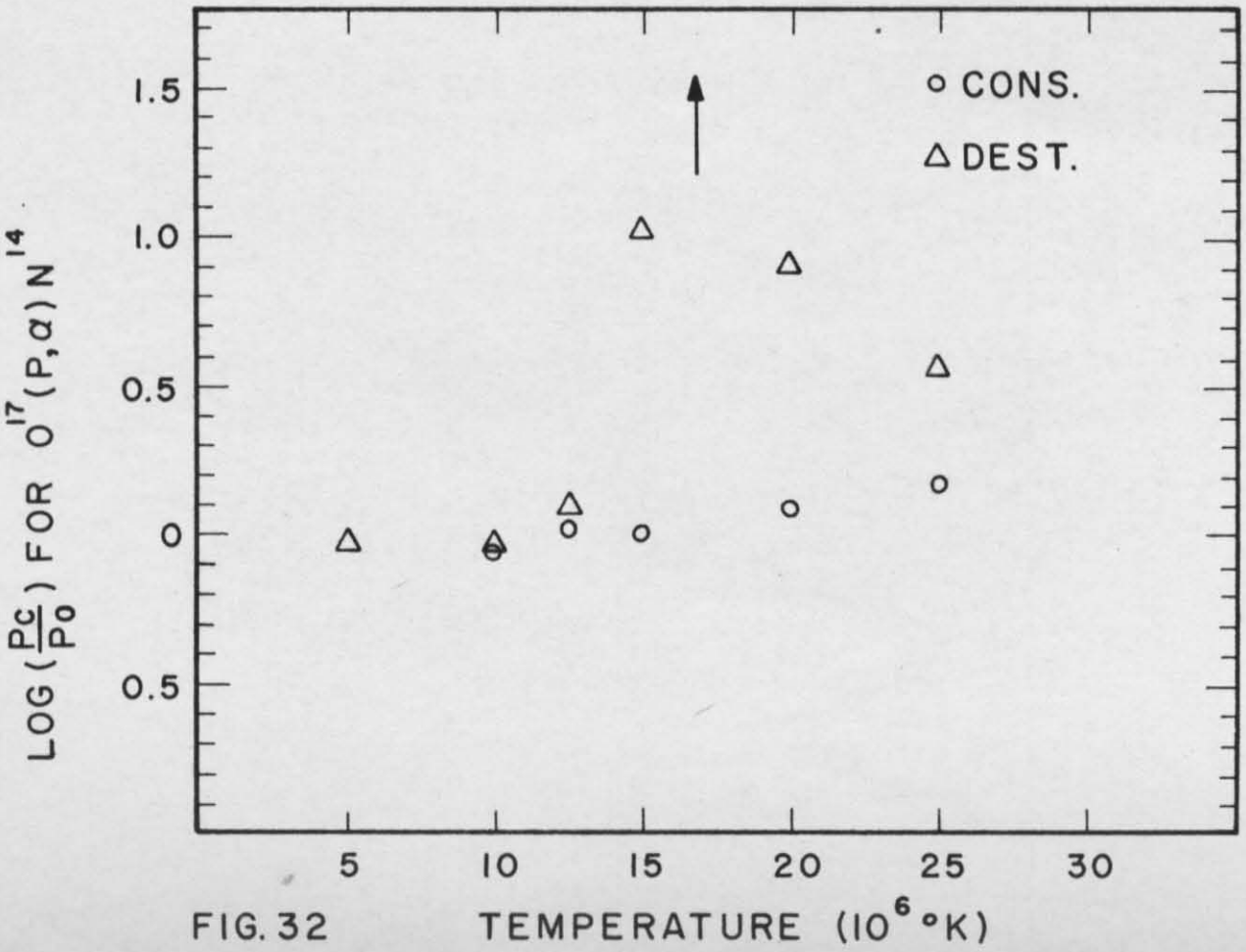
LOG $(\frac{Pc}{Po})$ FOR $O^{17}(P,\alpha)N^{14}$
1.5
1.0
0.5
0
0.5
5
10
15
20
25
30
TEMPERATURE (10^6 °K)
o CONS.
Δ DEST.

FIG. 32